The Philosophical Magazine

UNIVERSITY OF HAWAII
LIBRARY

FIRST PUBLISHED IN 1798

A Journal of Theoretical Experimental and Applied Physics

Vol. 5 August 1960 No. 56
Eighth Series

25s. 0d., plus postage
Annual Subscription £13 10s. 0d., payable in advance

ALERE FLAMMAM

Printed and Published by
TAYLOR & FRANCIS LTD
RED LION COURT, FLEET STREET, LONDON, E.C.4

THE PHILOSOPHICAL MAGAZINE

Editor
Professor N. F. Mott, M.A., D.Sc., F.R.S.

Editorial Board
Sir Lawrence Bragg, O.B.E., M.C., M.A., D.Sc., F.R.S.
Sir George Thomson, M.A., D.Sc., F.R.S.
Professor A. M. Tyndall, C.B.E., D.Sc., F.R.S.

Authors wishing to submit papers for publication in the Journal should send manuscripts directly to the Publishers.

Manuscripts should be typed in *double* spacing on one side of quarto (8 × 10 in.) paper, and authors are urged to aim at absolute clarity of meaning and an attractive presentation of their texts.

References should be listed at the end in alphabetical order of authors and should be cited in the text in terms of author's name and date. Diagrams should normally be in Indian ink on white card, with lettering in soft pencil, the captions being typed on a separate sheet.

A leaflet giving detailed instructions to authors on the preparation of papers is available on request from the Publishers.

Authors are entitled to receive 25 offprints of a paper in the Journal free of charge, and additional offprints can be obtained from the Publishers.

The *Philosophical Magazine* and its companion journal, *Advances in Physics*, will accept papers for publication in experimental and theoretical physics. The *Philosophical Magazine* publishes contributions describing new results, letters to the editor and book reviews. *Advances in Physics* publishes articles surveying the present state of knowledge in any branch of the science in which recent progress has been made. The editors welcome contributions from overseas as well as from the United Kingdom, and papers may be published in English, French and German.

The Thermoelectric Power of Pure Copper†

By A. V. GOLD‡, D. K. C. MACDONALD, W. B. PEARSON
and I. M. TEMPLETON
Division of Pure Physics, National Research Council, Ottawa, Canada

[Received February 24, 1960]

ABSTRACT

Measurements of the absolute thermoelectric power S of very pure copper samples (with residual resistivity ratios as low as $3{\cdot}1\times10^{-4}$) have been carried out between ~0·1°K and ~350°K. Several specimens were found to exhibit marked negative anomalies in S between 8°K and 9°K, whereas a very pure sample of 'natural' copper gave small but positive values of S at low temperatures. By emphasizing that S depends on the *relative* importance of the various scattering mechanisms we have been able to show that the anomalies occur whenever scattering by traces of *iron* becomes dominant, other impurities being of only minor importance. Moreover we are able to account for the occurrences of similar anomalies, as well as the resistance minima, in dilute alloys of oxygen-containing copper with various solutes (e.g. Ga, Ge, Sn . . .) *not* in terms of these particular solutes *directly*, but only in so far as they separate traces of iron from its oxide, thereby bringing it into solid solution. At about 70°K there is a positive peak in S which we ascribe to an Umklapp phonon-drag component.

§ 1. INTRODUCTION

THE absolute thermoelectric power, S, of a well-annealed copper specimen was shown by MacDonald and Pearson (1953) to be very small and negative below about 14°K, a typical value for S being about $-0{\cdot}04\,\mu$v/deg. at 5°K. However, extrapolation of thermoelectric data obtained recently (MacDonald *et al.* 1960) below 1°K on a sample of similar purity, but obtained from a different source, indicated a probable value of about $-3{\cdot}0\,\mu$v/deg. at 5°K, *i.e. differing by about two orders of magnitude from the previous result.* These contradictory results on specimens of almost identical residual resistivity are rendered even more astonishing when one bears in mind the prediction of conventional theory (Wilson 1953) that at low temperatures the thermoelectric power should be small ($S \doteqdot -0{\cdot}05\,\mu$v/deg. at 5°K for the free electron model) and *independent* of the amount and nature of impurities present, provided that the impurity concentration is not sufficient to alter appreciably the band structure of the otherwise pure metal. We have therefore been prompted to remeasure S for a variety of the purest samples of copper which we have been able to obtain to date, including a very pure sample of 'natural' copper. Our attention was at first confined to the temperature region between 2°K and 20°K, but in view of the diversity of the results obtained, we have also carried out measurements on the same samples between 80°K and 400°K; at such relatively high temperatures one would certainly expect a similar behaviour for all pure samples since the thermal scattering of the electrons far outweighs the scattering due to impurities.

---

† Communicated by the Authors.
‡ National Research Council Postdoctorate Fellow.

§ 2. EXPERIMENTAL

The experimental method for the measurement of S between 2°K and 20°K consists of the improved technique used by Christian *et al.* (1958) for the determination of the absolute thermoelectric power of lead, the superconducting Nb_3Sn specimen used in these experiments being replaced by the present copper samples. Thus S at any temperature is obtained as the difference between the observed thermoelectric power and the absolute value for lead. In order to make quite sure of our results, especially in cases where $S_{\mathrm{obs}} \doteqdot S_{\mathrm{Pb}}$ so that S is given by the difference between two large and nearly equal quantities, we have recalibrated the lead wiring of the apparatus against a fresh Nb_3Sn superconductor. In addition we have measured S for one sample directly against Nb_3Sn, but this procedure is in general impracticable, requiring samples in the form of long, thin wires. The measurements between 80°K and 400°K were also made relative to lead, the specimen being housed in an evacuated container which could be immersed in various constant-temperature baths. One end of the specimen was anchored to the container, and the temperature gradient, established by a heater at the other end, was measured by copper–constantan thermocouples. A sensitive galvanometer amplifier (MacDonald 1947) was used to measure the potentials from both the specimen and the thermocouples. In addition we have used the method of MacDonald and Pearson (1953) to follow S for two samples from 4·2°K to room temperature and have extended measurements on two further samples to temperatures below 1°K using the technique of MacDonald *et al.* (1960).

Most of the specimens were some 6 or 7 cm long, and 0·1 mm to 0·5 mm in diameter, with the lead potential wires and small copper thermal probes attached about 1 cm from either end with pure lead as solder. The 'natural' copper sample was of unfavourable dimensions being in the form of an irregular L-shaped 'wire', of length 8 mm and mean thickness about 0·3 mm, though there were several thinner spots. Details of the specimens concerning source, preparation, and residual resistance ratio are given in the table.

§ 3. RESULTS

Figure 1 illustrates the remarkable diversity of thermoelectric power which we have found in the various 'pure' copper samples below 20°K. Sample Cu 1 was prepared from the same commercial copper containing

Sample Cu	Source	Code in figs. 1, 2 and 3	$10^3\times\rho$ ($\rho=R_{4\cdot2}/(R_{293}-R_{4\cdot2})$)	S_{anom} (μv/deg. °c)	T_{anom} (°K)
1	‘J.T.H.’ commercial Cu containing oxygen. 0·002% Fe (present as oxide), traces Ca, Al and Mg	□	2·23	− 0·05	~5·5
2	A.S. and R. batch ‘A’ (long drawn wire; measured directly against Nb_3Sn)	+	2·75	− 3·2	9·5
3	A.S. and R. batch ‘B’ (drawn wire)	×	1·21	− 4·6	8·0
4	Do. (etched rod bent in mounting)	○	0·97	− 5·8	8·5
5	Do. (etched rod)	●	0·86	− 6·0	8·5
6	Do. (long drawn wire)	–·–·	1·05	− 5·2	~8·7
7	A.S. and R. batch ‘C’† (drawn wire)	△	0·65	− 1·8	~7·8
8	Do. (etched rod)	▽	0·48	− 2·9	~8·1
9	Natural copper from Keweenaw Peninsula, Lake Superior‡	◇	0·31	Positive S below 13°K	
10	‘J.T.H.’ Cu + 0·054 wt % Fe (drawn wire)	⬘	320§	~ −16·0	
11	A.S. and R. Cu (batch B) + 0·01% Sn (long drawn wire)	–··–··	25·2	− 1·58	14
Kropschot and Blatt (1959)	A.S. and R. (drawn wire)		1·85	− 1·9	~10
Powell *et al.* (1959)	A.S. and R. (drawn wire)		0·67		

Notes: Specimens 1–11 have been vacuum annealed at 530°c for 24 hours. Chemical analyses on A.S. and R. batches B and C give ~0·0001% Fe; spectrographic analyses by American Smelting and Refining Co. give similar amounts of As, Ni, Pb, S, Sb, Se, Sn and Te.

† Kindly supplied by Dr. J. Babiskin.

‡ Kindly supplied by Professor A. F. Kip and Dr. D. Langenberg.

§ At resistance minimum (26°K; Pearson 1955).

oxygen as used by MacDonald and Pearson (1953) and our findings of small and negative values of S confirm the results obtained earlier by a less accurate experimental technique. The results for this sample are also shown on a more expanded scale in fig. 2 (*a*). Samples Cu 2 to Cu 8, on the other hand, all exhibit a marked negative anomaly in S which reaches a maximum size between 8°K and 9°K. These samples were prepared from various batches of copper refined by American Smelting and Refining Co., and all have residual resistivities comparable with or lower than that of Cu 1. The extreme cases of Cu 1 and Cu 5 have values of S which differ by a factor of 120 at the anomaly! In samples taken from the *same* batch, the observed minimum value of S appears to increase as the purity of the metal, gauged by the residual resistivity, increases (see table).

Fig. 1

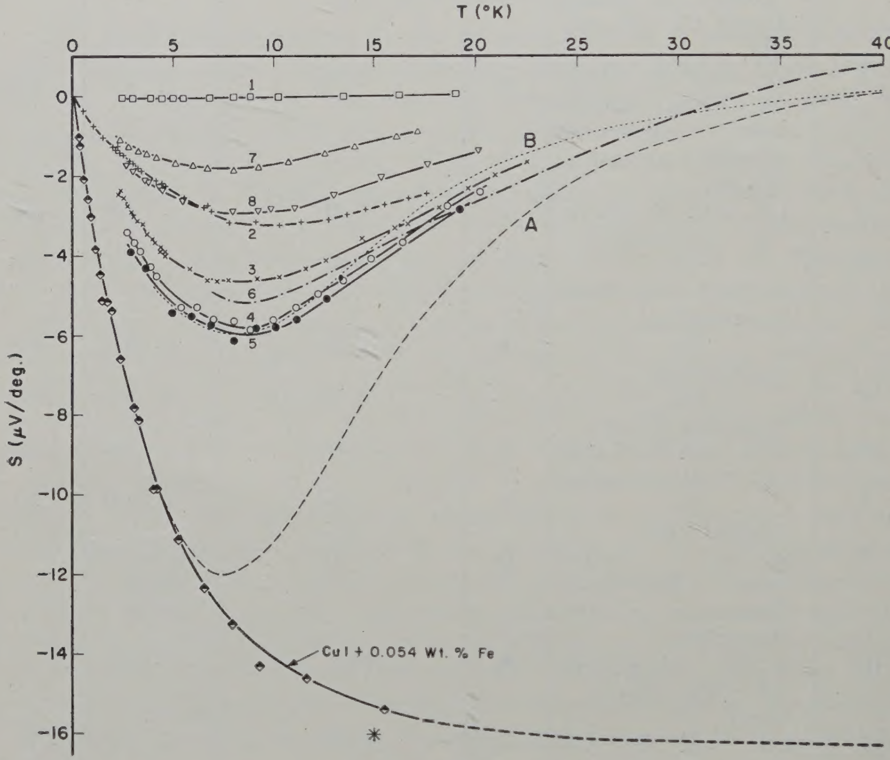

The low-temperature anomaly in S. Details of the specimens are given in the table. With this highly compressed scale of ordinates a linear extrapolation of the high-temperature results (fig. 3) and the free-electron variation of S (Wilson 1953) would both be indistinguishable from a horizontal line through the origin. A, B: calculated from eqn. (3) for a specimen with $\rho=0{\cdot}67\times10^{-3}$ and assuming, respectively, 100% and 50% of the impurity scattering to be due to iron. *, characteristic value of $S_{15^\circ\mathrm{K}}$ for Fe in Cu from fig. 4.

When, however, samples taken from *different* batches are compared there is generally speaking no correlation between overall purity and thermoelectric power.

Fig. 2

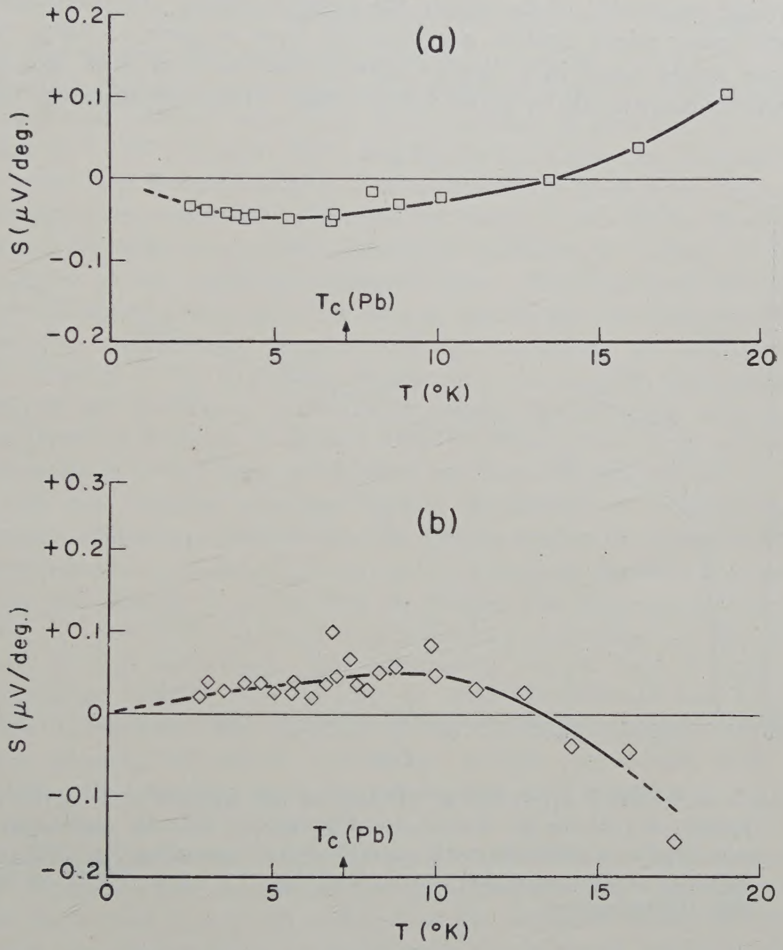

Low-temperature variation of S for (*a*) Cu 1 and (*b*) Cu 9 (natural copper), with the scale of the ordinates considerably expanded.

In addition to these remarkable results, we have now found a small but *positive* thermoelectric power at low temperatures for the 'natural' sample Cu 9, which, according to residual resistivity, is the purest of all our samples. The data for this specimen are presented on an enlarged scale in fig. 2 (*b*). Measurement of S for this very pure and inconveniently shaped sample was not easy because of the difficulty in setting up an adequate temperature gradient. We are in no doubt whatsoever that S is indeed positive below 7·2°K, where direct measurements are made relative to superconducting lead with zero thermoelectric power. However, we cannot be too sure of the reliability of the results above 7·2°K since S is then obtained as the difference between two large and nearly equal observed quantities. Because of the unfavourable dimensions of the specimen, with the lead solder joints for the potential and thermal probes occupying some 20% of its length, the experimentally observed thermoelectric power might contain a systematic error as great as 10%; such an error would result in a displacement of the value of S at, say, 18°K upwards or downwards by about 0·08 μv/deg. However, since the values of S turn out to be more or less the same when measurements are made either just below or just above 7·2°K, we are inclined to think that any error is not as large as this and that S does indeed change sign near 13°K.

Fig. 3

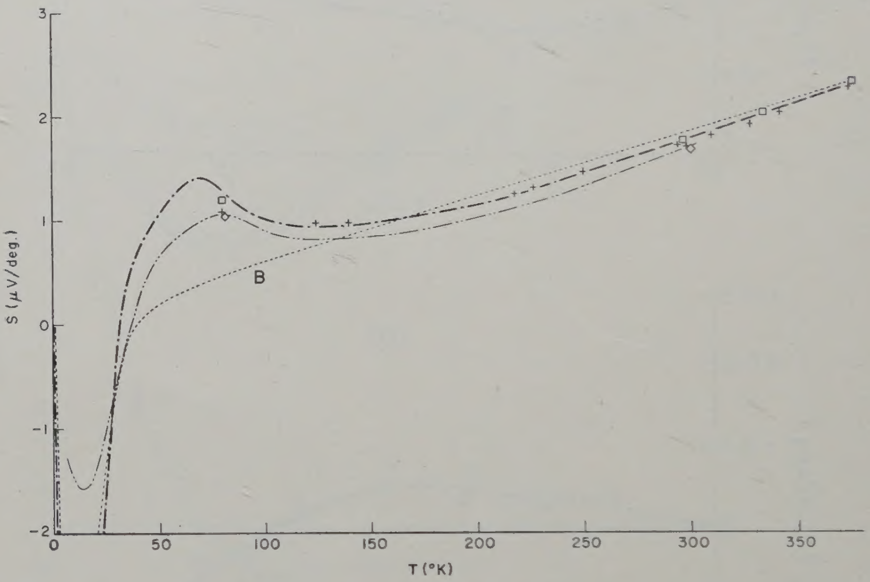

Variation of S with T up to 400°K. Details of the specimens are given in the table. —·—, Cu 6; —··—··, Cu+0·01% Sn; B, calculated from eqn. (3) for a specimen with $\rho = 0{\cdot}67 \times 10^{-3}$, assuming that 50% of the impurity scattering is due to iron and that $S = +5{\cdot}4 \times 10^{-3} T$ μv/deg. at high temperatures.

In contrast to the striking differences found at temperatures below 20°K, the thermoelectric powers above 100°K (fig. 3) do not differ significantly from sample to sample and are positive. Thus the data from Cu 1 (no low-temperature anomaly) and Cu 6 (large anomaly) are virtually indistinguishable at the higher temperatures. Also shown in fig. 3 is the curve obtained for an alloy with 0·01% Sn (see table). The results given recently by Kropschot and Blatt (1959) for a pure specimen with residual resistivity similar to that of some of our samples (see table) fall close to our Cu–Sn curve, while the earlier work of Borelius *et al.* (1930) (see also Nyström (1947)) for a nominally pure specimen of unknown residual resistivity gives slightly greater values of S than the present results.

§ 4. DISCUSSION

4.1. *The Anomalous Scattering and the Resistance Minimum*

The low-temperature anomalies found in samples Cu 2 to Cu 8 bear considerable resemblance to the results obtained when material similar to that of Cu 1 is alloyed with very small amounts of iron (see fig. 1, also Borelius *et al.* 1932, Pearson 1955), and we shall now propose, and justify as we proceed, that the anomalies in S arise specifically from some anomalous scattering of the conduction electrons by traces of *iron* rather than from scattering by other impurities, phonon-drag effects, or because of basic peculiarities in the electronic structure alone. Starting from this single hypothesis we are able to account for and coordinate a considerable range of hitherto unexplained experimental facts relating not only to the thermoelectric power in 'pure' copper but also to the thermoelectric power and the resistance minimum in several dilute copper alloys.

The presence of traces of around 0·0001% iron in the samples showing the anomaly in S has been established by chemical analysis (see table); from this fact, together with the residual resistivities of the samples and the known scattering cross section for iron in copper (cf. Pearson 1955), we conclude that scattering by iron is the dominant impurity scattering. Reasons will shortly be given why we believe the other impurities (e.g. As, Ni, ...; see table) to be of only secondary importance as far as the anomaly in S is concerned. The commercial copper Cu 1 is known to contain about 0·002% iron, *present as oxide* (MacDonald and Pearson 1955 a); if, however, this copper is melted under reducing conditions, a sizeable anomaly of about $-9\,\mu$v/deg. results, consistent with the supposition that the iron has now entered into solid solution.

On the other hand, it is tempting to regard the small yet positive S in our purest sample Cu 9 as being close to the true 'diffusion' thermoelectric power of pure copper, unaffected by any anomalous impurity scattering. In this connection it is worth noting that the values of slopes, dS/dT, at high and low temperatures are both approximately $+5\times10^{-3}T\,\mu$v/deg^2. This is, broadly speaking, in agreement with conventional theory (Wilson 1953) which predicts the slopes at high and low temperatures to be of the same (albeit negative) sign, with the former three times the latter.

As a starting point for further discussion of the low-temperature results we shall now make use of an expression, originally proposed by Kohler (1949)†, for thermoelectric power of a single-band conductor where two or more scattering mechanisms are present. If we assume these scattering mechanisms to operate independently of one another, each giving rise to a characteristic thermoelectric power $S_i(T)$ and a thermal resistivity $W_i(T)$, then, subject to certain restrictions, the resultant thermoelectric power should be given by:

---

† Kohler derived this result from his theory of electron transport based on a variational principle. The result can be derived in a direct manner with similar restrictions from a rather general model (Appendix I).

$$S=\sum_i W_i S_i \Big/ \sum_i W_i. \qquad \ldots\ldots\ (1)$$

Thus, unlike the thermal and electrical resistivities, the resultant thermoelectric power does *not* depend on the *total* amount of scattering but on the *relative* amounts of scattering, as gauged by the thermal resistivities W_i, of the individual mechanisms.

An application of (1), of which we shall make considerable use in what follows, concerns the low-temperature thermoelectric power in a metal in which two types of impurity are present. Since we are concerned with the residual resistance region, we may write $W_i=\rho_i/L_0T$ (L_0 is the Lorenz constant$=\pi^2k^2/3e^2$) and we obtain a relation which was in essence given by Nordheim and Gorter (1935; eqn. (9)):

$$S=\sum_i \rho_i S_i \Big/ \sum_i \rho_i=\frac{\rho_a}{\rho}S_a+\frac{\rho_b}{\rho}S_b=S_a+\frac{\rho_b}{\rho}(S_b-S_a), \qquad .\ (2a)$$

where S_a, S_b and ρ_a, ρ_b are the thermoelectric powers and electrical resistivities (or corresponding residual resistance ratios) which would be obtained if each of the impurities a, b were to be present by itself. Thus if we now start with a 'pure' metal with parameters S_a, ρ_a and measure the changes in S and ρ as the impurity b is added, then a plot of S against the total inverse residual resistance ratio $1/\rho$ should yield a straight line with intercept S_b as $1/\rho\to 0$, this value being independent of the parameters S_a, ρ_a of the starting material. We must emphasize that these conclusions assume that the only role of the added solute impurities is to scatter the electrons. In other words, we are specifically excluding any modification of the Fermi surface due to alloying. These predictions appear strikingly confirmed in fig. 4, which shows the effects of adding small amounts of nickel to the copper of samples Cu 1 and Cu 2. Although the two 'pure' starting metals have considerably different values of S_a, both plots extrapolate to approximately the same value of $S_b \doteqdot -1{\cdot}2\,\mu$v/deg., which is then the characteristic value of S for nickel in copper at 15°K. Thus, by constructing such S *versus* $1/\rho$ plots at a fixed temperature for any particular solute, we can determine the concentration-independent characteristic value of S for the solute at that temperature. In other words, when the scattering by the solute *dominates* the impurity scattering the observed thermoelectric power will be the characteristic thermoelectric power for that solute in the solvent considered.

We have determined the characteristic thermoelectric powers for the solutes Ag, Au, Cr, Ga, Ge, In, Si and Sn in copper (see fig. 5), as well as that due to physical imperfections introduced by cold-working pure copper

(Pearson 1960), and find that the characteristic values are all small, lying in the range between +1 and −1 μv/deg. at 15°K. However, there is one glaring exception to this scheme, namely *iron*, for which one finds the anomalously high value of −16·2 μv/deg. at 15°K (fig. 4)†.

Fig. 4

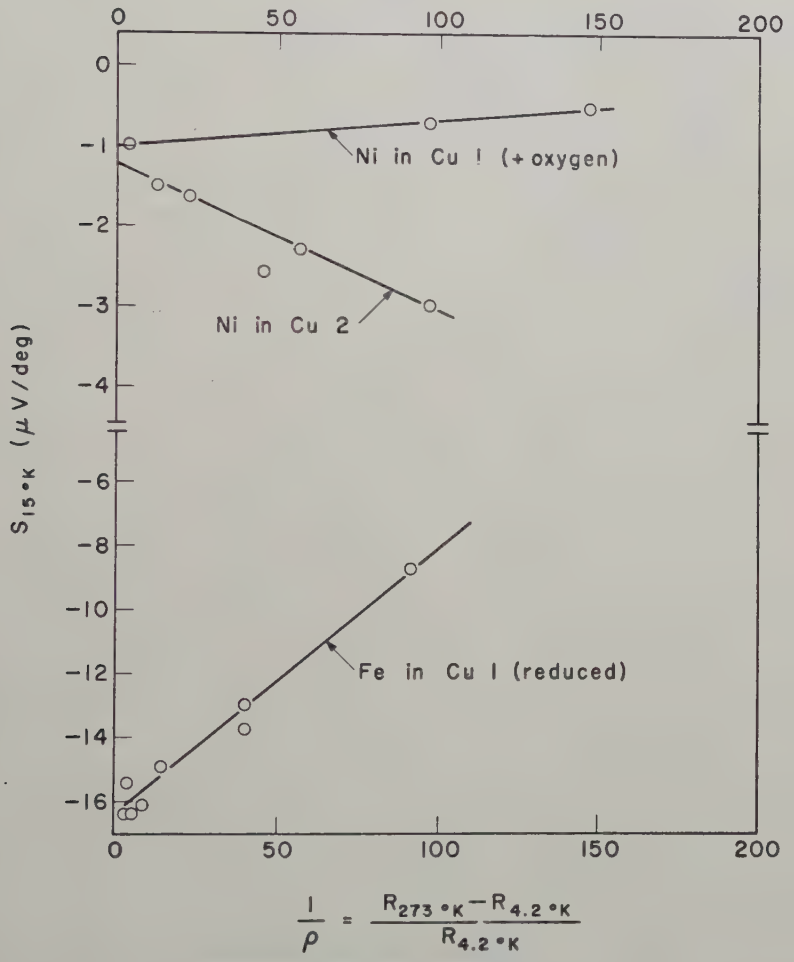

Variation of $S_{15°K}$ with inverse residual resistance ratio for dilute Cu–Ni and Cu–Fe alloys.

These results thus lay the foundation for our hypothesis that the low-temperature anomaly is primarily due to the dominant scattering of

---

† There is some evidence that the solutes Co, Mn and perhaps Bi and Pb, may have somewhat greater (negative) characteristic values of S at 15°K than −1 μv/deg.; we intend to re-investigate these alloys using our present much purer copper.

Fig. 5

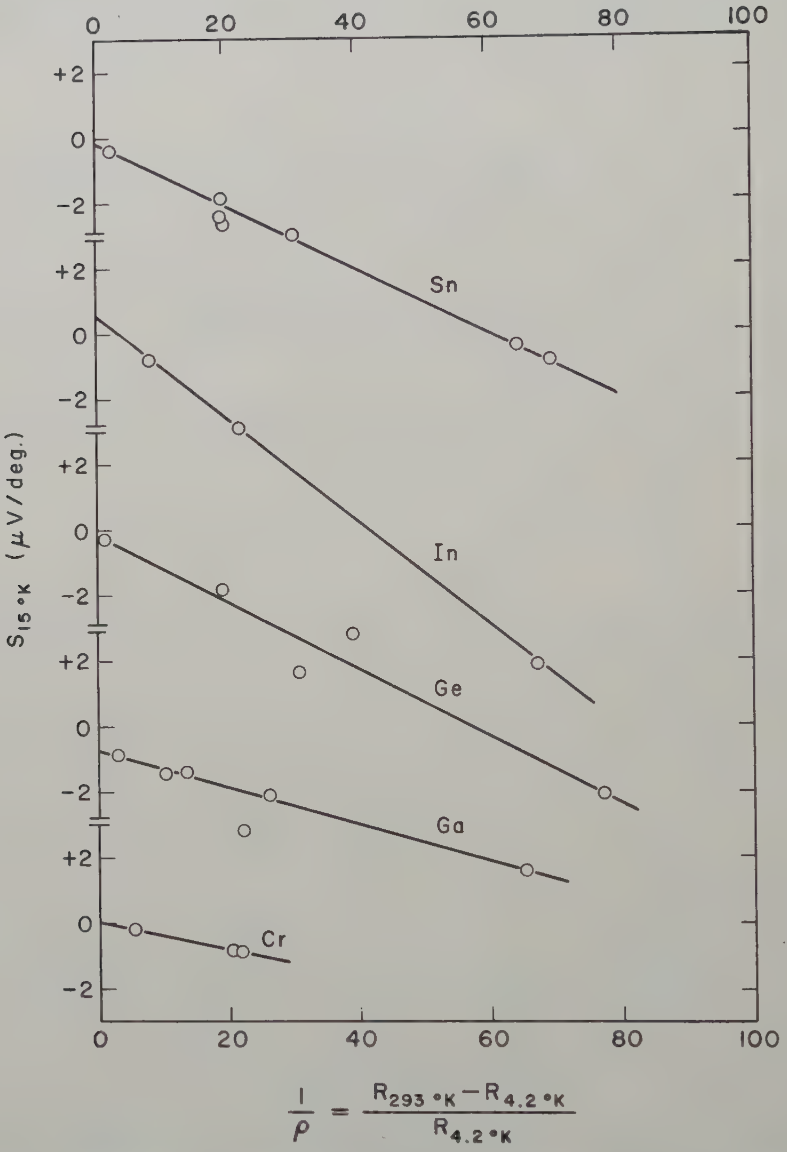

Variation of $S_{15^\circ\mathrm{K}}$ with inverse residual resistance ratio for dilute alloys of Cr in A.S. & R. Cu and Sn, In, Ge and Ga in Cu 1 (containing oxygen). The data for the latter four alloy series correspond to the region B C in fig. 10 (Appendix II); they were obtained by a less accurate experimental technique than that used for the Cu–Cr, Cu–Ni and Cu–Fe alloys which might give rise to errors corresponding to displacing the lines upwards or downwards by $\pm 0{\cdot}5\,\mu$v/deg. The same remarks hold for the data on alloys with the solutes Ag, Au and Si (not shown in figs. 4 and 5), all of which yield characteristic values of close to zero at 15°K.

small traces of iron and we shall now give a more quantitative discussion of the temperature dependence of S in the neighbourhood of the anomaly. Applying eqn. (1) to the case of impurity and thermal scattering, we have:

$$S=\frac{W_{\text{imp}}}{W_{\text{imp}}+W_{\text{th}}}S_{\text{imp(Fe)}}+\frac{W_{\text{th}}}{W_{\text{imp}}+W_{\text{th}}}S_{\text{th}}. \quad . \quad . \quad . \quad (3)$$

Since the characteristic value of S for iron in copper of $-16{\cdot}2\,\mu$v/deg. at 15°K lies close to the curve for the 0·054% Fe alloy in fig. 1, we shall take the curve for this particular alloy to approximate to the true curve of $S_{\text{imp(Fe)}}$, when all other scattering mechanisms are dominated by the scattering from iron. This curve 'saturates' at a value of about $-16\,\mu$v/deg., at least up to the limit of the impurity scattering region which occurs at about 100°K for this iron concentration (cf. fig. 2 of Borelius *et al.* (1932)). For the purely thermal scattering component we shall take $S_{\text{th}}=+5{\cdot}4\times10^{-3}T\,\mu$v/deg. from the Thomson heat measurements of Nyström (1947) above 350°K, where impurity scattering is negligible and phonon-drag effects are assumed to be small (§ 4.2)†. The temperature dependence of the thermal resistivity components W_{imp} and W_{th} for a copper sample of similar purity to ours has been given recently by Powell *et al.* (1959) (see table) and the resulting S–T variation calculated from eqn. (3) is shown as the curve A in fig. 1.

It is pleasing that this simple analysis accounts not only for the shape of the observed curves but also for the temperature at which the anomaly occurs. The discrepancy in the actual size of the anomaly can be attributed to the effect of scattering by all the remaining traces of chemical and physical impurities present in the copper, e.g. Ag, Au, Cr, ..., etc., which alone give very small values of S and yet give rise to approximately half of the impurity scattering in the thermal resistivity. In fact the curves for Cu 4, Cu 5 and Cu 6 can be well accounted for by supposing 50% of W_{imp} to be due to iron and the remaining 50% to be due to other impurities with small (effectively zero) S_{imp} (fig. 1, curve B). Likewise the fact that S for cold-worked copper is *positive* relative to annealed copper in this temperature region (cf. Pearson 1960, van Oijen 1957) is merely a reflection of the fact that the *relative* amount of scattering due to iron is reduced by the introduction of defects. Figure 3 also shows a considerable reduction of the anomaly when material of samples Cu 3 to Cu 6 is alloyed with 0·01% Sn, this being sufficient to 'swamp' most of the effect of the iron present ($\sim$0·0001%).

We have already pointed out that, with the notable exception of iron, all of the solutes in copper studied so far have *low* characteristic thermoelectric powers ranging between +1 and $-1\,\mu$v/deg. at 15°K. This at first sight does not seem to be in keeping with the fact that sizeable anomalies of as much as $-10\,\mu$v/deg. can be 'produced' when copper is alloyed with *some of these very elements* (MacDonald and Pearson 1955 a, b). The copper used for these experiments was the same as that of our sample Cu 1, viz. *containing oxygen*, and we now propose that these results arise from some metallurgical phenomenon whereby the particular solutes concerned separate the iron (~0·002%) from its oxide and that it is the iron which is primarily responsible for the anomalies. For example, tin is typical of such solutes and the dependence of the size of the anomaly on tin concentration is shown in fig. 6 (curve A). At tin concentrations above about 0·005 at. % all the iron has been brought into solid solution and the addition of further tin as solute merely cuts down the relative importance of the anomalous scattering by iron; this is the sole effect of the tin in alloys which have been prepared under *reducing* conditions (curve B). A further discussion of the Cu–Sn alloys is given in Appendix II.

---

† S varies linearly with T above 350°K in accordance with eqn. (4) to within the accuracy of Nystrom's Thomson heat results and of the absolute value of S at 350°K (fig. 3).

Fig. 6

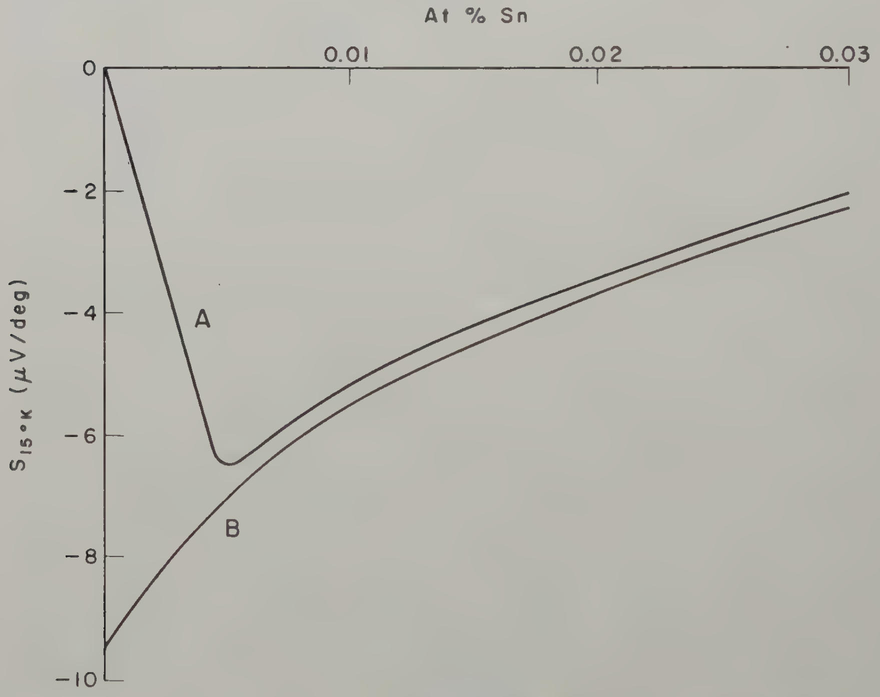

Dependence of size of the low-temperature anomaly on tin concentration in dilute alloys prepared from the oxygen-containing Cu 1 (curve A) and from the same copper, but under reducing conditions (curve B). (MacDonald and Pearson 1955a; somewhat schematic).

Similar conclusions about iron being the 'prime mover' in the dilute alloys studied by MacDonald and Pearson (1955 a, b) are arrived at from considerations of the resistance minimum which is closely related to the thermoelectric power anomaly. While the size of the thermoelectric power anomaly depends on the relative concentration of iron, the absolute size of the associated resistance minimum depends on the *total* amount of iron present (Pearson 1955). Thus we see from fig. 7 that the size of the resistance minimum in the Cu–Sn alloys remains constant once sufficient tin has been added to the oxygen-containing copper to bring all the iron into solid solution. Moreover, the size of the minimum obtained by reducing the initial copper is the same as the saturation value for the unreduced Cu–Sn alloys, this point lying on the straight line obtained by subsequently alloying with iron. The picture outlined so far is quite consistent with all the experimental data for various solutes in copper, but offers no explanation of the result of Pearson *et al.* (1959) that a resistance minimum can be created in oxygen-free Cu–Sn single crystals prepared from A. S. and R. copper simply by rendering them polycrystalline and annealing; the fact that the residual resistivity did not increase in this process would suggest that the specimens were not significantly contaminated by extraneous impurities†. In the present work we have found no significant evidence

Fig. 7

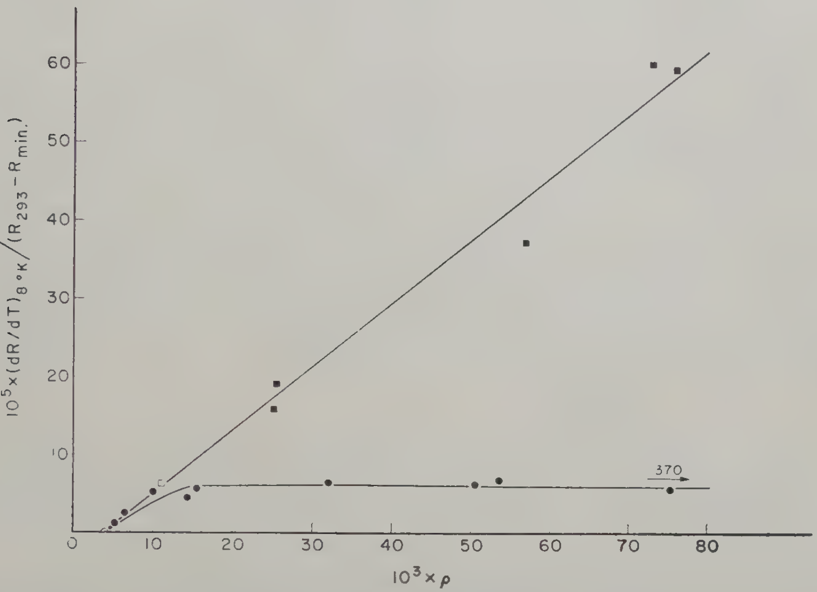

Dependence of absolute size of resistance minimum (gauged by $(dR/dT)_{8^\circ K}/(R_{293}-R_{\rm min}))$ on residual resistance ratio in dilute alloys prepared from the oxygen-containing Cu 1. ○, Cu 1; ●, Cu 1 + Sn; □, Cu 1 (reduced); ■, Cu 1 + Fe (reduced) (Pearson 1955). If instead we plot the size of the minimum, *relative* to the resistivity ρ at the minimum, against ρ, we obtain a cusp-shaped curve similar to curve A in fig. 6.

---

† Mr. E. Wallingford (private communication) has shown that no resistance minimum results if the oxygen-free A.S. and R. copper (with low iron content; see table) is alloyed with tin.

of a resistance minimum in our 'pure' copper samples, in spite of many having large thermoelectric power anomalies. This is, of course, to be expected in view of the minute quantities of iron concerned ($\sim 0{\cdot}0001\%$), the size of the minimum depending not on the relative but on the total iron concentration.

While we have so far been able to coordinate a variety of experimental facts relating to the low-temperature thermoelectric power anomalies and the resistance minima in 'pure' copper and in dilute copper alloys, we are still unable to account satisfactorily for the temperature dependence of the anomalous characteristic thermoelectric power of iron in copper (fig. 1). Let us emphasize that the 'flattening-off' of the curve at about $-16\,\mu$v/deg. is *not* due to scattering of electrons by thermal vibrations. Presumably we are concerned here with some highly energy-dependent inelastic scattering of the electrons by magnetic iron impurity ions (cf. Schmitt 1956; see also Korringa and Gerritsen 1953). Unfortunately, the recent theoretical work by Brailsford and Overhauser (1959) does not seem to be directly applicable to our case as far as calculating the thermoelectric power is concerned. These authors predict a quadratic dependence of the size of the resistance minimum on solute concentration whereas the size of the minimum in dilute Cu–Fe alloys is found to increase *linearly* with concentration (fig. 7; Pearson 1955).

4.2. *The Results at High Temperatures and Evidence for Phonon-drag*

According to the conventional theory (cf. Mott and Jones 1936, Wilson 1953) the diffusion thermoelectric power is given by the expression:

$$S=\frac{\pi^2k^2T}{3e}\left(\frac{\partial\log\sigma(E)}{\partial E}\right)_\zeta=\frac{\pi^2k^2T}{3e\zeta}\left(\frac{\partial\log\sigma(E)}{\partial\log E}\right)_\zeta, \quad . \quad . \quad . \quad (4)$$

where the derivative of the conductivity $\sigma(E)$ is taken at the Fermi level ζ and e is the electronic charge in magnitude and sign. Thus from the fact that S is positive at high temperatures (fig. 3) we infer that $(\partial\sigma(E)/\partial E)_\zeta$ is negative, of opposite sign to that predicted for free electrons (Wilson 1953). We believe that this sign reversal must in some way be connected with the fact that the Fermi surface in copper is distorted to the extent of contacting the Brillouin-zone boundary (Pippard 1957, Shoenberg 1960); S is also positive for both silver and gold, whose Fermi surfaces are now known to contact the zone faces (Shoenberg 1960). It might be worth noting that the high-temperature thermoelectric power in copper calculated from eqn. (4) for thermal scattering of free electrons, viz. $S=-8{\cdot}7\times10^{-3}\,T$ μv/deg. (taking $\zeta=7{\cdot}0$ ev and $(\partial\log\sigma/\partial\log E)_\zeta=2{\cdot}5$ (Jones (1956); Wilson (1953) gives $(\partial\log\sigma/\partial\log E)\zeta=3$)) is quite close to the observed result of $S\doteqdot+5{\cdot}4\times10^{-3}T$ μv/deg. (fig. 3), apart from the change in sign.

It will be seen from fig. 3 that the experimental results around 70°K lie considerably above the dashed curve B, which was calculated from eqn. (3) on the assumptions that 50% of the low-temperature impurity scattering was due to iron and that $S = +5{\cdot}4 \times 10^{-3} T$ μv/deg. at high temperatures. We interpret this difference as arising from a net positive Umklapp-type phonon-drag component in S. The detailed theory of phonon-drag in even the monovalent metals is complicated (Ziman 1959, Bailyn 1960), the resulting thermoelectric power depending on the relative frequencies of normal (N) and Umklapp (U) scattering processes (fig. 8), so that in what follows we shall make only a rough comparison of the phonon-drag contribution S_g with simple theory.

Fig. 8

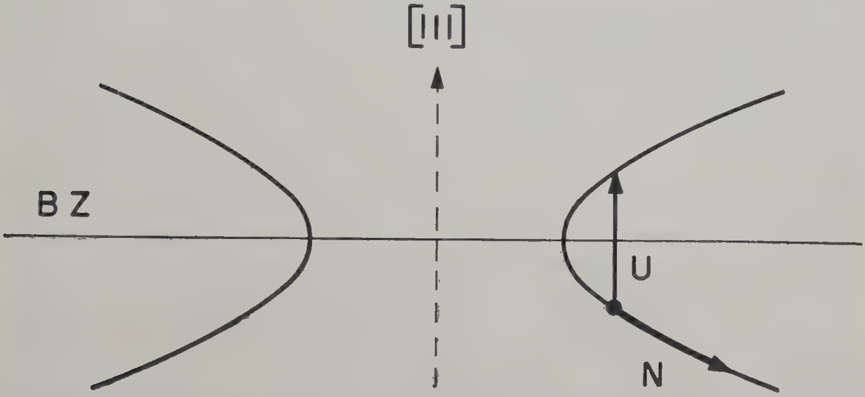

Illustrating scattering by N- and U-processes near the contact of the Fermi surface with the Brillouin zone.

A convenient expression for the phonon-drag thermoelectric power at temperatures low enough for the phonons to be scattered by electrons only, and assuming only N-scattering processes, was given by MacDonald (1954) and later in more exact form by Hanna and Sondheimer (1957) and is:

$$S_g = \frac{1}{3} \frac{1}{Ne} C_g, \quad \quad (5)$$

where C_g is the lattice specific heat and N is the number of electrons per unit volume. This gives for copper:

$$S_g = -1{\cdot}65 \times 10^{-4} T^3 \,\mu\text{v/deg.}, \quad \quad (6)$$

assuming one electron per atom and $\theta_D = 344$°K (cf. Corak *et al.* 1955). Now if the Fermi surface in copper were singly connected, the positive low-temperature contribution to S_g from U-processes would depend in an approximately exponential manner on T; since, however, the Fermi surface contacts the Brillouin zone, and so runs smoothly from one cell of the reciprocal lattice into the next, we might expect the contributions from both N- and U-processes (fig. 8) to vary more or less as T^3. Then by roughly fitting the difference between the observed curve for Cu 6 and curve B (fig. 3) to a T^3 law below the maximum we find:

$$S_{g(\mathrm{obs})} \doteqdot +1{\cdot}2 \times 10^{-5} T^3 \, \mu\mathrm{v/deg}. \quad . \quad . \quad . \quad . \quad . \qquad (7)$$

This is less than 10% of the magnitude given in eqn. (6) for N-processes alone, so that we conclude that the contributions to S_g from U-processes and N-processes very nearly cancel and that we have a small excess of the U-contribution. Although strictly it appears that Ziman's (1959) calculation is not applicable to the case where the Fermi surface touches the Brillouin zone, the observed maximum is, broadly speaking, in keeping with his general prediction of a U-type maximum in S_g at $T \sim \theta_D/10$ for monovalent metals with a distorted but singly-connected Fermi surface. At the lowest temperatures, however (i.e. where only phonons of low wave-number are excited) we would expect ultimately from fig. 8 the contribution from N-processes to be the larger, and it is suggested that this may be the reason why the results from our purest sample apparently become negative at about 13°K (fig. 2 (*b*)); any such trend in the A.S. and R. samples would be masked by the large anomaly.

At temperatures above the peak at 70°K, the phonon-drag term should fall off as T^{-1} on account of phonon–phonon scattering (Hanna and Sondheimer 1957), but it is difficult to verify this precisely since this obviously depends on the exact choice of our curve B at the higher temperatures. The reduction in the phonon-drag term due to phonon–impurity scattering is illustrated by the curve for the Cu + 0·01% Sn sample (fig. 3), and Pearson (1960) has discussed the reduction due to scattering of phonons by lattice defects.

Notes added in proof:

(i) Blatt and Kropschot (1960) have recently discussed the reduction in the phonon-drag 'hump' when copper is alloyed with various solutes.

(ii) The simple derivation of Kohler's formula (Appendix I) has also been pointed out by de Vroomen (1959) and de Vroomen *et al.* (1960); Kohler's formula has also been derived, but in a more complicated way, by van Oijen (1957).

(iii) de Vroomen (1959) has independently suggested that the thermoelectric power anomalies and the resistance minima in various dilute alloys may be due to transition metal impurities.

(iv) The high-temperature part of curve B (fig. 3) has been inadvertently drawn with slope $6{\cdot}0 \times 10^{-3}\,\mu\mathrm{v/deg}^2$ rather than $5{\cdot}4 \times 10^{-3}\,\mu\mathrm{v/deg}^2$; this is of no real consequence as far as the anomaly is concerned.

Acknowledgments

We are indebted to Professor A. F. Kip and Dr. D. Langenberg for kindly giving us the sample of natural copper, to Dr. J. Babiskin for kindly giving us a batch of very pure A.S. and R. copper, and to Dr. J. S. Dugdale for helpful discussions. We are also grateful to Mr. D. J. Huntley for carrying out some of the measurements, to Mr. J. W. Fisher for preparation of most of the specimens, and to Miss J. Spong for her help with the calculations.

APPENDIX I

Consider two conductors placed in series with one another as in fig. 9 (*a*) and having absolute thermoelectric powers S_1, S_2 and thermal resistances W_1, W_2, respectively. If then a (small) temperature difference, ΔT, be applied across the system as shown, this temperature difference will be divided in proportion to the thermal resistances W_1, W_2. Consequently,

Fig. 9

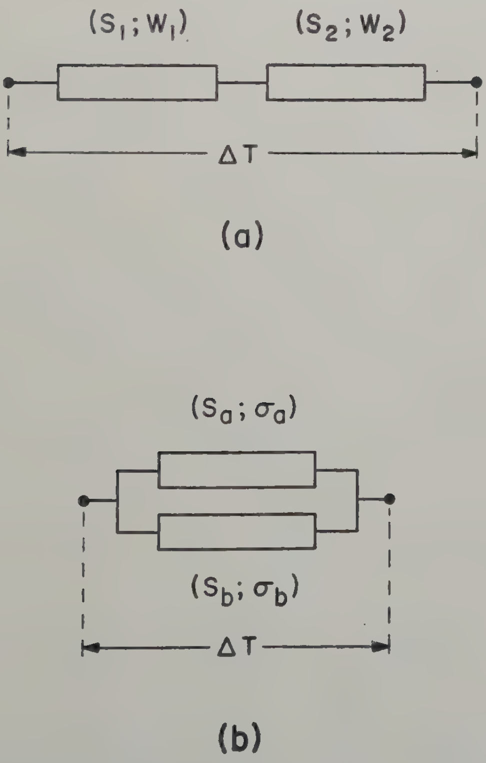

Illustrating the series and parallel circuit theorems.

a net open circuit potential difference, ΔV, will be generated across the series combination given by

$$\Delta V = S_1 \frac{W_1}{W_1+W_2} \Delta T + S_2 \frac{W_2}{W_1+W_2} \Delta T, \qquad (8)$$

i.e. the absolute thermoelectric power of the conductors in series is given by

$$S = \frac{W_1 S_1}{W_1+W_2} + \frac{W_2 S_2}{W_1+W_2} \qquad (9a)$$

or more generally

$$S = \sum_i W_i S_i \Big/ \sum_i W_i. \qquad (9b)$$

We now suggest that this result may be applied directly to a *single* conductor with various scattering mechanisms under the following conditions:

(i) We assume that the electrical conduction in the conductor may be treated in terms of a *single* homogeneous group of charge carriers (let us say electrons). We believe that this implies in particular that matrix elements for electron scattering should *not* depend explicitly on the electron wave vector, $\mathbf{k}$.

(ii) The electron scattering mechanisms are to be assumed as being entirely independent of one another, and such that any particular scattering mechanism (say the ith), if operating entirely alone, would give rise to a characteristic thermoelectric power, $S_i(T)$, at the temperature T appropriate to the conductor and a thermal resistivity due to electron scattering, $W_i(T)$. Effectively, what we assume is that each and every electron 'collision', whatever its cause, may be considered as independent of preceding or succeeding 'collisions'.

(iii) Where we are concerned with a variation in the intensity of any electron scattering mechanism (e.g. owing to variation in concentration of a solute or in the intensity of thermal scattering) we assume that the essential characteristics of the conduction electrons remain unchanged. Effectively this means that the electron density of states function is assumed to be unaffected.

(iv) The transport of *heat* (i.e. thermal conduction) in the conductor is supposed to be determined entirely (i.e. in practice dominantly so) by the conduction electrons.

It would appear that these restrictions are effectively those which are involved when Kohler's theorem is derived from a specific analysis of electron transport, although perhaps slightly less restrictive in some aspects. In particular, it would appear that these conditions usually restrict one to applying eqn. ($9a$, b) usefully to the analysis of diffusion thermoelectric power (but see immediately below).

Recently the problem of calculating thermoelectric power *due to phonon-drag* has been in prominence. A matter of some interest has been the relative contributions from 'normal' electron–phonon process and from the Umklapp processes in a conductor otherwise free from electron scattering mechanisms. It is improbable that eqn. (9 *a*, *b*) can be applied *strictly* to this situation because the electron–phonon scattering matrix elements, particularly for Umklapp processes, will presumably depend quite significantly on the electron wave vector, **k**. However, at least as a useful approximation, it appears that one might write for the thermoelectric power, S_g, due to phonon-drag:

$$S_g(T)=\frac{S_{gN}(T)W_N(T)}{W_N(T)+W_U(T)}+\frac{S_{gU}(T)W_U(T)}{W_N(T)+W_U(T)}.$$

This may be compared with the expression put forward by Ziman (1959) and Bailyn (1960).

One is tempted to try and generalize eqn. (9 *a*, *b*) if lattice thermal conduction is no longer negligible in comparison with electronic thermal conduction. We suggest that if this is the case, an approximate extension of eqn. (9 *a*, *b*) might run as follows: in eqn. (8) S_1 and S_2 remain as before, but W_1 and W_2 would be replaced by $W_1{}^*$ and $W_2{}^*$, where

$$W_1{}^*=(K_1+(1+\alpha)K_g)^{-1}; \quad W_2{}^*=(K_2+(1+\alpha^{-1})K_g)^{-1}$$

and

$$K_1=W_1{}^{-1}, \quad K_2=W_2{}^{-1}.$$

K_g is the lattice thermal conductivity, and $\alpha=N_2/N_1$, where N_1 and N_2 are the numbers of electron scattering centres corresponding to the electronic thermal resistivities W_1 and W_2 respectively. Thus if w_1 and w_2 are the apparent electron scattering cross-sections for thermal resistance corresponding to these two mechanisms, then $\alpha=W_2w_1/W_1w_2$.

This modified form of eqn. (8) means that S would no longer vary exactly as predicted in the text (p. 772) when two impurities are present at low temperatures; we should now look for deviations due to this cause from the expected linear dependence of S with $1/\rho$.

Although we make no use in this paper of a two-band model of a conductor it seems appropriate to point out here that an expression for the thermoelectric power in a two-band conductor may be derived in a rather similar manner. If we consider two conductors (*a*) and (*b*) in parallel (see fig. 9 *b*) having absolute thermoelectric powers, S_a and S_b, and electric conductances, σ_a and σ_b, then it is easy to show that the absolute thermoelectric power, S, of the System is given by

$$S=\frac{\sigma_a S_a}{\sigma_a+\sigma_b}+\frac{\sigma_b S_b}{\sigma_a+\sigma_b}; \quad . \quad . \quad . \quad . \quad . \quad . \quad . \quad (10\,a)$$

or if a number of conductors are in parallel:

$$S=\sum_j \sigma_j S_j/\sum_j \sigma_j. \quad . \quad . \quad . \quad . \quad . \quad . \quad . \quad . \quad (10\,b)$$

This result may then be applied quite generally to the case of a single conductor which has two independent groups of charge carriers, *a* and *b*, with conductivities σ_a and σ_b respectively, and such that each group *if acting alone* would contribute a thermoelectric power S_a and S_b respectively. As long as the condition of independent conduction by the two groups of carriers is strictly maintained, the result of eqn. (10 *a*, *b*) should be quite general and independent of any specific mechanism of thermoelectric power production. Equation (10 *a*) has been derived previously by various authors (Sondheimer 1948, Chambers 1952†, Wilson 1953) with varying degrees of generality.

Finally let us point out that the expression given by Mott and Jones (1936) for the diffusion component of thermoelectricity will also yield corresponding expressions within the range of its validity. Mott and Jones give:

$$S = \frac{\pi^2 k^2 T}{3e}\left(\frac{d \log \sigma(E)}{dE}\right)_{E=\zeta} \quad . \quad . \quad . \quad . \quad . \quad . \quad (11\,a)$$

for the absolute thermoelectric power, which may also be written

$$S = -\frac{\pi^2 k^2 T}{3e}\left(\frac{d \log \rho(E)}{dE}\right)_{E=\zeta} . \quad . \quad . \quad . \quad . \quad . \quad . \quad (11\,b)$$

Equation (11 *a*) was derived from a Boltzmann equation analysis, the solution of which depended on the assumption of a relaxation time, and, as mentioned above, is applicable only to the diffusion component of thermoelectricity. Mott and Jones themselves say: "It is valid both for pure metals and for alloys at temperatures above the characteristic temperature θ, and at lower temperatures provided the 'Restwiderstand' ["residual resistance"] is large compared with the resistance due to the thermal motion of atoms. It is not, however, valid for *pure* metals if $T < \theta$." If eqn. (11 *a*) is now applied to a metal or other conductor, in which we assume that there are two independent bands of carriers, then we may write as before (cf. eqn. (10 *a*)):

$$S = \frac{\sigma_a S_a}{\sigma_a + \sigma_b} + \frac{\sigma_b S_b}{\sigma_a + \sigma_b} . \quad . \quad . \quad . \quad . \quad . \quad . \quad . \quad (12)$$

If, instead, we start from eqn. (11 *b*) and regard the conductor as made up of a single band of carriers which encounter two separate scattering mechanisms (both of which must satisfy the requirements of the original formula) and if we write the electrical resistivities corresponding to each of these mechanisms as ρ_1 and ρ_2, and the corresponding absolute thermoelectric powers that would be observed if either were acting independently alone as S_1 and S_2 respectively, then we may write:

$$S = \frac{\rho_1 S_1}{\rho_1 + \rho_2} + \frac{\rho_2 S_2}{\rho_1 + \rho_2} , \quad . \quad . \quad . \quad . \quad . \quad . \quad . \quad (13)$$

---

† Chambers' derivation appears to be based on the most general assumptions for a two-band model of a conductor and he points out that concern with a two-band model dates back as early as Riecke (1898). A similar equation to (10 *a*) was derived by Fowler (1936) for the case of a semiconductor with conductivity arising from two bands.

which is essentially the result of Nordheim and Gorter (1935). Equation (9*a*) (Kohler's formula) of course reduces to this when we can write $W=\rho/L_0T$ (where L_0 is a *constant*) and this is valid either in the residual resistance region where impurity scattering is entirely dominant, or at 'high' temperatures ($T \gtrsim \theta$) where the thermal scattering becomes essentially classical in character, which are just the regions of validity of the Mott and Jones formula.

APPENDIX II

We give here a further discussion of the effect of adding tin to our oxygen-containing copper in terms of the S *versus* $1/\rho$ plot of fig. 10. Curve A B C gives the variation of the size of the anomaly as the tin concentration is increased; the point C for $1/\rho \to 0$ then gives the characteristic value of $S_{15^\circ\mathrm{K}}$ (~ 0) for tin in copper. If, on the other hand, the alloys are prepared under reducing conditions, the addition of tin reduces the size of the anomaly which is already present in the starting material (D B C). Furthermore when iron is deliberately added to the reduced copper, the points lie on the continuation of the line A D (giving the characteristic value of $S_{15^\circ\mathrm{K}}$ for iron in copper at E), which is consistent with the hypothesis that hydrogen-reduction brings the iron in the initial oxygen-containing copper into solid solution. Since iron is the only impurity in the copper with a greater negative characteristic thermoelectric power than $-1\,\mu$v/deg. at 15°K, it is proposed that the tin does not in itself 'produce' the anomaly in the oxygen-containing copper A, but that it brings the iron into solid solution until the point B is reached where the amount of iron in solid solution is constant (corresponding to D). Thereafter (B C) the addition of more tin reduces the relative amount of anomalous scattering by iron so that the

Fig. 10

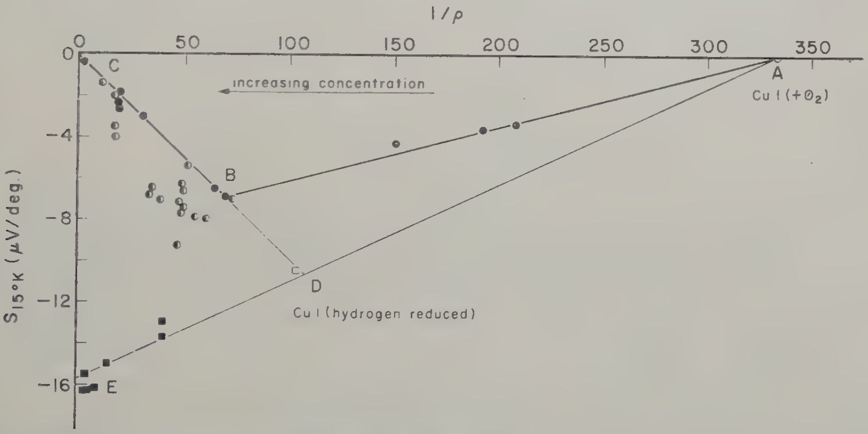

Variation of $S_{15^\circ\mathrm{K}}$ with inverse residual resistance ratio for dilute alloys prepared from the oxygen-containing Cu 1. ○, Cu 1; ●, Cu 1+Sn; □, Cu 1 (reduced); ■, Cu 1+Fe (reduced); ◐, Cu 1+Sn (reduced).

size of the anomaly decreases; likewise it is the reduction by the tin of the effectiveness of the iron scattering which results in the oxygen-containing alloys following the path A B C rather than A D C. It is interesting to note that many of the points for the *reduced* tin alloys lie *below* the line D B C, which suggests that alloying with an excess of tin is not alone sufficient to bring *all* the iron into solid solution.

REFERENCES

BAILYN, M., 1960, *Phil. Mag.* (in the press).

BLATT, F. J., and KROPSCHOT, R. H., 1960, *Phys. Rev.*, **118,** 480.

BORELIUS, G., KEESOM, W. H., JOHANNSON, C. H., and LINDE, J. O., 1930, *Proc. Acad. Sci. Amst.*, **33,** 17 (Leid. Comm. 206a); 1932, *Ibid.*, **35,** 25 (Leid. Comm. 217e).

BRAILSFORD, A. D., and OVERHAUSER, A. W., 1959, *Phys. Rev. Letter*, **6,** 331.

CHAMBERS, R. G., 1952, *Proc. phys. Soc.* A, **65,** 903.

CHRISTIAN, J. W., JAN, J.-P., PEARSON, W. B., and TEMPLETON, I. M., 1958, *Proc. roy. Soc.* A, **245,** 213.

CORAK, W. S., GARFUNKEL, M. P., SATTERTHWAITE, C. B., and WEXLER, A., 1955, *Phys. Rev.*, **98,** 1699.

DE VROOMEN, A. R., 1959, *Thesis*, University of Leiden.

DE VROOMEN, A. R., VAN BAARLE, C., and CUELENAERE, A. J., 1960, *Physica*, **26,** 19.

FOWLER, 1936, *Statistical Mechanics* (Cambridge: University Press).

HANNA, I. I., and SONDHEIMER, E. H., 1957, *Proc. roy. Soc.* A, **239,** 247.

JONES, H., 1956, *Handbuch der Pyhsik* (ed. S. Flügge), **19,** 227.

KOHLER, M., 1949, *Z. Phys.*, **126,** 481.

KORRINGA, J., and GERRITESN, A. N., 1953, *Physica*, **19,** 457.

KROPSCHOT, R. H., and BLATT, F. T., 1959, *Phys. Rev.*, **116,** 617.

MACDONALD, D. K. C., 1947, *J. sci. Instrum.*, **24,** 232; 1954, *Physica* **20,** 996.

MACDONALD, D. K. C., and PEARSON, W. B., 1953, *Proc. roy. Soc.* A, **219,** 373; 1955 a, *Acta Met.*, **3,** 392; 1955 b, *Ibid.*, **3,** 403.

MACDONALD, D. K. C., PEARSON, W. B., and TEMPLETON, I. M., 1960, *Proc. roy. Soc.* (in the press).

MOTT, N. F., and JONES, H., 1936, *Theory of Metals and Alloys* (Oxford: Clarendon Press).

NORDHEIM, L., and GORTER, C. J., 1935, *Physica*, **2,** 383.

NYSTRÖM, J., 1947, *Ark. Mat. Astr. Fys.* A, **34,** No. 27.

PEARSON, W. B., 1955, *Phil. Mag.*, **46,** 911; 1960, *Phys. Rev.* (in the press).

PEARSON, W. B., RIMEK, D. M., and TEMPLETON, I. M., 1959, *Phil. Mag.*, **4,** 612.

PIPPARD, A. B., 1957, *Phil. Trans.* A, **250,** 325.

POWELL, R. L., RODER, H. M., and HALL, W. J., 1959, *Phys. Rev.*, **115,** 314.

RIECKE, E., 1898, *Wied. Ann.*, **66,** 545, 1199.

SHOENBERG, D., 1960, *Phil. Mag.*, **5,** 105.

SONDHEIMER, E. H., 1948, *Proc. roy. Soc.* A, **193,** 484.

SCHMITT, R. W., 1956, *Phys. Rev.*, **103,** 83.

VAN OIJEN, D. J., 1957, *Thesis*, University of Delft.

WILSON, A. H., 1953, *The Theory of Metals* (Cambridge: University Press).

ZIMAN, J. M., 1959, *Phil. Mag.*, **4,** 371.

Observations of the Decomposition of Crystals of Lead Iodide in the Electron Microscope†

By A. J. Forty
H. H. Wills Physics Laboratory, University of Bristol

[Received January 24, 1960]

Abstract

Thin crystals of lead iodide grown from solution have been examined in transmission in the electron microscope. The crystals are sufficiently stable in the electron beam to allow dislocations to be observed, but it is found that after prolonged periods of observation at high beam intensities decomposition commences, and proceeds through a number of stages to completion. The initial and intermediate stages are accompanied by the climb of pre-existing dislocations, the formation of new dislocations and the creation of other features which might be interpreted as cavities in the crystal. These can be understood to some extent as a result of the formation of vacancies in the crystal under irradiation with the electron beam. In the final stage the crystals appear to decompose completely leaving an aggregate of dense crystallites which are probably metallic lead. This is presumably accompanied by the release of iodine gas. The mechanism for this final stage of decomposition is not yet understood.

§ 1. Introduction

The application of transmission electron microscopy to the study of thin crystalline films during the past few years has led to a remarkable advance in our knowledge of the formation and behaviour of dislocations and other imperfections in crystals. The observations have, however, been made almost entirely on metal crystals. This is not altogether surprising since dislocation theory finds its most direct application in attempts to explain the mechanical behaviour of metals. Moreover, metal films are relatively stable in the beam of the electron microscope whereas other inorganic crystals, such as sodium chloride, for example, are known to decompose very rapidly, presumably because of their low thermal and electrical conductivities. Recent attempts to correlate the step structure on growth surfaces of crystals with internal imperfections by direct observation have, however, indicated that there are some inorganic crystals, notably lead iodide and cadmium iodide, which are moderately stable in the electron beam for periods sufficient to allow observations on dislocations to be made, and that these can provide a useful contribution to this field of study.

The correlation expected from this study has not been found, but, as will become evident later, this is not altogether surprising since the interaction of the electron beam with the thin crystals used here leads to a slow but controllable decomposition of the crystals in such a manner as to modify existing dislocations and generate new ones. The observations which have been made on this process of decomposition are thought to be sufficiently interesting to be reported in this paper.

---

† Communicated by the Author.

It is impossible at this stage to determine whether the decomposition is induced directly by irradiation of the crystals in the electron beam or whether it occurs indirectly as a result of the heating of the crystals. In either case it can be considered to some extent to represent a form of radiation damage, and, moreover, a form of damage which can be observed directly in progress. It is not impossible that similar effects might be found in metal crystals but to a greatly lesser degree so that these have hitherto escaped observations.

§ 2. EXPERIMENTAL

The observations to be described have all been made on crystals of lead iodide. Cadmium iodide and other members of this family of compounds show similar effects and have also been examined in some detail. These will not be discussed here.

Large plate-like crystals of lead iodide can be grown from a solution in alcohol by saturating the solution at about 100°C in a water bath and allowing this to cool slowly to room temperature. The crystals can then be transferred to an electron microscope specimen grid by depositing a drop of the stirred solution and allowing it to evaporate, leaving several large crystals resting across the bars of the grid. An alternative but less reliable method is to place the grid in a drop of the solution between a glass slide and a cover slip, heat gently to about 100°C and then allow to cool to room temperature. In this way a few crystals grow in contact with the grid which can then be dried by extracting the excess solution with a filter paper.

The crystals have a marked platelet habit and lie flat on the specimen grid without a supporting film. Prepared in this way, a good many of them are sufficiently thin for direct transmission microscopy. It is thus possible to examine as-grown crystals without further preparation.

The crystals have been examined in a Philips 100 kv electron microscope. This allows direct transmission microscopy with facilities for tilting the specimen through large angles and for deflecting the beam through small angles. Moreover, facilities for electron diffraction are available so that crystallographic orientations and some contrast effects in the microscope image can be fairly readily determined as the observations are made.

§ 3. THE CRYSTAL STRUCTURE OF LEAD IODIDE

In the following sections reference to directions and other special features of the lead iodide structure will frequently be made. These are summarized in fig. 1† which shows one unit of the structure. It will be seen that this consists of a sandwich of a hexagonal array of lead ions between two close-packed layers of iodine ions. The crystal is built of a stack of such sandwiches so that a layer sequence in the familiar a, b, c notation can be described as

---

† Figures 2–15 are shown as plates.

$$(a\gamma b)\,(a\gamma b)\,(a\gamma b)\ldots$$

where Roman letters represent iodine ions and Greek letters represent lead ions. In view of the relative sizes of the lead and iodine ions it is possible to regard this structure simply as a hexagonal close-packing of iodine ions with interstitial lead ions placed in the octahedral holes between alternate pairs of layers. The basal plane defined by the direct contact of two iodine layers without interstitial lead provides a cleavage plane and a plane of easy glide.

Fig. 1

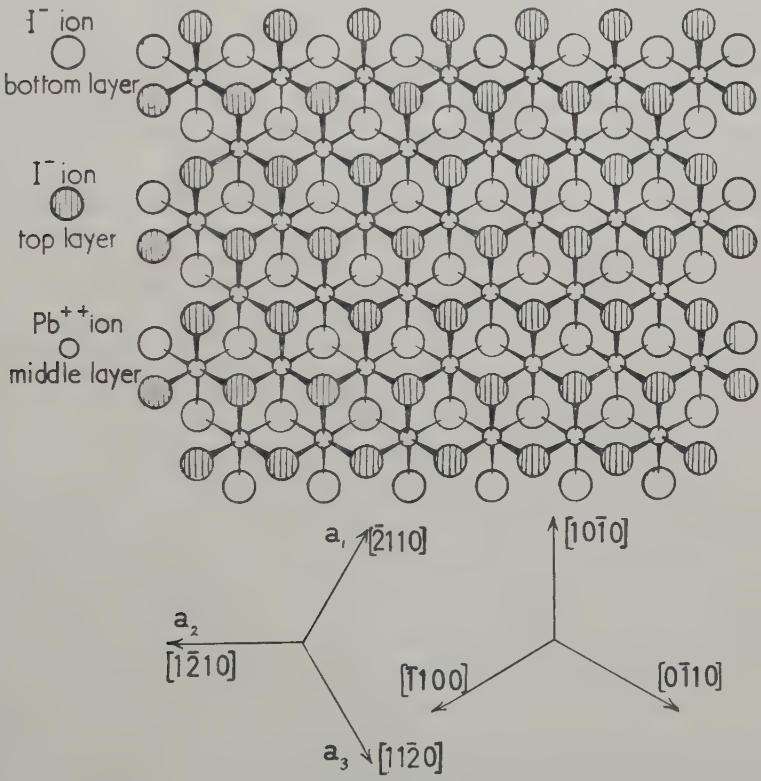

A single sandwich of lead iodide. Note the strong ionic bonding within the sandwich.

§ 4. Observations

Dislocations can be seen in the crystals as soon as observation commences. These are generally individual lines or wide-meshed networks of dislocations lying in the plane of the platelet. This is the basal plane (0001) and is the plane in which glide or other deformation is likely to occur most readily. It is also the plane on which the steady thickening of the platelet has taken place (Forty 1952) during growth. It is therefore possible that these pre-existing dislocations have been introduced during growth or by deformation through transferring the crystals from the solution to the specimen grid.

This simple pattern gradually becomes more complex during a prolonged period of observation as the crystal begins to decompose. The rate at which decomposition develops and proceeds depends on the intensity of the electron beam; that is, on the filament current, condenser current and the operating voltage applied. Most of the observations to be described have been made at 80 kv although some have been made at the full 100 kv. In the latter case decomposition is often catastrophic.

It is convenient to describe the observations separately in the early, intermediate and final stages of decomposition, although it must be emphasized that the process is one which evolves and progresses steadily, varying at each stage only in the degree of decomposition reached.

Decomposition invariably starts at the centre of the illuminated portion of the crystal, presumably where the beam is most intense. A zone of decomposed crystal eventually grows and spreads outwards over the whole platelet. Thus, after a prolonged exposure to the beam it is possible to observe at any one time the early stage of decomposition at places well removed from the centre with the intermediate and final stages nearer the centre.

§ 5. DISLOCATIONS IN THE CRYSTALS BEFORE DECOMPOSITION

The crystals are by no means perfect even before decomposition. Figure 2, for example, shows part of a thin platelet containing an extensive array of dislocations. This array appears to be lying parallel to the basal plane although, owing to the large depth of focus of the microscope, one cannot be certain that it is confined to a single plane. It will be noticed that the dislocations are crossed by a number of extinction contours so that the contrast varies from point to point in the array. This distribution of contours is typical for these crystals and indicates a marked degree of buckling. Some of the buckling is probably a natural result of growth but some must also have been introduced by mounting the crystals across the specimen grid without a supporting film.

Arrays are usually confined to a few regions of the crystal and can often be described as large families of loops of dislocation. These may have been introduced during growth or by deformation during mounting. The latter possibility is favoured since a network introduced during growth is more likely to extend throughout the crystal and would probably show crystallographic features. Moreover, the arrays are usually localized near holes and other gross imperfections in the crystal where shear stresses can be expected to be concentrated during handling. The array shown in fig. 2, for example, can be described as a fairly complex system of several independent families of loops lying in parallel basal planes which have been generated from the large hole and tear in the crystal under the high stresses imposed during mounting. Members of these families have subsequently interacted to produce the hexagonal and more complex networks. Such a possibility has been indicated by observations on a number of simple systems where this behaviour can be followed with some certainty. Figure 3 shows one of these systems consisting of at least five families of loops all originating from a single hole in the crystal. The system is in the early stage of formation but already some interaction has occurred between families B and C. The formation of these loops in the basal plane by a glide process must mean, of course, that the Burgers vectors of the dislocations also lie in this plane. This has not been confirmed by direct diffraction studies but there is some evidence for it from observations of the climb of the dislocations which indicates that the slip direction is probably the $[10\bar{1}0]$ direction.

The arrays in the freshly prepared crystals become modified after a short period of observation in a manner which suggests that dislocation climb is occurring. This is the first indication that the electron beam is damaging the crystal and forms part of what has already been described as the early stage of decomposition. The resulting pattern of dislocations is often extremely complex but there are instances where the climb of individual dislocations can be resolved. Dislocation climb is associated with the condensation of point defects, vacancies or interstitials; the examples described in the following section serve to illustrate that, since this kind of interaction is indeed occurring, point defects are being produced in the early stage of decomposition. They also illustrate a number of interesting features of the climb process.

§ 6. THE EARLY STAGES OF DECOMPOSITION

The condensation of point defects in a crystal can lead to the climb of existing dislocations or to the formation of new prismatic loops of dislocation. Both climb and loop formation have been observed in the lead iodide crystals after short periods of exposure to the electron beam. The two processes often occur in the same region of the crystal, although climb is sometimes observed in the absence of detectable loop formation. This seems to indicate that, as might be expected, the supersaturation of defects required for nucleation of isolated aggregates is larger than that required for climb.

The climb of a dislocation in the edge orientation results only in a simple translation of the line in the climb plane. The fact that such simple translations are often observed during climb with some component in the plane of observation (i.e. in the basal plane) indicates that the climb plane is not a prismatic plane of the hexagonal structure but is inclined at some intermediate angle. This feature will be discussed more fully later when it will become apparent that such a plane might well be of the type $(10\bar{1}1)$.

The climb of a dislocation in the screw orientation, or of any dislocation having a screw component, can proceed only by the line adopting a helical configuration so as to extend it in the edge orientation. Helical dislocations have been studied extensively by Amelinckx *et al.* (1957) in crystals of fluorite internally decorated with metallic silver and have also been observed with the electron microscope in thin films of aluminium–copper alloy by Thomas and Whelan (1959). In both cases the formation of helices can be associated with conditions in which a supersaturation of vacancies is known to exist. Helical dislocations are frequently observed in the lead iodide crystals after decomposition commences and figs. 4 and 5 show examples of these. That shown in the centre of fig. 4 is clearly a rounded helix of irregular radius and pitch and is very similar to those observed by Thomas and Whelan. The dislocations shown in fig. 5 and also at the bottom of fig. 4 are more typical of those generally observed. They appear to have a characteristic zig-zag configuration which might be interpreted as the projected image of a segmented helix. This can be taken to indicate that there are preferred crystallographic planes for dislocation climb in these crystals. It is interesting to notice in fig. 5 that the zig-zags appear to form parts of a single loop of dislocation terminating on a large hole. This loop is probably one formed at the hole in the crystal by deformation prior to observation and which has subsequently climbed out of the basal plane. The zig-zags follow the parts of the dislocations in the screw orientation whilst the outermost curved portion probably represents the edge component. This appears to have climbed completely out of the crystal at one end. Such a description is consistent with the suggestion that the pre-existing dislocations lie in the basal plane and have their Burgers vector in this plane and also with the idea that the climb plane is some inclined pyramidal plane.

Figure 6 shows another mechanism by which point defects can interact with dislocations. Aggregation can occur preferentially at a point in the dislocation line, leading to a bulge if the dislocation is in the edge orientation or to a single helical loop in the line if it has a screw component. Both forms occur in fig. 6 but the large loop in the vertical line is probably the most striking feature here. There appears to be one and a half turns of helical loop. Figure 6 is especially interesting since it illustrates at the same time several long segmented helices and also the appearance of a large number of small isolated loops of dislocation. The occurrence of such loops will be discussed shortly.

Figure 7 shows a more complex example of the climb of isolated segments of the original dislocation lines. In this case chains of elongated loops protrude from the connecting dislocations, as if formed by the successive nucleation of new loops in a single plane. Alternatively, the protrusions might be accounted for by the growth of a single elongated loop on an inclined plane and the subsequent displacement of parts of it by glide in the basal plane to produce the twisted appearance. The orientation of the crystal by electron diffraction shows that the elongation of the protrusions follows the three $\langle 11\bar{2}0 \rangle$ directions. Clearly these are the preferred directions for the growth of prismatic loops in lead iodide.

The occurrence of small isolated loops in the early stages of decomposition has already been pointed out in the description of fig. 6. The loops in this photograph are extremely small but nevertheless it is possible to see that the line has uniform contrast. It might be inferred from this that the loops lie in the plane of observation. There are instances, however, as in fig. 8, where loops show a variable contrast. It has been pointed out by Whelan (1959) in connection with similar observations in quenched metal films that these can be interpreted as loops inclined to the plane of observation, with the more steeply inclined parts showing poor contrast. This interpretation, together with the crystallographic orientation established from the electron diffraction pattern from this region of the crystal, indicates that the loops in fig. 8 are inclined to the basal plane about a direction close to $[11\bar{2}0]$.

§ 7. The Intermediate Stage of Decomposition

After a prolonged period of observation other features appear in the crystals close to the centre of the illuminated patch. The most striking of these is the appearance of sharply defined bright patches less than one micron in diameter which form in this region and spread outwards through the crystal. They appear gradually and in comparatively small numbers at low beam intensities but catastrophically if the intensity of illumination is increased. At the same time, the dislocation climb already described becomes more pronounced. Clearly the generation of point defects is increasing. There appears to be no definite correlation between the points at which the bright patches are formed and the occurrence of other imperfections or singularities, although the edges of the crystals are favoured to some extent. The patches usually appear where the irradiation is most intense.

At high rates of formation the patches are rounded in outline but at low rates or after reduction of the beam intensity they develop a hexagonal shape with edges following the $\langle 10\bar{1}0 \rangle$ directions in the basal plane. The latter shape is illustrated in fig. 9. The bright contrast is consistently observed under most diffracting conditions, although the degree of brightness varies considerably. Such a variation is clearly illustrated in fig. 10 where patches can be seen on and either side of a strong extinction contour. Moreover, the superposition of two patches invariably leads to enhancement of the brightness (see fig. 9 for example). These observations suggest that although some of the contrast might arise from irregular diffraction of the electron beam in the neighbourhood of the patches a large part of it can be accounted for by a diminished absorption if they represent voids or cavities in the crystal. This explanation is not entirely satisfactory, however, since such a marked degree of brightness requires that the cavities should occupy a large fraction of the thickness of the crystal and, further, some evidence will be presented shortly which shows that the bright contrast can be removed and even reversed in some circumstances by a slight tilting of the crystal, favouring an interpretation in terms of a diffraction phenomenon.

At high beam intensities the bright patches drift through the crystal at speeds of several microns per second, and the direction of movement is generally outwards from the centre of the illuminated area. Their movement is frequently checked by obstacles in the crystals, such as dislocations lying in arrays ahead of the advancing patches or shallow etch pits extending into the crystal. This, together with the observation that complex clusters can always be resolved into a number of individual patches overlying each other, suggests that the bright patches represent internal imperfections disposed at various levels through the depth of the crystal.

The movement of the patches can be controlled fairly readily by adjusting the operating conditions of the microscope correctly. This allows sequences of photographs like that shown in fig. 10 (*a*), (*b*), (*c*), (*d*) to be recorded to illustrate the movement and occasional merger of patches. This particular sequence illustrates also the very interesting observation that trails of dislocation lines are often associated with the movement of patches. The trailing dislocations are sometimes single loops but are often multiple like those in fig. 10. The outward movement of patches and the extension and interaction of the trailing dislocations results in an extensive structural breakdown of the crystals. The development of this breakdown in its early stage is illustrated by fig. 10 and, in particular, by (*d*). Figure 11 shows the completed state of deformation left after a wave of bright patches has crossed a crystal in this way. This pattern has been produced entirely by the complex interaction of loops from each patch with some simultaneous modification by dislocation climb.

§ 8. THE FINAL STAGE OF DECOMPOSITION

The formation and migration of bright patches leaves the crystal in a densely dislocated condition. At this stage, electron diffraction reveals that the structure is still essentially a single crystal. If exposure to a high intensity electron beam is continued, however, the crystal rapidly breaks down into its final decomposed state. The beginning of this final stage is illustrated by fig. 12. This shows a rapidly decomposing zone at the bottom of the photograph. A wave of bright patches is leaving this zone and some of the patches are trailing loops of dislocation. In the decomposed zone itself there remains an aggregate of dense crystallites. Some of these are roughly triangular or hexagonal in outline. This characteristic form is more clearly illustrated by fig. 13 which shows a similar area where decomposition is nearing completion. In this case the crystallites appear to be similarly oriented. It is thought that the crystallites are metallic lead and this has been partially confirmed by electron diffraction from the region shown in figure 13. The crystallites are occasionally embedded in a thin film of crystalline matrix but more frequently appear to be suspended only in the carbon film which becomes deposited on the specimen during observation. Presumably lead iodide completely decomposes in the final stage to form metallic lead and iodine gas.

§ 9. DISCUSSION

It is clear that the decomposition of the crystals, at least in the early stages and probably in all stages, is proceeding by the generation of point defects, produced either directly or indirectly by the electron beam. It is unlikely that the disordering of the structure which we observe in the initial stages is a direct result of irradiation. At most, it might be expected that the electron beam will produce ionization of thermally produced defects, leading to the formation of complexes such as F-centres or V-centres. It is more likely that the defects responsible for climb are produced indirectly due to the heating of the crystals by the high energy beam, although we cannot be certain of this until the observations are repeated under more closely defined conditions in which the temperature of the crystals is recorded and varied by external control.

According to Lidiard (1957) in a discussion of Tubandt's work (1932), lead iodide is likely to develop Shottky disorder on heating to temperatures around 200–300°C. That is, it might be expected that mobile single ion vacancies of either kind will be produced during the exposure of the crystals to an electron beam of sufficient intensity to raise the temperature to this degree. We might also expect molecular vacancies (i.e. associated groups of lead and iodine ion vacancies) to be produced. Although there is no direct evidence to support this, some indication can be obtained from the observation that lead iodide evaporates in molecular form under gentle heating (Lister and Sutton 1941). The structure of lead iodide, in which there is strong ionic bonding in the sandwiches of PbI_2 but only weak binding between them, is likely to ensure that the association of lead and iodine ion vacancies thus created is preserved to some extent.

The observations of the formation of loops and the climb of dislocations to form helices and zig-zags in the early stages of decomposition can be accounted for by suggesting that vacancies are created in the centre of the illuminated patch of crystal and that these migrate and aggregate in the outer regions. The orientations of loops and zig-zags indicate that the climb plane or plane preferred for aggregation intersects the basal plane along $\langle 11\bar{2}0 \rangle$ directions and is therefore one of the family $\{10\bar{1}n\}$. The tilting of the loops clearly indicated in some of the photographs suggests that the climb planes might well be the pyramidal planes $\{10\bar{1}1\}$. It is interesting to notice that these are single planes in the crystal structure which are followed closely by slightly corrugated surfaces having a simple molecular composition, and are therefore planes in which molecular vacancies might prefer to aggregate. It might even be considered that these are the planes in which molecular vacancies are most readily created since they provide the correct geometrical conditions by which the non-linear molecules of lead iodide may leave the structure without distortion. We may conclude that decomposition in the early stages probably proceeds with the formation of mobile molecular vacancies by the evaporation of lead iodide molecules and that these aggregate to produce the climb of existing dislocations and the creation of new loops.

It is more difficult to understand the mechanism of decomposition in the intermediate stage. The remarkable degree of brightness and sharpness in the patches produced at this stage can be accounted for in terms of absorption contrast only if they represent thick prism-shaped cavities. Such cavities might be formed by the condensation of vacancies. It is interesting to notice here that the particular orientation found for the hexagonal patches is the only one for which a corresponding hexagonal prism-shaped cavity can be created in the crystal with no net configurational charge. In other words, the cavities can be formed by the condensation of molecular vacancies or equivalent numbers of single lead and iodine ion vacancies in layers parallel to the basal plane. The cavity model is consistent with a number of the observed properties of the bright patches. For example, the marked interaction between the patches and arrays of pre-existing dislocations might be explained by the elastic interaction between cavities and dislocations. This interaction might well be repulsive for a dislocation on one side of a cavity and attractive on the other, depending on the Burgers vector of the dislocation and the nature of the walls of the cavity. In the present experiments we frequently observe instances where moving bright patches initially repel dislocations but retain them by close attraction after cutting through. Many of the observations of dislocation loops being trailed behind bright patches (fig. 10 for example) may be accounted for in this way. The structural breakdown associated with the movement of patches in the intermediate stage of decomposition might therefore arise from an extension of existing dislocations rather than the creation of new ones.

The movement of the bright patches is an ordered process, all drifting in the same direction and generally outwards from the centre of decomposition. Such a movement can be accounted for by an electrolytic process if the patches represent cavities containing some iodine gas. This might indeed be the case since the internal decomposition of lead iodide to form metallic lead and iodine gas is likely to commence at the beam intensities required to induce movement of the patches (see fig. 12, for example). The crystal, being non-uniformly charged by the electron beam, is likely to carry a radial potential gradient and this can transport ions across the cavities to deposit lead iodide on the inner surfaces and remove it from the outer surfaces. Some simple calculations of the magnitude of current required to account for the simultaneous movement of a typical system of bright patches by this process have been made, and this represents only a small fraction of the total current incident on the crystal. An electrolytic process is not therefore unreasonable. A similar argument using distillation of lead iodide down the temperature gradient over the crystal can be applied but this leads to an inward movement of cavities towards the centre of illumination. It is possible that the movement observed is due to a combination of thermal and electrolytic processes.

The cavity model, although successful in accounting for many of the observed properties of the bright patches, is not completely satisfactory. One of the difficulties encountered is illustrated by fig. 14 (*a*) and (*b*). These show the change in appearance of a field containing a number of bright patches as the electron beam is deflected through a small angle. In the initial setting the patches have the usual bright contrast whereas in the second setting the brightness of some has disappeared. At the same time a complex array of dislocation loops associated with the patches has appeared. It will be noticed also that some of the patches now appear as small isolated loops (as at A, B, C for example) inclined to the plane of observation. This kind of behaviour is further illustrated by fig. 15 (*a*), (*b*) which show a complete reversal of contrast for a number of patches following a slight deflection of the electron beam. These observations are exceptional but indicate that at least some of the appearance of the patches arises from a form of diffraction contrast. No completely satisfactory explanation of this behaviour is available.

The final stage of decomposition of lead iodide is not fully understood at present. Clearly, the process involves the formation and aggregation of metallic lead and the corresponding release of iodine gas, but it is not yet clear how this is assisted, if at all, by vacancies or other defects produced in the earlier stages. This is a feature of the observations which requires further investigation under carefully controlled thermal and electrical conditions.

Acknowledgments

The author wishes to thank Professor F. C. Frank for many useful and interesting discussions during the course of this work. He is also grateful to Miss E. Harris for her able assistance and instruction in the use of the Philips 100 kv electron microscope.

References

Amelinckx, S., Bontinck, W., Dekeyser, W., and Seitz, F., 1957, *Phil. Mag.*, **2,** 355.

Forty, A. J., 1952, *Phil. Mag.*, **43,** 72.

Lidiard, A. B., 1957, S. Flügge's *Handbuch der Physik*, Vol. 20, p. 246.

Lister, M. W., and Sutton, L. E., 1941, *Trans. Faraday Soc.*, **37,** 406.

Thomas, G., and Whelan, M. J., 1959, *Phil. Mag.*, **4,** 511.

Tubandt, C., 1932, *Handbuch der Experimentalphysik*, Vol. 12 (1), p. 383.

Whelan, M. J., 1959, *J. Inst. Met.*, **87,** 392.

Dislocations with Burgers Vectors of $a\langle 100\rangle$ in Crystals of Silver Bromide†

By J. T. Bartlett and J. W. Mitchell
H. H. Wills Physics Laboratory, University of Bristol‡

[Received March 7, 1960]

Abstract

Experimental observations of the combination, in crystals of silver bromide, of two dislocations with Burgers vectors of $\frac{1}{2}a\langle 110\rangle$ at right angles to form a single dislocation with a Burgers vector of $a\langle 100\rangle$ are described in this paper. It is believed that this is the first occasion upon which the interaction has been definitely established for dislocations on glide planes.

§ 1. Introduction

The conditions under which dislocations combine or dissociate were first discussed by Frank (1949) who pointed out that cases occurred in the cubic system in which a pair of dislocations could have the same energy as a single combined dislocation.

The object of the present paper is to describe interactions of this kind in crystals of silver bromide between two dislocations with Burgers vectors of $\frac{1}{2}a\langle 110\rangle$ at right angles which combine to form a single dislocation with a Burgers vector of $a\langle 100\rangle$. Many examples of this interaction have now been observed in different crystals. Fourteen of them have been partially analysed and eight of these have been fully analysed. The experimental observations on one of these interactions are reported in detail in this paper. The intersecting dislocations were always nucleated at the surfaces of the crystals. The dislocation loops expanded on their different glide planes under the influence of the applied stress and the interactions occurred where they intersected.

Amelinckx (1958 a) has presented some evidence that dislocations with an $a\langle 100\rangle$ Burgers vector can appear in crystals of potassium chloride as a result of the above interaction. The dislocations which he observed formed segments of nets on sub-boundaries where there was a relatively high density of dislocations. They were decorated by a method (Amelinckx 1958 b) requiring the crystals to be heated to a temperature at which climb could occur through the interaction of the dislocations with mobile Schottky defects. Amelinckx suggested that the presence of a third dislocation, interaction with which would tend to bring the combining dislocations into a parallel orientation, might be a necessary condition for the reaction.

---

† Communicated by the Authors.

‡ Now at the Department of Physics, University of Virginia, Charlottesville, Va.

In the present work, the interacting dislocations were generated at the surfaces of initially dislocation-free crystals. Both the dislocation lines and the associated surface terraces were decorated with particles of colloidal silver by exposing the crystals to light at room temperature after they had been strained. This allows the glide planes to be determined and the nature of the interactions to be fully established. In these experiments, the dislocations are observed in the configuration which they have at a particular stage of their glide motion.

§ 2. Experimental Observations

Full details of the experimental method are given in our previous paper (Bartlett and Mitchell 1960). Here we will describe one of the eight examples of the interaction which has now been fully established by detailed experimental measurements. The orientations of the silver bromide crystals were determined from back-reflection Laue x-ray diffraction photographs. The orientation of the crystal in which the particular interaction which will be illustrated was observed is represented in the stereographic projection of fig. 1. It will be seen that the surface of the crystal was very nearly parallel to the (001) crystallographic planes. The relative positions of the decorated surface terraces and of the dislocation lines below the surface are shown diagrammatically in fig. 2. The decorated surface terraces are illustrated in the photomicrograph of

Fig. 1

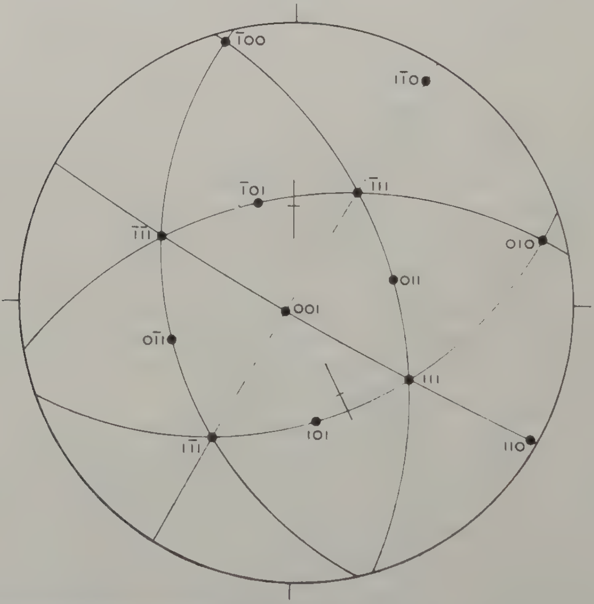

Stereographic projection showing the orientation of the crystal and the poles of the glide planes of the interacting dislocations.

fig. 3 (Pl. 109) and the corresponding dislocation lines at a distance of 4 microns below the surface are shown in fig. 4 (Pl. 109). The crystal was displaced on the microscope stage between the two photographs as will be evident from fig. 2.

Fig. 2

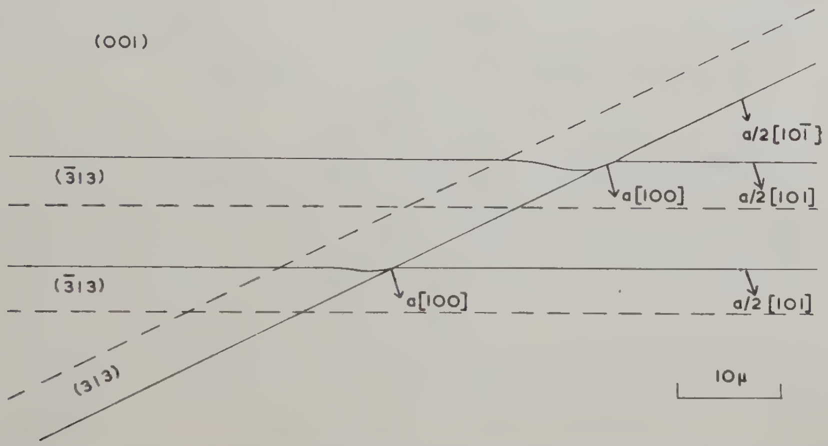

Diagram showing the relative positions of the surface terraces (dotted lines) and of the dislocation lines. The indices of the glide planes are given together with the Burgers vectors of the dislocations.

Our observations indicated that the oblique dislocation in the illustrations was the intersected dislocation and that the two parallel dislocations were the intersecting dislocations. The extremely small depth of focus of a high-power, large-aperture microscope objective is used to advantage in this work as it allows us to focus accurately upon the surface terraces and the dislocation lines. We have determined the glide planes of the intersected and intersecting dislocations from measurements with a calibrated micrometer eyepiece and the calibrated fine focusing adjustment of the microscope. Angular relationships with respect to the orientation of the crystal were measured with a microscope eyepiece with a graduated circular vernier scale. The results of these observations are presented in figs. 1 and 2. The crosses on the arcs in fig. 1 show the mean experimental values for the location of the poles of the glide planes and the lengths of the arcs indicate the spread of the individual observations. Even when the microscope is in very good adjustment, there is inevitably a considerable error in the depth measurement which has also to be corrected to allow for the relatively high refractive index of silver bromide.

As all our observations establish that the glide planes of dislocations in silver bromide crystals contain an $a\langle 110\rangle$ lattice vector, we deduce that the glide planes of the intersected and intersecting dislocations in the neighbourhood of this interaction are the (313) and ($\bar{3}$13) planes, respectively. The only possible Burgers vectors for these dislocation lines are therefore

$\frac{1}{2}a[10\bar{1}]$ and $\frac{1}{2}a[101]$ and the interaction must be represented by one of the following equations depending on the sense of the Burgers vectors:

$$\tfrac{1}{2}a[101]+\tfrac{1}{2}a[10\bar{1}]=a[100], \quad . \quad . \quad . \quad . \quad . \quad . \quad . \quad (1)$$

$$\tfrac{1}{2}a[101]+\tfrac{1}{2}a[\bar{1}01]=a[001]. \quad . \quad . \quad . \quad . \quad . \quad . \quad . \quad (2)$$

Our experimental observations do not allow us to distinguish between these two alternatives. For purposes of discussion, we have therefore represented the reaction as though it occurred in accordance with eqn. (1) and this is consistent with the fact that the plastic deformation resulted from the establishment of a tensile stress in the crystal. The interaction leads to the formation of a segment of dislocation line with a Burgers vector of $a[100]$ and, within the limits of experimental error, this combined dislocation is parallel to the [010] direction in the crystal. This means that its glide plane is the (001) plane. Both the combining dislocations and the resultant dislocation are almost in the pure edge orientation.

§ 3. DISCUSSION

The resultant edge dislocation with a Burgers vector of $a[100]$ in the (001) plane could dissociate into two dislocations of mixed character as follows:

$$a[100]=\tfrac{1}{2}a[110]+\tfrac{1}{2}a[1\bar{1}0]. \quad . \quad . \quad . \quad . \quad . \quad . \quad . \quad (3)$$

We have no experimental evidence for this dissociation but it might be possible if the energy of a dislocation were less in the screw than in the edge orientation (see, Huntington *et al.* 1955). Complete dissociation on the (001) plane is unlikely to occur as the interacting dislocations would be pinned at the nodes and the force between the two dissociated dislocations should be small. It is also evident that the resulting system could glide only with difficulty, even if dissociation did occur, as the dislocations meeting in the nodes could not move simultaneously on their three intersecting glide planes. We have, moreover, never observed dislocations with {100} glide planes in silver bromide crystals (see, Bartlett and Mitchell 1960).

ACKNOWLEDGMENTS

This work was carried out during the tenure of a Research Studentship awarded by the Department of Scientific and Industrial Research to J. T. Bartlett. The photomicrographs were taken with equipment purchased with a special grant from the Department of Scientific and Industrial Research. This assistance is gratefully acknowledged. We are also grateful to Kodak Ltd., for financial support and to J. H. Burrow and G. D. Freke for valuable assistance.

REFERENCES

AMELINCKX, S., 1958 a, *Nuovo Cim.*, **7,** 569; 1958 b, *Acta Met.*, **6,** 34.
BARTLETT, J. T., and MITCHELL, J. W., 1960, *Phil. Mag.* **5,** 445.
FRANK, F. C., 1949, *Physica*, **15,** 132.
HUNTINGTON, H. B., DICKEY, J. E., and THOMSON, R., 1955, *Phys. Rev.*, **100,** 1117.

The Atomic Diffusion of Platinum in Gold†

By A. J. Mortlock, A. H. Rowe and A. D. Le Claire
Metallurgy Division, Atomic Energy Research Establishment,
Harwell

[Received March 15, 1960]

Abstract

Measurements are reported of the diffusion of platinum at tracer concentrations in gold over the temperature range 800°c to close to the melting point of gold. Above about 900°c the results obtained can be fitted to the following equation: $D=(7{\cdot}6^{+4\cdot7}_{-2\cdot9})\exp[-(60\,900\pm1200)/RT]$ cm²/sec. The magnitude of the observed activation energy relative to that corresponding to self-diffusion in gold is in qualitative agreement with current theories.

Below about 900°c the observed diffusion coefficients appear to be enhanced relative to those expected by extrapolation from higher temperatures; possible explanations of this effect are discussed.

§ 1. Introduction

In recent years careful experiments using radio-tracers have shown that activation energies for the diffusion of impurities at near-zero concentration in a given solvent may be greater or smaller than that associated with the self-diffusion of the solvent. This is in contrast to earlier experimental results which suggested that, in general, impurities diffuse with activation energies less than that for the solvent: see, for example, the collections of data given by Seitz (1943) and Le Claire (1949).

A considerable advance in the understanding of the results of these more recent experiments came when Lazarus (1954) introduced a simple electrostatic model in order to explain the observed differences in activation energies. This model was based on the earlier Mott (1936) picture of an impurity of valence $Z+1$ dissolved in a monovalent solvent and screened by the conduction electrons, the resultant potential distribution around the impurity being found by solving a linearized form of the Thomas–Fermi equation. The change in the energy of vacancy formation was considered by Lazarus to be simply the change in the lattice binding energy of a nearest neighbour in the screened potential of the impurity atom. The change in the energy of motion was supposed to be due to a corresponding change in the elastic constants controlling a particular distortion of the lattice capable of moving the impurity atom towards the adjacent vacancy.

This model yielded the following equation for ΔH, the amount per atom by which the activation energy for impurity diffusion exceeds that for solvent self-diffusion:

$$\Delta H=-[1-(q^2a^2-5qa-5)/4](Ze^2/a)\exp(-qa) \quad . \quad . \quad . \quad (1)$$

---

† Communicated by the Authors.

where q, a and e are respectively the screening parameter, interatomic spacing and electronic charge. Substitution in this shows that the activation energy for the diffusion of electropositive (+ve Z) impurities should be less than that for solvent self-diffusion and, for electronegative impurities (−ve Z), greater.

Good agreement between theory and experiment was found for the electropositive impurities, cadmium, indium, tin and antimony diffusing in silver, see Lazarus (1960), but was poor in the case of analogous impurities in copper. Similar, although scarcer data for electronegative impurities also appeared to be in poor agreement with the simple theory. For example, Mackliet (1958) found that, while nickel, cobalt and iron diffuse in copper with activation energies greater than that for copper self-diffusion, as expected, the sign of the change in activation energy in going from one element to the other was opposite to what one would expect on the basis of eqn. (1).

Alfred and March (1956) later showed how a more accurate working out of the model could be obtained if exact numerical solutions of the applied Thomas–Fermi equation were employed. Their analysis indicated that the right hand side of (1) should in fact be multiplied by a factor α which was a decreasing function of Z, being >1 for −ve Z's and <1 for +ve Z's. Application of this result produced little improvement in the agreement between theory and experiment for electropositive impurities but indicated the possibility of relatively large values of ΔH for electronegative impurities. Results recently obtained by Pierce and Lazarus (1959) on the diffusion of ruthenium in silver seem to verify this particular prediction.

Manning (1958) has pointed out that this earlier theoretical work neglects a possible temperature dependence of the correlation factor, f, which takes account of inequalities in the probability of diffusion jumping in different directions in any formula for the diffusion coefficient based on a purely random walk analysis. If f is in fact temperature dependent then the observed activation energy per atom, Q, is related to the calculated sum, H, of the energy of movement and energy of formation, by the equation

$$Q = H - k[d \ln f/d(1/T)] \qquad . \quad . \quad . \quad . \quad . \quad (2)$$

where k is Boltzmann's constant and T is the temperature in degrees Kelvin.

For impurity diffusion f depends not only on the frequency of impurity–vacancy jumps but also on that of vacancy exchanges with neighbouring solvent atoms. These jump rates generally will involve several different activation energies so that f will be temperature dependent and the second term on the right in eqn. (2) may represent a small but nevertheless significant contribution to Q. For the particular case of self-diffusion f is only a geometrical constant so that the second term is zero. Thus, it is possible to write

$$\Delta Q = \Delta H - k[d \ln f/d(1/T)] \qquad . \quad . \quad . \quad . \quad . \quad (2a)$$

where ΔQ is the observed difference in activation energy between impurity and solvent self-diffusion and the second term on the right continues to refer to impurity diffusion only; the relative importance of this term is greatly increased when applied in this way since its magnitude is usually of the same order as that of ΔH.

An alternative theoretical derivation of ΔQ, as opposed to ΔH only, has recently been proposed by Le Claire (1960); it also is based on the electrostatic model of the dissolved impurity. The change in the energy of vacancy formation is calculated as before but the change in the energy of motion is considered to be simply the difference in energy between the electrostatic configuration corresponding to the impurity atom at the saddle point and that with it at the equilibrium position. For this purpose the saddle point configuration is taken to correspond to a charge Ze situated between two half vacancies of charge $-\frac{1}{2}e$ each. The centroids of the supposedly hemispherical charge shapes of the half-vacancies are taken to be the effective charge centres. For electronegative impurities where the controlling jump frequency is that due to impurity atom–vacancy exchange, the correlation factor correction is negligible so that in this case

$$\Delta Q = \Delta H = (16\alpha Ze^2/11a)\exp(-11qa/16). \quad . \quad . \quad . \quad (3)$$

It is clear that particular interest attaches to new experimental data on the diffusion characteristics of electronegative impurities in the monovalent metals, as the various theories of ΔQ diverge to a greater extent in this region than for electropositive impurities. Furthermore, the lack of a correlation factor correction in this region makes for a less complicated comparison of the theoretical model with experiment. For these reasons a series of measurements has been made of the diffusion of the electronegative impurity platinum dissolved in the monovalent noble metal, gold.

§ 2. MATERIALS

The gold used was supplied by Johnson Matthey in the form of flat circular discs of about 2 cm diameter and 4 mm thick with a nominal purity of 99·98%. A full spectrographic analysis revealed that the major impurity was silver with a concentration of about 44 p.p.m. Other impurities were present in negligible concentrations, suggesting that the overall purity could be appreciably better than the nominal figure.

The platinum was also supplied by Johnson Matthey; in this case the purity was given as 99·999%.

§ 3. METHOD

The technique employed in these experiments was the fairly standard one in which a thin layer of radioactive solute is laid down on one face of a solvent metal specimen and diffused in by heat treatment. The resultant concentration versus penetration distance profile is then determined by first serially sectioning with a precision lathe and then subjecting each individual section to radioactive assay. Provided the surface concentration of solute falls to a very small level in a time which is short compared to the total diffusion time, then the calculated diffusion coefficient can be taken as applying to effectively zero concentration of solute.

§ 4. EXPERIMENTAL DETAILS

The diffusion specimens were prepared in the following manner.

Where single crystals were required the as-received gold discs were remelted in a graphite crucible-mould of high purity suspended in an argon atmosphere in a vertical tube furnace. The crucible was then lowered through a sharply decreasing temperature zone, the single crystal being nucleated at a vee-shaped depression near the bottom of the crucible-mould. The near-circular discs so produced were finely ground on one face and etched with a 40% solution of boiling aqua regia. This process was repeated several times until a flat and nominally cold-work-free surface was produced. The specimen was then annealed for about three days at about 1000°C, usually in vacuum, and the single-crystallinity and freedom from large scale cold work tested by taking Laue back reflection X-ray photographs of the surfaces.

Those discs which were finally given a diffusion annealing as polycrystals were finely ground on one face but were usually not subjected subsequently to any etching or pre-diffusion annealing. The grain size of this material was about 1 mm^2.

Pile-activated platinum contains the radioactive isotopes ^{191}Pt, ^{193}Pt, ^{195}Pt, ^{197}Pt and ^{199}Pt, of which ^{199}Pt (half-life 30 min) decays to the stable isotope ^{199}Hg via the radioactive daughter ^{199}Au (half-life 3·2 days). This means that it is necessary either to remove this impurity before deposition onto the gold discs or else to discriminate against it during the radioactive assay of the sections. As an extra precaution in the present case both procedures were followed.

Before deposition onto the prepared surfaces of the gold specimens the active gold impurity was removed from the pile-activated platinum by preferential distillation, at least two days having been allowed to elapse so that practically all the gold impurity destined to be produced by decay was present. The relative absence of active gold was checked with a scintillation counter-pulse height analyser arrangement by comparing the 165 kev gamma peak due to ^{199}Au decay with the 65 kev gamma peak due to the combined decay of the remaining platinum isotopes; this technique was originally described by Kidson and Elsdon (1958). The correctness of the association of the observed 65 kev gamma peak with platinum decay was checked by half-life measurement. The observed effective half-life of this peak was found to be 3·5 days, in fair agreement with the figure of 3·7 days obtained by Kidson and Elsdon from measurements extending over 10 days. The present measurements extended over a period of 9 days following a 'cooling' period of about 6 days and after removal of the gold impurity.

Deposition of the purified platinum onto the gold specimens was carried out in the special vacuum evaporator described by Rowe (1959). A bead of platinum was supported in a glazed thoria crucible contained in a silica vacuum vessel. A suitable flux concentrator was mounted around this vessel and the bead heated by radio-frequency induction. Layers of not more than about 1000 Å were deposited in this way and calculation showed that in the worst case the maximum concentration of platinum in the diffusion zone fell to about 1% in a time which was negligible compared to the total annealing time.

The platinum deposited gold discs were sealed in vacuum in small silica tubes and annealed for periods ranging from a day to three weeks. Temperature uniformity in the temperature-controlled annealing furnaces was assisted by the use of hollow metal (stainless steel or nickel) blocks into which the silica tubes were placed. The temperature measurement was made with specially calibrated Pt–(Pt + 13% Rh) thermocouples which were checked regularly for drift by melting a small piece of gold wire welded across their hot junctions. Suitable corrections were also applied for the diffusion which took place during heating up, no correction being necessary for cooling down as the specimen was usually quenched in water. Overall, the stated temperatures cannot be in error by more than about ± 2°c.

Sectioning was carried out in the manner described earlier by Makin *et al.* (1957). In this case, however, the individual cuts were dissolved in aqua regia and counted as a liquid in a well-type scintillation counter, attention being restricted to the 65 kev gamma radiation due to the active platinum isotopes. By taking the ratio of the measured activity of each section to the mean measured activity of the first section, used as a standard and counted immediately before and after each other section, the relative activities of all sections were obtained in a manner independent of radioactive decay or change in counter characteristics. Subsequent measurements of the ratios corresponding to individual sections were occasionally carried out as an additional running check of their constancy in time and therefore of the purity of the diffusing metal. If there had been a contaminating radioactive impurity present with half-life and diffusion characteristics different from those of platinum, the magnitude of the ratio corresponding to a particular section would not have been independent of time.

§ 5. Results

The logarithm of the relative activity of each section was plotted against the square of the penetration distance and a straight line fitted by least squares analysis. Where necessary any points corresponding to small or large penetrations which appeared to be inconsistent with the general slope of this line were neglected. The diffusion coefficient, D, was calculated from the slope of this line via the following equation

$$\ln (C/C_0) = -x^2/4Dt \quad . \quad . \quad . \quad . \quad . \quad . \quad . \quad . \quad (4)$$

in which (C/C_0) is the concentration of platinum at a penetration distance x relative to that at the surface after a diffusion annealing for effective time t.

In fig. 1 two plots are given corresponding to data obtained from the simultaneous diffusion annealing of a single crystal and a polycrystal at 1039°c. The fact that the operative diffusion coefficients are in close agreement in this case indicates that the presence of a highly worked surface layer is unimportant at relatively high temperatures. That this is so is evident when it is remembered that the single crystal had been finely ground, etched and pre-annealed prior to the final diffusion annealing whereas the polycrystal had only been finely ground.

Diffusion Coefficients of Platinum in Gold at Various Temperatures

Temperature (°c)	Diffusion coefficient (cm²/sec)	
1055·5	$7{\cdot}33 \times 10^{-10}$	
1039·0	5·67	(SC)
1039·0	5·52	
1030·2	4·42	
1007·7	3·16	
977·0	1·62	
950·9	$9{\cdot}80 \times 10^{-11}$	
925·9	6·35	
845·0	1·23	(SC)
845·0	1·23	(SC)
801·0	$5{\cdot}54 \times 10^{-12}$	(SC)
799·0	5·00	(SC)

Diffusion coefficients obtained with single crystal specimens are labelled (SC).

At low temperatures where short-circuiting diffusion is of greater importance a more exact test was felt to be necessary in order to demonstrate that the diffusion coefficients obtained were independent of the preliminary treatment of the specimen surface. Especially was this the case because x-ray evidence suggested that a small proportion of the lattice defects introduced by grinding sometimes remained after etching and pre-annealing. Also, a polycrystal annealed at 802°c had shown definite signs that material transfer via grain boundaries represented an appreciable proportion of the total transfer at these temperatures. For these reasons a comparison was made at 800°c between a single crystal specimen in the as-grown condition and one which had been worked, etched and pre-annealed: as before no significant difference in behaviour was detected. The log (C/C_0) versus x^2 plot corresponding to the as-grown single crystal is given in fig. 2 together with that obtained using the polycrystal referred to above.

Fig. 1

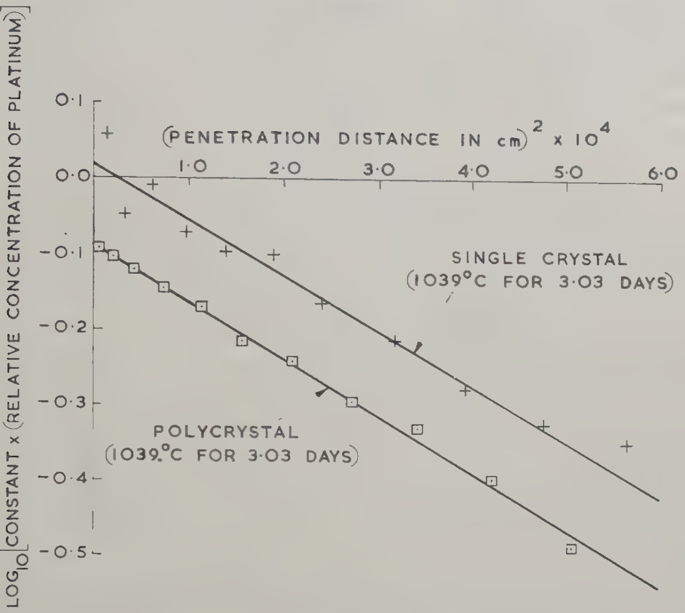

Concentration distributions for a single crystal and a polycrystal gold specimen after annealing at 1039°c.

Fig. 2

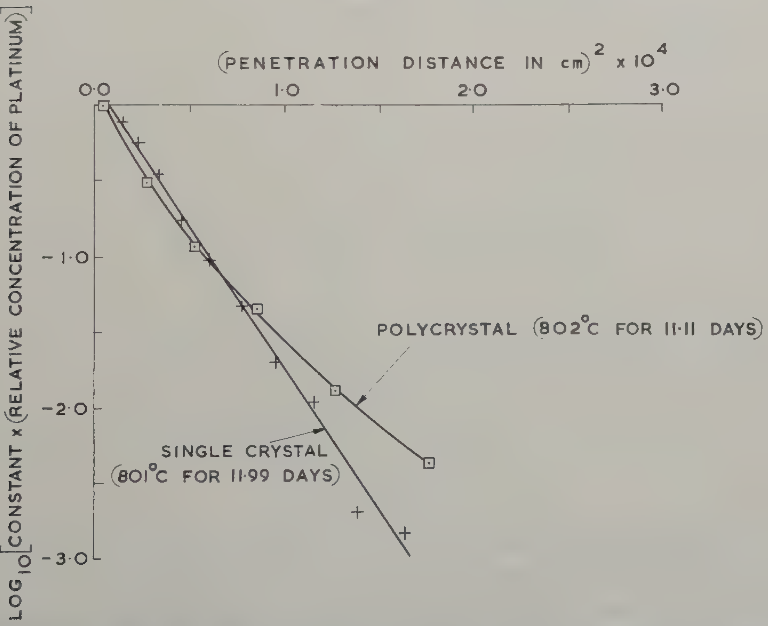

Concentration distributions for a single crystal and a polycrystal gold specimen after annealing at 801°c and 802°c respectively.

In the table the diffusion coefficients obtained and the temperatures to which they apply are listed. Figure 3 is a plot of log D versus $(1/T)$. The equation to the straight line fitted by least squares analysis to the region corresponding to temperatures in excess of about 900°c is:

$$D=(7{\cdot}6^{+4{\cdot}7}_{-2{\cdot}9})\exp\left[-(60\,900\pm1200)/RT\right]\ \mathrm{cm}^2/\mathrm{sec} \qquad . \quad . \qquad (5)$$

where R is the gas constant in calories per gramme molecule per degree Kelvin, and the errors are standard errors based on the scatter of the individual diffusion coefficients.

Fig. 3

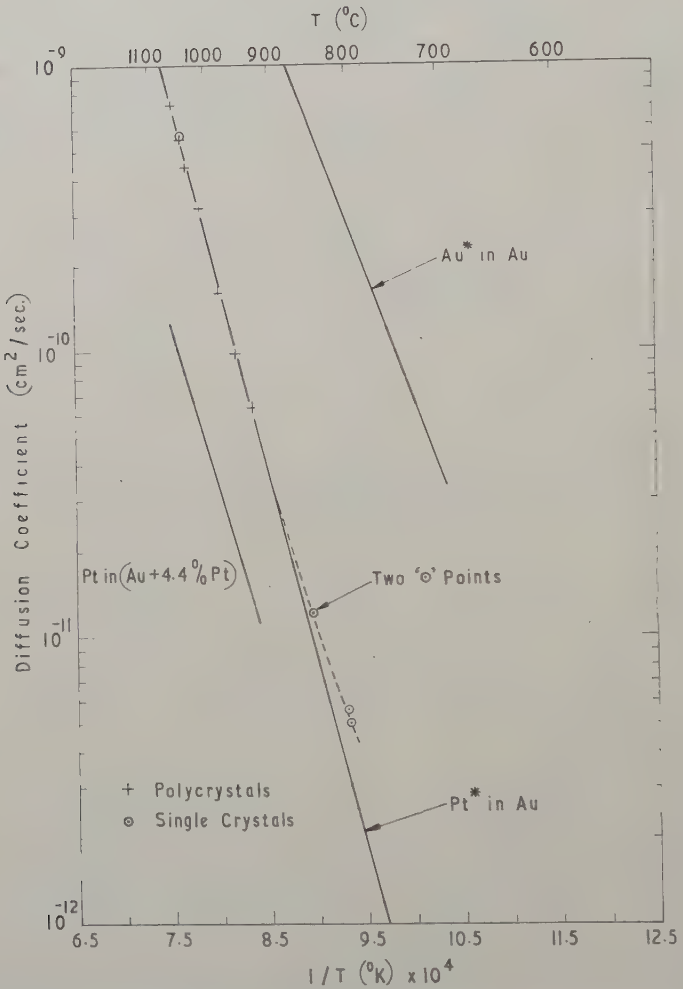

Arrhenius plot of experimental data for the diffusion of platinum in gold and, for comparison, self-diffusion in gold.

§ 6. Discussion

The only other data available on the diffusion of platinum in gold with which a comparison is worthwhile are those due to Bolk (1959). This author determined the partial diffusion coefficient of platinum in gold-platinum alloy at an average concentration of 4·4% platinum (atom fraction). The results obtained correspond to the equation

$$D = 0{\cdot}09 \exp\left[-(54\,000 \pm 7000)/RT\right] \mathrm{cm}^2/\mathrm{sec},$$

which has also been plotted in fig. 3. It is clear that the activation energy observed is not inconsistent with that found in the present investigation. No significance can be attached to the large disagreement in the pre-exponential factors because of the very low accuracies involved.

The anomalously enhanced diffusion evident at low temperatures needs some comment. It is similar to that observed by Mackliet (1958) when studying the diffusion of iron and cobalt in copper. The effect is clearly not due to the presence of short-circuiting diffusion along grain boundaries because of the use of single crystals. Also, the presence of an unwanted impurity would only be expected to enhance the overall diffusion in the manner observed if it were very fast-moving in gold compared to gold itself. This follows from the possibility that the diffusion of platinum in impure gold can be expressed as a linear function of that in pure gold and the diffusion coefficient of the impurity itself in gold: see, for example, Hart *et al.* (1957). As it is reasonable to suppose that the activation energy for the diffusion of the hypothetical impurity in impure gold is less than that for platinum in pure gold, the effective 'activation energy' for the diffusion of platinum in impure gold could then be an increasing function of temperature, as observed.

In order to settle this point a rough measurement was made of the diffusion of silver (the major impurity present) at tracer concentration in gold: a figure of $2{\cdot}7 \times 10^{-9}$ cm²/sec at 900°C was obtained. This is not much different from that for self-diffusion in gold at the same temperature ($1{\cdot}5 \times 10^{-9}$ cm²/sec) so that the operation of this mechanism in producing the observed enhancement is unlikely.

Hart (1957) has suggested that short-circuiting diffusion along dislocations can enhance bulk self-diffusion at sufficiently low temperatures. Later, Mortlock (1960) pointed out that segregation towards these defects could amplify this effect in the case of solute diffusion. The total enhancement in D, ΔD, is then given by

$$\frac{\Delta D}{D_1} = n f_0 \left(\frac{D_d}{D_1}\right)\left(\frac{C_d}{C_1}\right) \quad . \quad . \quad . \quad . \quad . \quad . \quad . \quad . \quad (6)$$

where n is the number of sites that go to make up a typical cross-sectional area of the dislocation pipe, f_0 is the fraction of all atoms situated in the cores of the pipes, D_d/D_1 is the ratio of the diffusion coefficient in the pipe to that in the lattice, and C_d/C_1 is the ratio of the fractional concentration in the pipe to that in the lattice.

A rough value of $3 \cdot 1 \times 10^4$ for D_d/D_l was found by applying the equation given by Fisher (1951) for bulk diffusion transfer via grain boundaries and lattice to the linear portion of a log C versus x plot of the data obtained with the polycrystal annealed at 802°c.

Taking n to be 10 and f_0 to be between 6×10^{-10} and 6×10^{-8} (corresponding to dislocation densities lying between 10^6 and 10^8 lines/cm^2), C_d/C_l then turns out to be in the range 4×10^3 to 4×10, to account for the observed enhancement of D. This corresponds to solute atom-dislocation binding energies of the order of a few tenths of an electron volt, which are not unreasonable. Furthermore, the average concentration levels operative in the diffusion specimens annealed at 800°c are a few tenths of a per cent, so that values of C_d/C_l not exceeding a figure in the range $\sim 10^2$ to 10^3 are allowable before the change in the overall effect produced by the dislocations becoming saturated must be considered.

The equation given above for $\Delta D/D_l$ does not take account of the fact that solute atom jumps in a dislocation pipe at right angles to the axis of the pipe do not contribute fully to the observed overall diffusion coefficient due to partial reflection from the pipe wall. At the worst only diffusion parallel to the axis of the pipe will be observed and, as the effective number of pipes which are parallel to any given direction is a third of the total, a factor k' which is less than unity but greater than a third should be introduced on the right hand side of eqn. (6). Therefore, if indeed dislocation diffusion is the whole cause of the observed diffusion coefficient enhancement, it would be more correct to regard the values of C_d/C_l calculated from eqn. (6) as lower limits.

An attempt was made to test the explanation of the observed diffusion coefficient enhancement based on the presence of dislocations by measuring the diffusion of platinum in a single crystal which had been so deformed that the dislocation density was appreciably larger than that in an as-grown crystal. The deformation was introduced by bending a special single crystal shaped in the form of a rectangular prism about an axis perpendicular to its two principal faces. One of these faces was then deposited with radioactive platinum in the usual way and the diffusion into the crystal following an annealing of about ten days duration at 800°c measured in a direction parallel to the bend axis. Unfortunately recrystallization occurred during this annealing and the penetration profile obtained was characteristic of a polycrystal at this temperature.

Before the agreement between theory and experiment can be discussed in relation to the activation energy problem, the question of the value of Z to be assigned to platinum dissolved in gold must be settled. Magnetic susceptibility data given by Vogt (1932) indicate that the rate of increase of the susceptibility of Au + Pt alloys as the platinum content is increased is considerably less than that to be expected on a simple compositional basis (which would be the case if the platinum atoms were unaffected by their surroundings), at least up to about 90% (atom) platinum. This suggests that the electronic structure of the dissolved platinum atom tends to be similar to that of gold; thus, the operative value of Z is best taken as -1.

Using this value, the initial theoretical analysis of the activation energy problem by Lazarus which was described earlier predicts that ΔQ is equal to 2·0 kcal/mol. If the correction due to Alfred and March is applied this becomes 3·0 kcal/mol. The recent treatment by Le Claire of the same problem gives 8·5 kcal/mol. If the activation energy for self-diffusion in gold is taken as 41·7 kcal/mol, Makin *et al.* (1957), then the experimental value for ΔQ comes out to be 19·2 kcal/mol. It is clear, therefore, that Le Claire's model yields the closest agreement between theory and experiment. At least part of the large discrepancy remaining can be put down to the possibility that the potential distribution around an impurity atom of negative excess valence is not in fact accurately defined by the equation $V=(\alpha Ze/a)\exp(-qa)$ given by Alfred and March (1956), March (1959, private communication).

A calculation of the total entropy of activation using the observed value for the pre-exponential factor yields a figure of 7·2 k units, k being Boltzmann's constant. The sign of this result is in agreement with theoretical calculations due to Huntingdon *et al.* (1955) which predict a magnitude of about 0·9 k units. If due account were taken of the fact that a platinum atom is smaller than a gold atom, thereby producing less crowding at the saddle point during the elementary diffusion movement, the theoretical estimate would be higher.

§ 7. PRINCIPAL CONCLUSIONS

The activation energy associated with the diffusion of platinum at tracer concentrations in gold has been measured and found to be much larger than for self-diffusion in gold. This is qualitatively consistent with current theories, but numerical agreement is poor.

The diffusion observed at temperatures below about 900°C was found to be greater than expected on the basis of extrapolation from higher temperatures. Calculations indicate that this effect could be due to short-circuiting diffusion of segregated platinum along dislocations.

ACKNOWLEDGMENTS

The assistance of Miss A. Nunley and Mr. C. Layton in carrying out some of the observations and numerical calculations is gratefully acknowledged. In addition, the authors wish to thank Dr. J. Makin and his colleagues for operating the single crystal growing furnace.

REFERENCES

ALFRED, L. C. R., and MARCH, N. H., 1956, *Phys. Rev.*, **103,** 877.
BOLK, A., 1959, *Het Kirkendall-Effect in Het Systeem Goud-Platina* (Delft: Grafisch Bedrijf Avanti): Delft Technical Institute Doctor Thesis.
FISHER, J. C., 1951, *J. appl. Phys.*, **22,** 74.
HART, E. W., 1957, *Acta Met.*, **5,** 597.
HART, E. W., HOFFMAN, R. E., and TURNBULL, D., 1957, *Acta Met.*, **5,** 74.

Huntington, H. B., Shirn, G. A., and Waja, E. S., 1955, *Phys. Rev.*, **99,** 1085.

Kidson, G. V., and Elsdon, W. L., 1958, *J. appl. Radiat. Isotopes*, **3,** 252.

Lazarus, D., 1954, *Phys. Rev.*, **93,** 973; 1960, *Advances in Solid State Physics*, Vol. 10 (New York: Academic Press Inc.).

Le Claire, A. D., 1949, *Progress in Metal Physics*, Vol. 1, 370–372 (London: Butterworths Scientific Publications Ltd.); 1960, *Phil. Mag.* (to be published).

Mackliet, C. A., 1958, *Phys. Rev.*, **109,** 1964.

Makin, S. M , Rowe, A. H., and Le Claire, A. D., 1957, *Proc. phys. Soc. Lond.* B, **70,** 545.

Manning, J. R., 1958, *Phys. Rev. Letters*, **1,** 365.

Mortlock, A. J., 1960, *Acta Met.*, **8,** 132.

Mott, N. F., 1936, *Proc. Camb. phil. Soc.*, **32,** 281.

Pierce, C. B., and Lazarus, D., 1959, *Phys. Rev.*, **114,** 686.

Rowe, A. H., 1959, *A.E.R.E. Report* No. 3113.

Seitz, F., 1943, *The Physics of Metals*, 181 (New York: McGraw-Hill Book Company, Inc.).

Vogt, E., 1932, *Ann. Phys., Lpz.*, **14,** 23.

Charged Dislocations in Lithium Fluoride†

By R. L. SPROULL
European Research Associates, Brussels, Belgium‡

[Received March 14, 1960]

ABSTRACT

The application of strong electrostatic fields to bent LiF crystals produced small motions (0·1 to 6 Å) of the bends which were analysed in terms of the motion of charged dislocations. The charge on the dislocation core was positive and of the order of 10^{-4} to 10^{-3} e.s.u./cm, and it presumably arose from the inequality of the free energies of formation of positive ion and negative ion vacancies. Estimates of the electrostatic contribution to the critical shear strength based on these values of charge substantiate the suggestion by Eshelby, Newey, Platt, and Lidiard that much of this strength may be electrostatic in origin.

§ 1. INTRODUCTION

THE purpose of this experiment was to learn if dislocations in an ionic crystal could be electrostatically charged and, if so, to study the behaviour of such dislocations in an applied field. Eshelby *et al.* (1958) have recently pointed out that dislocations in ionic crystals should generally be charged and have suggested that a substantial part of the critical shear stress of such crystals is attributable to the electrostatic attraction between a dislocation and its surrounding charge cloud. They have also proposed several interesting consequences of the charge on dislocations for the mechanical behaviour of ionic crystals, including the proposal that a sufficiently strong electric field might produce plastic deformation.

The present experiment had a different objective, namely to produce *elastic* deformation by an applied electric field. It was expected that the phenomena would be somewhat simpler than plastic deformation and that the effect, if any, could be studied as a function of the field in order to distinguish it from spurious effects.

The basic plan of the experiment was to apply a strong electric field to the dislocations forming a bend in a crystal and thereby to cause the whole dislocation pattern constituting the bend to move a short distance. A crude sketch showing how the measurement was accomplished is presented in fig. 1. One end of the bent crystal was rigidly mounted, and the motion of the other end (the displacement x) was transmitted to an electromechanical transducer. Such an experiment requires the measurement of very small values of the displacement x, from a few hundredths

---

† Communicated by the Author.
‡ Present address: Cornell University, Ithaca, New York.

Fig. 1

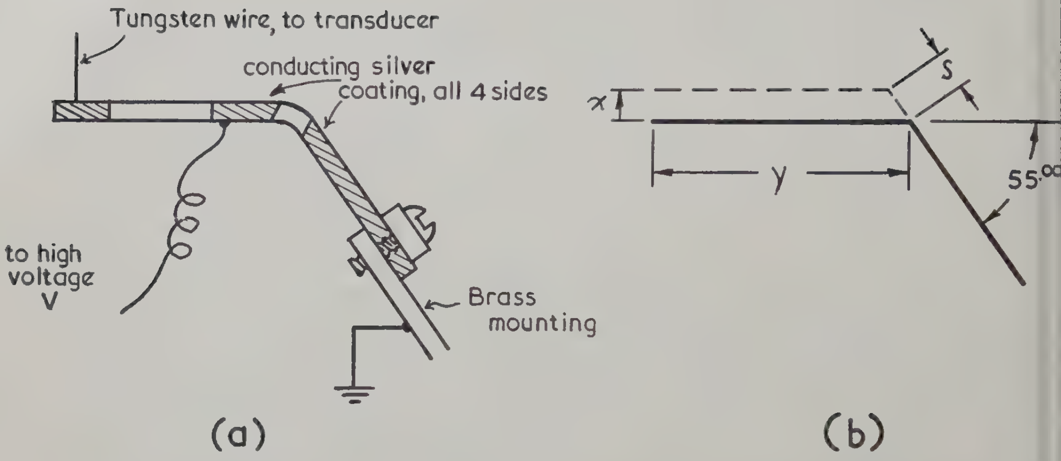
Tungsten wire, to transducer
conducting silver coating, all 4 sides
to high voltage V
Brass mounting
(a)
x
S
y
55.0
(b)

(*a*) Bent crystal. Motion of the left end is communicated through the tungsten wire to the transducer. (*b*) The relation between a displacement *s* of the bend and a displacement *x* of the transducer.

Fig. 2

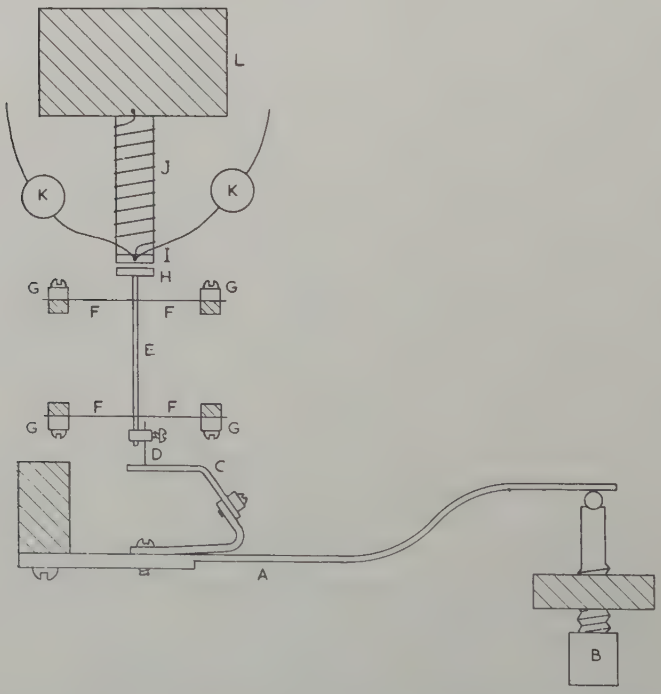

Schematic plan view of apparatus. The shaded parts are fastened rigidly to the base plate.

of an angstrom to several angstroms, but it proved practical to accomplish this measurement with a rather simple apparatus.

§ 2. APPARATUS AND TECHNIQUE

A schematic diagram of the apparatus appears in fig. 2. A brass bar A was rigidly mounted at the left end. The gradation in thickness and the length (18 cm) of the bar were such that 1/11 revolution of the micrometer head B moved the tip of the crystal in contact with D a distance of $1\,\mu$. (This micrometer motion was used both for adjustment and for calibration.) The bent crystal C was clamped to the brass bar, and motion of the free end of C was transmitted through the 0·2 mm diameter tungsten wire D and the brass rod E to the 1 cm diameter plate H of a parallal plate condenser. The part E and H was supported by four $1{\cdot}5\,\text{mm} \times 0{\cdot}02\,\text{mm}$ Cu–Be legs F: these legs confined the motion of E to one dimension and provided a light spring action to hold D against C. The other plate I of the condenser was cemented to the end of a 1 cm outside diameter quartz tube on which were wound 57 close-spaced turns of 0·03 mm diameter wire. One end of this coil J was earthed and the other was connected to I; the resonant circuit thus formed and the two $2\,\mu\mu\text{F}$ coupling condensers K constituted the feed-back (frequency controlling) network of a two-transistor oscillator developed by Dr. J. Van Cakenberghe and Mr. L. Tremouroux (the circuit diagram will be provided on request). The transistors were embedded in a large brass block L to retard temperature drifts. Dust prevented use of condenser plate separations closer than 3 or $4\,\mu$; at this separation, the oscillator frequency was about 5 Mc/s, and a typical calibration was a change of about 0·3 Mc/s per micron of motion of the crystal end (30 c/s per Å). This high value was attained partly because of the flatness of the condenser plates which (as with the rest of the apparatus) were skilfully prepared by Mr. M. Fievet, and partly because the plates could easily be made nearly parallel. Parallelism was accomplished by loosening the clamps G, holding the two plates H and I together by a loop of thread, and then tightening the clamps.

The assembly of fig. 2 (except the tip of the micrometer head) was enclosed in a massive brass box which in turn was enclosed in foamed plastic and shielded from draughts. The batteries powering the oscillator were also protected from rapid temperature changes. Thus although only crude temperature compensation was built into the apparatus, under favourable conditions a drift in one minute of < 10 c/s ($\frac{1}{3}$ Å) was often observed, and data could be taken at much higher drift rates. Frequency fluctuations superimposed on the drift, presumably microphonic in origin, were $\sim \pm 3$ c/s in each measuring period of 2 sec; averaging repeated measurements reduced uncertainty from this source. The frequency was measured with a Hewlett–Packard 524B frequency meter which usually was set to count the number of cycles in a 1 sec interval and to plot the last two or the last three digits of this number on a strip-chart recorder. Thus full scale on the recorder was 100 cycles (~3 Å) or 1000 cycles (~30 Å).

Single crystals about $1{\cdot}7 \times 6 \times 35$ mm were cleaved from LiF purchased from the Harshaw Chemical Company. Each crystal was bent by forcing it into a notch in an aluminium block pre-heated to 200°c. The crystal was cooled quickly to room temperature and contained a 55° bend about 4 mm in length; this angle was a compromise between too non-uniform an electric field (too large angles) and too small a ratio of x to the amount of motion of the bend (too small angles). Conducting silver electrodes were painted onto the crystal as sketched in fig. 1 (*a*), and the surface of the crystal in the region of the electric field was coated with a thin polystyrene solution. A 0·25 mm copper wire of which one end was embedded in the silver paint connected the high-voltage output of a radio-frequency power supply to the central electrode of the crystal (corona currents with a threshold at ~3000 v were observed when the size of this wire was decreased to 0·1 mm).

After the crystal was mounted in the measuring apparatus and the temperature allowed to stabilize for 16 hours or more, measurements were begun. The cycle of measurement was as follows: with no voltage, the frequency meter counted cycles for 1 sec; this number was transmitted to the recorder (but it took nearly 2 sec for the recorder pen to attain its final position). After 1 sec of counting, the counter was idle for 1 sec; a second count was then made. Immediately after this count was completed, the high voltage was switched on, applying a negative potential to the high-voltage lead. Two readings were made with a negative potential. Then two zero readings and two readings with a positive voltage the same in magnitude as the negative voltage completed the cycle. (Switching of the applied voltage occurred in less than $\frac{1}{3}$ sec and therefore was complete before a new count was made.) Occasionally zero readings were omitted in order to switch with maximum speed from minus-to-plus-to-minus, etc., to combat drift when the effect of reversing the voltage was very slight.

Usually 10 or 20 such cycles of eight frequency readings each were taken with 500 v, then a similar group with 1000 v, and so so. After the entire series of measurements, calibration was made in order to convert frequency changes to angstroms of motion.

§ 3. Experimental Results

Two sections of the recorder chart for a series of readings on one crystal are reproduced in fig. 3. At low voltages a *positive* potential applied to the high-voltage electrode *increased* the frequency, and a negative potential decreased the frequency. At higher voltages, decreases in frequency were produced by potentials of either sign, but the decrease was smaller in magnitude when the potential was positive. An increase in frequency corresponded to an increase in condenser plate spacing, which in turn would have been produced by motion of the bend in the crystal toward the end where it was rigidly mounted.

Fig. 3

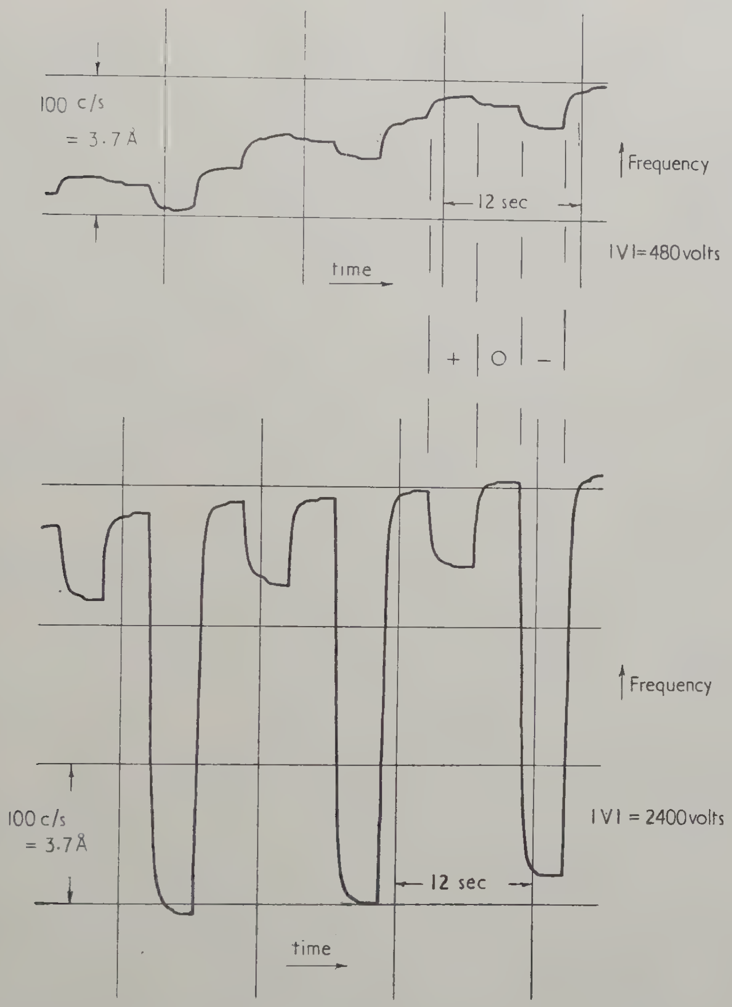

Strip-chart recordings for two magnitudes of $|V|$. The symbols O, +, and − refer to the values of V during each 4-second period.

It is clear from data like that in fig. 3 that at least two processes with different voltage dependencies occurred. Progress in separating these processes can evidently be made by determining the component of the displacement x which is an even function of voltage and the component which is an odd function. Let

$$x = aV + bV^2 + cV^3 + dV^4 + \dots .$$

Then if x_1 is the displacement at voltage V and x_2 the corresponding displacement at voltage $-V$,

$$(x_1+x_2)/2=bV^2+dV^4+\ldots, \qquad (1)$$

$$(x_1-x_2)/2=aV+cV^3+\ldots. \qquad (2)$$

Experimental values of the former (even) function are plotted as a function of V^2 in fig. 4. It appears that b is positive and that d and higher even coefficients are nearly zero. The value of b varied from one crystal to another or even with different electrodes on the same crystal. Analysis in the Appendix shows that this even function quite probably arose from electrostriction and is not of primary interest in this investigation.

Data for the odd function of V on the same crystal used for fig. 4 are plotted in fig. 5, in which the ordinate is $-(x_1-x_2)/2$, hereafter called $-\bar{x}$. Evidently both a and c are negative. In all the data taken, $\bar{x}$ was always a distinctly non-linear function of V, and the non-linearity was always in the same sense and about the same in magnitude. Curves nearly identical to those of fig. 5 were found for three other Harshaw LiF crystals, with the same values ± 30% of a and c. Similar phenomena, but with smaller and more variable values of a and c, were observed on Leitz and Harshaw NaCl crystals.

Several possible disturbing effects are considered in the Appendix, and it is there shown that the displacements plotted in fig. 5 are probably not the result of heating, electrostriction, converse piezoelectric effect, or the motion of vacancies. Although there may be other spurious effects not properly considered, there are two arguments in favour of the dislocation motion interpretation of the data:

(1) $\bar{x}$ as a function of V is non-linear; furthermore, c/a has the sign and about the magnitude expected, as will be shown in § 4.

(2) A bent crystal was polygonized by heating to 600°C and slowly cooling in air. Etching carried out by Mr. M. Reynders and Dr. E. Votava, according to the Gilman and Johnston (1956) prescription, showed that most of the isolated dislocations climbed into small angle boundaries as a result of this treatment. Polygonization reduced the odd-function-of-V effect by a factor of 8 and did not change the even function. Since this treatment changed the internal arrangement of dislocations but not the external shape of the crystal, it provided some evidence to support the connection between the observed phenomena and the properties of dislocations.

The transducer motion $\bar{x}$ could have arisen either because of a change in the bend angle or a change in the bend position. The former type of motion is sensitive to the distance y defined in fig. 1 (b), whereas the latter (illustrated in that figure) is not. Only limited advantage was taken of this different behaviour because an electrostatic shield around the high-voltage electrode prevented the use of small values of y, but experiments on the same bent crystal mounted with different values of y

Fig. 4

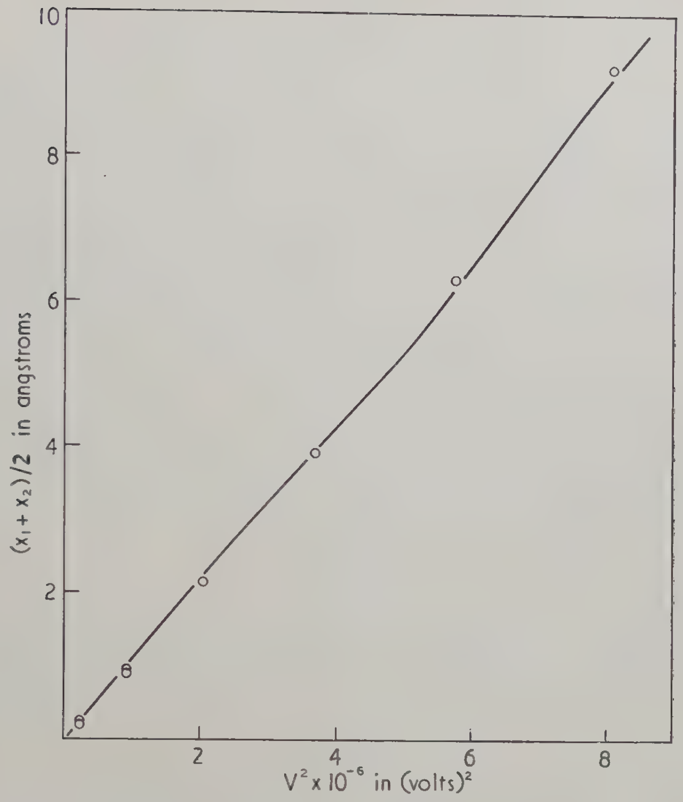

The part of x that is an even function of V plotted *vs* V^2.

Fig. 5

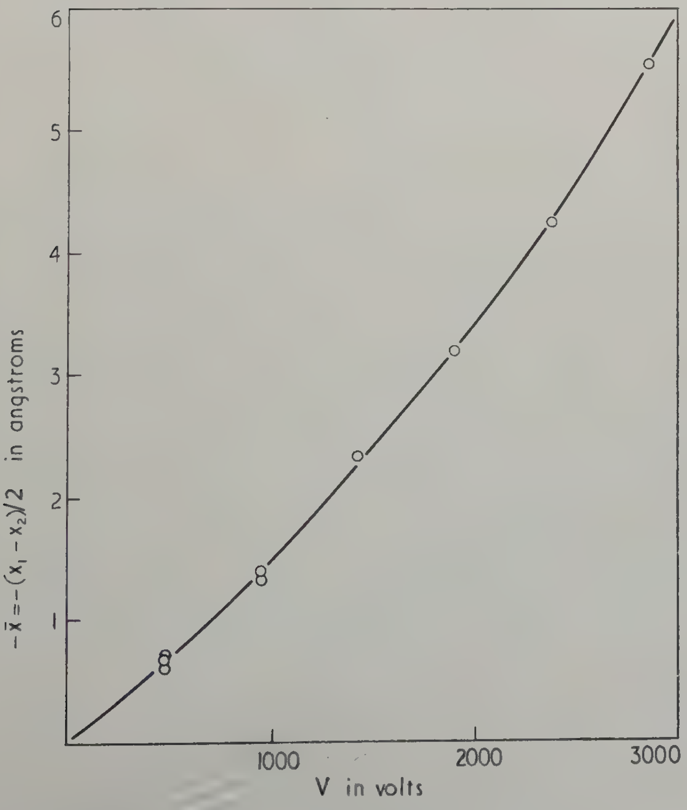

The part of x that is an odd function of V plotted *vs* V.

indicated that the motion $\bar{x}$ was of the type illustrated in fig. 1 (*b*), that is, a change in the position of the bend. A more convincing experiment consisted of bending a crystal into a half-circle of radius ~ 1 cm, mounting the crystal at one end of the diameter, and permitting the other (free) end to actuate the transducer through a tiny quartz rod. In this configuration, azimuthal electric fields failed to produce measurable displacements of the free end, whereas any change in the angle of bending would have caused larger displacements than those observed in the usual (fig. 1) configuration.

§ 4. Discussion

The data from fig. 5 at $\bar{x} = -1$ Å and $\bar{x} = -4$ Å will be considered here, but other experiments on the same crystal and on other LiF crystals gave substantially the same results. If these displacements $\bar{x}$ were produced by a motion s of the 55° bend,

$$\bar{x} = s \sin 55°.$$

The edge dislocations constituting the bend move on the (110) and (110) glide planes at an angle of 45° to the (100) planes forming the surfaces of the crystal (fig. 6). The distribution of dislocations within the bend is complicated when the angle of bending is so large, but a dislocation on a (110) plane and one on a (110) plane can be approximately replaced (insofar as their effect on the external shape of the crystal is concerned) by a single dislocation of larger [010] Burgers vector, as sketched in fig. 6 by dotted lines. The motion to the left of these does not change the radius of curvature of the bend, but some dislocations at the left side move into a previously straight section of crystal, and some at the right leave a curved section and make it straight. Thus the bend as a whole moves a distance $s = r/\sqrt{2}$ along the length of the crystal when the individual dislocations move a distance r along their glide planes. Thus

$$r = \sqrt{2}\bar{x}/\sin 55°. \qquad \text{(3)}$$

Fig. 6

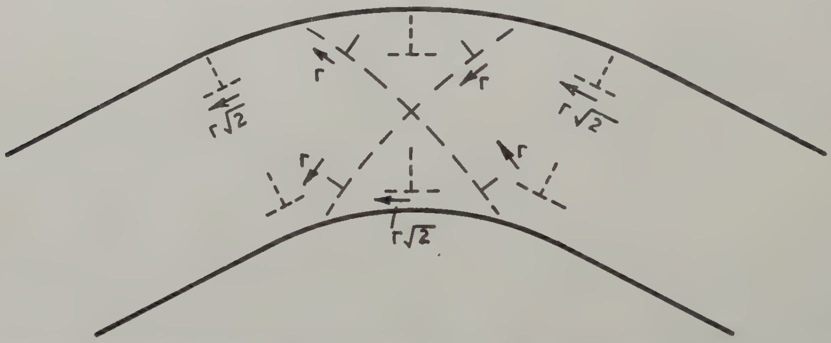

Schematic diagram showing the relation between the motion r of dislocations along glide planes and the motion s of the bend.

Attention will next be directed toward the theory of the motion r as a function of the applied electric field. Lehovec (1953) showed that a space-charge layer should occur at the surface of an ionic crystal because vacancies cannot be formed inside the perfect crystal and because the free energies of formation of positive and negative ion vacancies are in general different. Pratt (1957) and Eshelby *et al.* (1958) made the important advance of suggesting that a similar space-charge region should occur around a dislocation, since dislocations can serve as sources and sinks for vacancies. Equal concentrations n_+ of positive ion vacancies and n_- of negative ion vacancies must occur in the regions of the crystal remote from dislocations in order to preserve electrical neutrality. But if the free energy of formation of a positive ion vacancy, g_+, does not equal the free energy of formation of a negative ion vacancy, g_-, an electrostatic potential difference must occur between the core of the dislocation and the remote regions. If $g_+ < g_-$, as is likely in the alkali halides, the core of the dislocation becomes positively charged, and there is a negative space charge surrounding the core. Thus the further emission of positive ion vacancies (negatively charged) is opposed by the electrostatic field. The dislocation then contains an excess of jogs (Seitz 1950, 1951) of positive sign.

Fig. 7

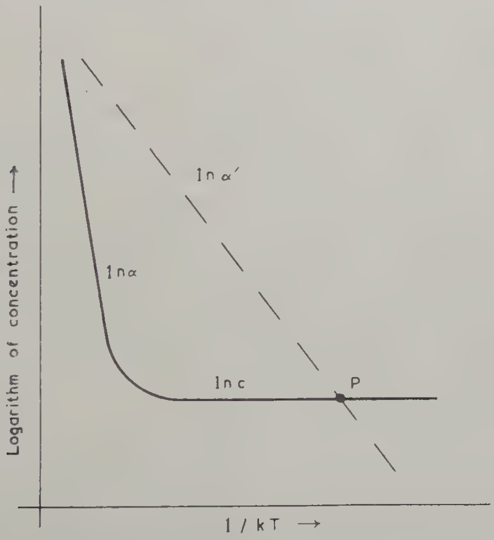

Schematic diagram of the logarithm of the concentration of positive ion vacancies as a function of reciprocal temperature.

The presence of divalent ions in an alkali halide modifies this analysis, since the concentration α of positive ion vacancies then approaches at low temperatures the concentration c of divalent ions. The situation is shown schematically in fig. 7, in which the dashed line is $\alpha' = \exp(-g_+/kT)$ and the solid line is $\alpha = \exp[-(g_+ + g_-)/2kT]$ at high temperatures and $\alpha = c$ at low temperatures. α' is the concentration of positive ion vacancies that would obtain in the absence of the requirement of electrical neutrality, and α is the actual concentration. Dislocations are positively charged when the temperature is above that at the 'isoelectric point' P and negatively charged below. Eshelby *et al.* (1958) have also considered the effects of vacancy–impurity association and impurity precipitation, which add complications to fig. 7.

Eshelby *et al.* (1958) found an approximate expression for the force per unit length F pulling a dislocation toward the centre of its charge cloud when the dislocation was displaced a distance r:

$$F = \frac{-2\sigma^2\kappa}{\epsilon}\left[(\kappa r)^{-1} - K_1(\kappa r)\right]. \qquad . \quad . \quad . \quad (4)$$

Here σ is the dislocation charge per unit length (e.s.u./cm), ϵ is the dielectric constant, K_1 is the Bessel function of imaginary argument (Watson 1952), and κ is defined by

$$\kappa^2 = 8\pi e^2 N\alpha/\epsilon kT,$$

with N the number of cation cites per cm³. Thus κ^{-1} is the characteristic radius of the cylindrical charge cloud surrounding a dislocation. Equation (4) was based on several approximations which limit its quantitative application, especially if the temperature is more than ~20°C from an 'isoelectric' point (the point P in fig. 7).

Eshelby *et al.* (1958) were concerned only with the maximum value (0·40) of the bracket in eqn. (4) in estimating the critical shear stress to pull the dislocation from its cloud, but the interest in the present experiment centres on small values of κr. It is therefore worthwhile to expand $K_1(\kappa r)$ about $\kappa r = 0$ using

$$K_1(\kappa r) = \frac{1}{\kappa r} + \frac{\kappa r}{2}\left(\ln\frac{\kappa r}{2} + 0{\cdot}0772\right) + \frac{(\kappa r)^3}{16}\left(\ln\frac{\kappa r}{2} - 0{\cdot}6728\right) + \ldots \qquad (5)$$

from Watson (1952). Neglecting the term in $(\kappa r)^3$ in (5) makes an error of only 1% at $\kappa r = 0{\cdot}08$, and therefore only the first two terms need be retained when considering small displacements of dislocations.

The force F' on the dislocation by the electric field E is $F' = E\sigma$. In the steady state with field applied, the sum of this force and the force from eqn. (4) is zero, and

$$E\sigma = \frac{-\sigma^2\kappa^2}{\epsilon} r\left(\ln\frac{\kappa r}{2} + 0{\cdot}0772\right). \qquad . \quad . \quad . \quad . \quad (6)$$

The peculiar behaviour of this equation as a function of σ is caused by the assumption that no restoring force other than the electrostatic one is applied, and if σ is too small, this is clearly a poor assumption. On this assumption, however, (6) becomes

$$r\left(\ln\frac{\kappa r}{2} + 0{\cdot}0772\right) = -\frac{\epsilon}{\sigma\kappa^2}E, \qquad . \quad . \quad . \quad . \quad . \quad (7)$$

in which $\ln(\kappa r/2)$ is always <0. It should be noted that $r(E)$ is distinctly non-linear even at extremely small values of κr; the logarithmic derivative is 0·81 at $\kappa r=0{\cdot}01$ and is 0·92 at $\kappa r=0{\cdot}00001$.

The assumption has been made in the above that the charge cloud is fixed. The data of Haven (1950) would indicate appreciable mobility for the positive ion vacancies in LiF at 22°C, however. Any motion of the charge cloud evidently reduces the magnitude of the dislocation motion but should not make a qualitative difference unless the charge cloud motion changes the shape of the crystal.

There is no requirement that the average displacement of the dislocation lines be an integral number of Burgers vectors, or even that the displacement of a single line be limited in this way, since only parts of the line may move. Although dislocations in LiF are in general loops with large screw components (Gilman and Johnston 1957), only the edge components determine the amount and position of the bend. Therefore this analysis is concerned only with these components which are the 'necessary' dislocations to produce the bend.

From the above picture of the effect of an electric field on the charged dislocations, it would be expected that the motion r (or x) would be a completely odd function of V. Thus the non-linearity of the data, analysed according to the procedure of § 3, can be compared with the theory without considering possible errors by loss of terms in even powers of V.

One must resist the temptation to determine the magnitude of α by comparing the non-linearity in $r(E)$ from (7) with the non-linearity of $\bar{x}(E)$ from fig. 5, since clearly too many and too crude approximations have been made in reaching (7). Instead, α will be estimated from ionic conductivity measurements made on these crystals and from the mobility data of Haven (1950) extrapolated to 22°C. This procedure yields a very low value of α, $\alpha_1=2{\cdot}2\times10^{-7}$, which is so low compared to the probable divalent ion impurity concentration that considerable association of vacancies or precipitation of impurities must be occurring. It is quite possible that the space-charge layer could be constructed in part from less mobile species than positive ion vacancies (e.g. divalent ions, charged vacancy aggregates). It may therefore be worth while also to carry through the analysis of the data with $\alpha_2=10^{-5}$ which may be more typical of the concentration of charges available for forming the space-charge cloud.

The corresponding values of κ at 22°C are $\kappa_1=4{\cdot}2\times10^{-5}\,\mathrm{cm}^{-1}$ and $\kappa_2=2{\cdot}8\times10^{-6}\,\mathrm{cm}^{-1}$. From fig. 5, eqn. (3), and the geometry of the crystal, we obtain the pair of data points:

$$\bar{x}=1\,\text{Å},\quad r=1{\cdot}73\,\text{Å},\quad V=710\,\text{v},\quad E=5{\cdot}25\,\text{e.s.u./cm};$$

$$\bar{x}=4\,\text{Å},\quad r=6{\cdot}9\,\text{Å},\quad V=2260\,\text{v},\quad E=16{\cdot}7\,\text{e.s.u./cm}.$$

From the assumption $\alpha=\alpha_1$, we obtain $\sigma_1=2{\cdot}0\times10^{-3}$ e.s.u./cm from the 1 Å data and $\sigma_1=2{\cdot}1\times10^{-3}$ e.s.u./cm from the 4 Å data. The excellent agreement between these two values demonstrates the agreement between the theoretical and observed non-linearity of $r(E)$. From the assumption $\alpha=\alpha_2$, we obtain $\sigma_2=6\cdot6\times10^{-5}$ e.s.u./cm from the 1 Å data and $\sigma_2=8\cdot7\times10^{-5}$ e.s.u./cm from the 4 Å data. The non-linearity no longer is in such good agreement. Although the precise amount of non-linearity in (7) is, of course, dependent on the accuracy of the assumptions and approximations, a non-linearity of this same sense (more rapid than linear dependence of r on E) would be expected from the nature of the physical situation. The assumption that the temperature is near an isoelectric point ($\sinh p\simeq p$ in the notation of Eshelby *et al.* 1958) is well satisfied for $\alpha=\alpha_2$ but not for $\alpha=\alpha_1$.

The values of σ thus obtained are not unreasonable in that jogs in the dislocation lines could provide enough excess charge of one sign, but the σ_1 values ($\sim4\times10^6$ electrons/cm) approach the upper limit of credibility.

Eshelby *et al.* (1958) estimated the critical shear stress Y of electrostatic origin as

$$Y=0\cdot80\sigma^2\kappa/\epsilon\mathbf{b},$$

where $\mathbf{b}$ is the Burgers vector (2·98 Å in LiF). Values of Y corresponding to σ_1, κ_1, and σ_2, κ_2 are $Y_1=5000$ g/cm^2 and $Y_2=50$ g/cm^2. The former of these is unreasonably large, since Gilman and Johnston (1957) have found yield stresses of the order of 1000 g/cm^2 at 300°K. It is noteworthy, however, that the experimental data here for σ and reasonable values of κ predict Y values comparable to the observed yield stress. To some extent this confirms the suggestion of Eshelby *et al.* (1958) that the electrostatic stress is a substantial part of the critical shear stress in ionic crystals.

The *sign* of the charge σ is obviously of interest. It is apparent from the sense of the observed motion (first paragraph of § 3) and the analysis associated with fig. 6 that the dislocations were positively charged. Thus the isoelectric point P of fig. 7 must have been below room temperature. If no vacancy–impurity association or impurity precipitation occurred, it is possible to estimate crudely the value of g_+ for LiF. This task was carried out by using the sign and magnitude of σ, the theory of Eshelby *et al.* (1958), and the value $g_++g_-=2\cdot68$ ev for LiF from Haven (1950). The slope of $\ln\alpha'$ *vs.* $1/kT$ in fig. 7 was adjusted until the vertical separation of the two lines at 22°C was the value computed from the measured σ. The σ_1 results placed P about 100°C below room temperature and led to a very low value of g_+. The σ_2 results, which are probably nearer the actual situation, placed P at about 0°C and led to $g_+=0\cdot3$ ev. Although there appear to be no other experimental or theoretical determinations of g_+, this value is unreasonably low, and therefore a more complicated interpretation of the data involving precipitation or association may be necessary.

It remains to suggest an explanation for the substantial reduction in $r(E)$ after polygonizing the crystal. The dislocation walls after this treatment were about 0·0022 cm apart on the average, and since the curvature in the bend was about 3 radians/cm, the tilt angle in each wall was on the average approximately 0·007 radian, and the dislocations making up the wall were ~400 Å apart. At this separation the individual charge clouds begin to coalesce (especially under the assumption $\alpha=\alpha_1$), and the restoring force at a displacement r is greater than if the dislocations were isolated. This explanation is rather tenuous, especially if $\alpha=\alpha_2$, however, and it may be that immobilization of dislocations by Cottrell atmospheres is the real cause of the reduction in $r(E)$ in the polygonized crystals.

§ 5. CONCLUSION

Evidence has been presented here to indicate that dislocations in LiF at room temperature are charged and can be moved measurable distances by an electric field. The observed magnitude of the charge in part confirms the suggestion by Eshelby *et al.* (1958) that a substantial part of the strength of ionic crystals is electrostatic in origin. It should be possible to use experiments such as the present one to learn interesting features of vacancy formation energies, association, and precipitation in ionic crystals, and such experiments might have an important bearing on the questions of plasticity, hardening, creep, and the temperature dependence of the yield stress in non-metallic crystals. Amelinckx *et al.* (1959) have also observed the effects of charged dislocations in an ingenious experiment quite different from the present investigation.

An obviously important handicap of the present experiment was the inability to vary the temperature over an appreciable range, whereas a variation of 50° or 100° could provide a crucial test of the dislocation interpretation of the effect studied and of some of the assumptions in the analysis. Another interesting experiment would be to bend a crystal, polygonize it, and then straighten it at a temperature $<200°$c; in this way it might be possible to measure the effect of isolated dislocations but with a completely rectangular crystal geometry, which should permit the application of a symmetrical electric field and minimize complicating effects. Among the additional experiments that would be worth while are studies of other ionic crystals, of alkali halides with known concentrations of divalent ion impurities, and of crystals with various heat treatments.

ACKNOWLEDGMENTS

In addition to the help acknowledged in the text, it should be noted here that the assistance of Dr. J. Van Cakenberghe, Mr. P. L. Moentack, and Mr. L. M. Tremouroux was indispensable in this investigation. The encouragement and suggestions of Dr. R. H. Gillette were invaluable. The author is also grateful to Dr. W. W. Webb for a critical study of this work and to the Union Carbide Corporation for its support.

APPENDIX

Whenever an apparatus sensitive to shape or length changes of the order of 1 Å is employed, it is obvious that many possibilities exist for spurious and subsidiary effects to complicate the data and perhaps to hide or to simulate the effect sought. It is never possible to be sure that all such disturbing effects have been avoided or accounted for, but it may be worth while to comment on some of the possible disturbances.

Heating

A temperature rise in the crystal could have caused a decrease in oscillator frequency simply by thermal expansion or by an expansion of the crystal at the inside of the bend that was greater than at the outside. Calculations based on observed currents showed that this displacement x was $< 0{\cdot}05$ Å at $V = 1500$ v. Furthermore, the displacement produced by such expansion should have had a time constant > 1 sec, instead of much < 1 sec as observed, and should have been an even function of V.

Heating by corona currents in the air around the crystal was more troublesome. In early experiments with a 0·1 mm wire connecting the high voltage to the crystal, phenomena simulating plastic deformation (continuous increase of x with time for several minutes) occurred, but these were traced to corona heating which was not the same for positive and negative V's. Corona was identified as the cause by measuring the current drawn from the high voltage supply with and without a crystal in place, and by showing that the 'plastic' effect was proportional to the power dissipated in corona (which had a distinctive voltage dependence). This effect was absent for $V < 3000$ v, even with the 0·1 mm wire, and absent at all voltages used with the 0·25 mm wire.

Electrostriction

Electrostriction is by definition (Cady 1946, Forsbergh 1956) that part of the strain in a substance produced by an electric field which is an even function of the field. No data appear to be available for LiF, but a typical magnitude in other solids is about $10^{-14}E^2$, where E is the electric field in v/cm (Cady 1946).

The longitudinal electrostriction coefficient in LiF was estimated by measuring $x(V)$ for a straight crystal mounted with its long dimension (direction of E) in the direction of the axis E (fig. 2). The strain was closely proportional to E^2, where E is the electric field in v/cm, and was about $5 \times 10^{-16}E^2$. (The transverse coefficient was estimated by a similar experiment with the straight crystal at right angles to the direction of motion of the transducer, and a value $3 \times 10^{-15}E^2$ was computed for the strain.) With the same measuring cycle described in § 2, the displacement x was always the same for positive and negative voltages.

The combination of electrostriction and polarization could have produced a displacement which was not exactly an even function of field, since the internal field would not have had the same magnitude when the external potential difference was reversed in sign. When a strong (10 000 v/cm) polarizing field had been applied for several minutes to the straight crystal described in the preceding paragraph and the usual procedure was then followed for taking data, a small effect of reversing the field was observed, the length of the crystal being greater when the applied field was opposed to the polarizing field. This effect disappeared in about 15 sec after the polarizing field was removed. A similar experiment was performed on a bent crystal. a potential difference of 2000 volts was applied for $1\frac{1}{2}$ min, and then data were taken at 500 v in the usual way. A small spurious effect of reversing V was observed in the first few cycles, but it disappeared in 30 sec. This experiment should have greatly exaggerated the effect of the combination of electrostriction and polarization. The dielectric relaxation time of LiF at room temperature can be estimated from its dielectric constant (9·27) and measurements of the ionic conductivity at room temperature (about $1{\cdot}5\times10^{-10}$ mho/cm for the LiF samples used). This time is about one minute, and therefore polarization fields cannot be sustained for long times. The cycle of taking data was ordinarily strictly timed to prevent the application of voltage of one sign for a longer time than that of the other. Occasionally a voltage of one sign would be sustained for 5 or 10 sec to accentuate any polarization–electrostriction effect, but such an effect never appeared in the experiments described in §§ 2 and 3.

There is another argument against the possibility that the combination of polarization and electrostriction may have created the observed odd-function-of-V effect in bent crystals: if the internal polarization field is E_0, the external applied field is E, and k is a constant, electrostriction would have produced a displacement

$$x=k(E+E_0)^2=kE^2+2kEE_0+kE_0^2.$$

Thus the contribution to x which is an odd function of E (or V) should have been strictly linear in V, and this definitely did not agree with the data.

Electrostriction is quite probably the cause of the V^2 term evident in fig. 4, since E was undoubtedly larger at the inside of the bend than at the outside, and thus electrostriction produced a decrease in oscillator frequency (increase in x). The approximate magnitude of **b** in (2) could be estimated from the electrode geometry and agreed well with the observed magnitude. Furthermore the sign of d could be changed and its magnitude increased a factor of 4 upon exaggerating the non-uniformity in field by the electrode configuration of fig. 8. In principle, then, this even function of V could be reduced to zero by careful design of the electrodes, but this process would be tedious and unnecessary.

Converse Piezoelectric Effect

Although a piezoelectric effect cannot occur in a crystal with the NaCl structure, which has a centre of symmetry, the excess of dislocations of one geometrical sign removes this symmetry. If this interpretation of the effect shown in fig. 5 be assumed, a piezoelectric coefficient of $\sim 4 \times 10^{-11}$ cm/v is computed. This is of the same order of magnitude or an order of magnitude smaller than the piezoelectric constants in crystals for which the effect is permitted by symmetry. It seems quite unreasonable to expect that the small deviation from inversion symmetry produced by bending could produce such a large coefficient.

Surface Effects

It is very difficult to analyse the possibilities of spurious deflections caused by surface charges, but the choice of LiF should have reduced the effects of water adsorption, and the polystyrene coating should also have helped. It should be noted that one crystal was measured before coating with polystyrene and again after coating ; no observable changes in $x(V)$ occurred.

Fig. 8

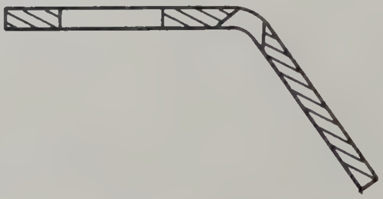

Crystal with electrodes shaped to exaggerate the electrostriction effect.

Electrostatic Effects

Electrostatic forces should have been strictly proportional to V^2. Also, in most of the experiments an electrostatic shield connected to the high voltage (and mechanically supported from the base of the apparatus, *not* from the crystal) surrounded the high-voltage electrode on the crystal. This shield did not even alter the V^2 term appreciably and had no effect at all on the odd function.

Motion of Vacancies

Since there is appreciable ionic conductivity in these crystals at room temperature, the possibility arises of a change in shape or length by ion motion. The dominant mobile species in LiF is the positive ion vacancy (Haven 1950). Whether it expands or contracts the lattice is not known with certainty, but the expansion or contraction cannot be much more than one Li^+ atom volume per vacancy. If this magnitude be assumed, the effect of ionic motion on the shape of the crystal was negligible in the present experiment. Furthermore, such a process should have produced an x which changed continuously for many minutes after the voltage was applied, whereas the observed displacements reached their terminal values in a fraction of a second.

REFERENCES

AMELINCKX, S., VENNIK, J., and REMAUT, G., 1959, *J. Phys. Chem. Solids*, **11**, 170.

CADY, W. G., 1946, *Piezoelectricity* (New York : McGraw-Hill).

ESHELBY, J. D., NEWEY, C. W. A., PRATT, P. L., and LIDIARD, A. B., 1958, *Phil. Mag.*, **3**, 75.

FORSBERGH, P. W. Jr., 1956, *Encyclopedia of Physics*, Vol. **17** (Berlin : Springer), p. 264.

GILMAN, J. J., and JOHNSTON, W. G., 1956, *J. appl. Phys.*, **27**, 1018; 1957, *Dislocations and Mechanical Properties of Crystals* (New York : Wiley), p. 129.

HAVEN, Y., 1950, *Rec. trav. Chim. Pays-Bas*, **69**, 1471.

LEHOVEC, K., 1953, *J. chem. Phys.*, **21**, 1123.

PRATT, P. L., 1957, *Monogr. Ser. Inst. Metals*, **23**, 99.

SEITZ, F., 1950, *Phys. Rev.*, **80**, 239; 1951, *Rev. mod. Phys.*, **23**, 341.

WATSON, G. N., 1952, *Theory of Bessel Functions* (Cambridge: University Press), pp. 78, 80 and Table II.

Electron Microscope Observations on the Annealing Processes Occurring in Cold-worked Silver†

By J. E. Bailey
Crystallographic Laboratory, Cavendish Laboratory, Cambridge

[Received April 1, 1960]

Abstract

Electron microscope observations on the dislocation structure of cold-worked polycrystalline silver and on the processes occurring during annealing are described.

In silver deformed 25% in tension the dislocations are arranged in a cell structure and the stored energy is released in two stages, a recovery stage followed by recrystallization. During the recovery stage there is no observable change in the dislocation distribution but there is a possibility of small-scale dislocation rearrangements within the cell boundaries. Recrystallization occurs by the migration of the grain boundaries originally present in the metal and this process is discussed in some detail.

Observations made on heavily rolled silver annealed either inside the electron microscope on a heating stage or outside the microscope are also described.

§ 1. Introduction

Microcalorimetric experiments reported in a previous paper (Bailey and Hirsch 1960) have shown that the energy stored in cold-worked polycrystalline silver is released in two distinct annealing stages which differ in the form of their annealing kinetics. One of these stages is accompanied by recrystallization, as shown by x-ray diffraction patterns. The other process, called recovery, begins prior to recrystallization when the specimen is annealed isothermally for a short period of time. The present paper reports some results obtained using the transmission electron microscopy technique to elucidate the mechanisms occurring during recovery and recrystallization. One particular aim of the experiments was to determine the nature of the recrystallization nuclei.

Observations were made both on specimens which had just been annealed in bulk outside the microscope and then thinned by electropolishing and on specimens which had been thinned first and then annealed on a heating stage inside the electron microscope.

---

† Communicated by P. B. Hirsch.

§ 2. PREPARATION OF THE SILVER FOILS

Polycrystalline silver specimens (99·99% purity) were deformed 25% in tension in the manner described previously (Bailey and Hirsch 1960) and by cold rolling by varying amounts up to 95% reduction. The cross sections of the specimens prior to deformation were so chosen to give final foil thicknesses of ~0·005 in. The silver foils were then thinned by electropolishing (for solution used see Bailey and Hirsch 1960) and examined in the electron microscope.

Pieces of the foils, deformed 25% in tension or cold rolled to 95% reduction, were annealed in the bulk for various times at temperatures at which complete recrystallization occurred in 15–20 hours, and after thinning were examined in the electron microscope. Some of the heavily rolled specimens were thinned before annealing and examined on a heating stage (Whelan 1957) in the electron microscope.

§ 3. OBSERVATIONS ON FOILS ANNEALED IN BULK

3.1. *Dislocation Arrangement after Cold Work*

In specimens deformed 25% in tension the dislocations are arranged in a cell structure shown in fig. 1 (*a*)†, which was discussed in a previous paper (Bailey and Hirsch 1960). The misorientations across cell walls are small, ~1°, the diffraction patterns from an area covering one cell wall being typical of those from single crystals (fig. 1 (*c*)). The cell boundaries appear to consist of dense 3-dimensional networks: they are not simple dislocation walls.

Foils rolled to 20% reduction had dislocation distributions similar to those found in the extended specimens. With increasing reduction, however, the dislocation density and the misorientations across the cell boundaries increase. Figure 2 shows a series of micrographs of specimens after reductions of 20, 40, 60 and 95% and fig. 3 corresponding diffraction patterns from areas of ~$\frac{1}{3}\,\mu$ diameter. The table lists the average spread in orientation per diffraction spot or cluster of spots for these specimens. It is clear from the diffraction patterns and from the table that not only does the average range of orientations increase with greater deformation, but some of the cells develop into distinct sub-grains, the misorientation increasing considerably. Diffraction patterns were taken from areas including a single cell boundary; for the specimens rolled to 95% reduction, it appears that quite large misorientations, even up to ~10° occur. Some of the boundaries are quite well defined, e.g. fig. 4.

It is interesting to compare the misorientations in the table with those found in previous x-ray work (Gay and Kelly 1953). In the latter experiments the angular spread along a Debye–Sherrer arc from an area of specimen ~20 μ in diameter was measured. These results are also shown in the table. Although the area of examination is many times greater in the x-ray than in the electron case, the misorientations are only greater by a factor of 3 or so. This shows that the orientation does not change in the same sense across a grain but fluctuates about a mean orientation.

---

† With the exception of fig. 12, all figures are shown as plates.

It is difficult to give a precise estimate of the dislocation density in the foil rolled to 95% reduction, an order of magnitude estimate being $\sim 5\times 10^{11}$ cm/cm^3 compared with 7×10^{10} cm/cm^3 for a specimen extended about 25% in tension.

Whereas the grain boundaries in the foils extended 25% in tension generally appear quite straight and do not show any large scale (>1000 Å) discontinuities, it is very difficult to recognise the original grain boundaries in the rolled specimens.

Misorientations in Rolled Foils

Silver (present investigation)		Copper (Gay and Kelly 1953)	
Reduction (%)	Total angular misorientation from $1\frac{1}{2}\,\mu$ diameter region (°)	Reduction (%)	Total angular misorientation within one grain ($20\,\mu$) (°)
		10·8	$3\frac{1}{2}$
20	<2	19·6	6
		28·9	8
40	~ 4		
		49·0	15
60	~ 7		
95	~ 12		

3.2. *Observations on Partially Annealed Specimens*

3.2.1. *Silver foil deformed 25% in tension*

The process of recrystallization was found to be very inhomogeneous on the scale of the electron microscope observations. In the same specimen large areas were recrystallized, while in others no obvious change had taken place as a result of the annealing treatment. In order to study the recrystallization mechanism at an early stage, observations were made on specimens annealed for 1 hour at 200°c; at this temperature complete recrystallization occurs in 15–20 hours. Figure 1 (*b*) shows a typical region of such a specimen which had not recrystallized. Although a small amount of stored energy ($\sim 5\%$) is released during this time (Bailey 1959), there is no observable change in dislocation distribution, as can be seen from a comparison of fig. 1 (*a*) and (*b*). Observations after much longer periods of recovery, corresponding to a larger release of stored energy ($>20\%$), also failed to reveal any observable change in dislocation distribution. However, small rearrangements of dislocations within the complex networks cannot be ruled out.

In other areas of similar specimens the original grain boundaries show bulges which are the result of grain boundary migration during annealing. Examples are shown in figs. 6 and 7. It should be emphasized that after deformation and before annealing, the grain boundaries are generally quite straight (fig. 5). Figure 6 (*a*) and (*b*) show an early stage of the migration process. In fig. 6 (*a*) the original position of the grain boundary is clearly along the line joining the two straight lines on either side of the bulge. The region through which the boundary has moved has a comparatively small dislocation density. This shows that most of the dislocations forming the cell structure are not connected to the boundary and presumably do not originate there. Some dislocations however, do end on the boundary and these increase in length as the boundary moves forward; examples are seen in fig. 6 (*a*). Figure 6 (*c*) shows a later stage in the migration process, the recrystallizing grain A has the same orientation as the cold-worked grain B and the original position of the grain boundary was presumably along the line joining points C and D. Figure 7 shows a case where neighbouring sections of a boundary appear to have moved into adjacent grains.

These observations suggest that recrystallization in these specimens takes place by migration of the original grain boundaries. This process will be considered in more detail in § 5. All the observations to date are consistent with this process of recrystallization. Occasionally completely enclosed recrystallizing grains are observed, as for example in fig. 8. Such grains are thought to originate from movement of original grain boundaries previously above or below the section of the specimen examined.

3.2.2. *Silver foil cold rolled to* 95% *reduction*

Whereas in the specimens deformed 25% in tension no polygonization was observed, in the heavily rolled foils sub-grains are formed as a result of short anneals. Figure 9 (*a*) shows an example of the sub-grains present after a 20 min anneal at 110°c, to be compared with the cold worked structure shown in fig. 2. These specimens recrystallize in 15–20 hours at 110°c.

Figure 9 (*b*) shows an example of the early stage of recrystallization. As in the case of the specimens deformed 25% in tension, recrystallization appears to take place by the migration of a high angle boundary. However, as the original grain boundaries cannot be distinguishd in the cold-worked metal, it is not possible to decide whether the moving boundary formed part of an original grain boundary or of a sub-grain boundary produced during deformation, or as a result of polygonization during annealing. It should be noted that in this material large misorientations across sub-grain boundaries are present after the deformation so that to some extent the difference between the original and newly formed boundaries disappears.

§ 4. OBSERVATIONS ON HEAVILY ROLLED SPECIMENS USING A HIGH TEMPERATURE STAGE

For these experiments silver cold-rolled to 95% reduction was thinned by electropolishing and placed on the mount of the high temperature stage. The foil is heated by passing a d.c. current through the specimen mount. A calibrated ammeter enables the foil to be heated to any required temperature by the operation of a variable rheostat. The high temperature stage was designed by Whelan (1957).

To avoid certain difficulties in operating the stage, e.g. specimen drift, the following procedure was usually adopted: The area selected for observation was heated to the appropriate temperature, allowed to cool down and observed again and this operation was repeated as required; during the heating and cooling operation the electron beam was switched off.

The results obtained on heating these thin foils in the electron microscope showed that they behave in many respects differently to the bulk material.

Figure 10 shows a set of micrographs taken using the technique described above. The micrographs are all taken from the same area and associated diffraction patterns were taken from the central area ($\frac{4}{3}\,\mu$ diameter). Figure 10 (*a*) shows the area at room temperature. Owing to the high dislocation density, dislocations cannot be resolved individually and the area is generally opaque. Heating for four minutes at 200°C and then cooling gave the result shown in fig. 10 (*b*). The micrograph shows clearly that some changes have occurred; sharp boundaries have appeared producing sub-grains at A, B and C. If the sequence of micrographs is followed through it is seen that more sub-grains form and that some grow slightly.

The diffraction patterns taken with the sequence of micrographs show that the greater part of the orientations present originally remains the same throughout the sequence. This observation supports the suggestion that the sub-grains form by a polygonization process. Numerous series of observations similar to these were made.

It is not possible however, to account for all the spots occurring on the diffraction patterns. Several possibilities arise: It is not certain that the diffraction aperture is placed on exactly the same area for each diffraction pattern and therefore new orientations were possibly introduced. Furthermore, during sub-grain growth, neighbouring sub-grains with a new orientation may grow into the region. Finally, the variation in the amount of buckling of the foil during the heating will cause some spots to be excluded and others to be introduced.

The results obtained on annealing these very thin foils in the electron microscope differ considerably from the results obtained on annealing the bulk material. As compared with the bulk material, in which recrystallization produces a grain size of $\sim 20\,\mu$ at 110°C, in these thin foils, a small amount of sub-grain growth occurs rapidly at higher temperatures, and results in a small sub-grain or grain size of $\sim 1\,\mu$.

Further observations on these thin foils suggest that the grain size is a function of the foil thickness. Figure 11 (*a*), (*b*) and (*c*) was taken after heating a specimen to a high temperature in the electron microscope. Figure 11 (*a*) was taken close to an edge of the foil, fig. 11 (*b*) was taken further in from the edge (from such areas most of the previously described observations have been made), fig. 11 (*c*) as far inside the specimen as possible. It is seen that the grain size ($\sim \frac{1}{2}\mu$) near the edge of the foil (fig. 11 (*a*)) increases to several microns far inside the foil (fig. 11 (*c*)). This observation that the grain size increases continuously with increasing thickness of the foil suggests that no new recrystallization mechanism is occurring in the thinner parts of the foil but that the mobility of grain boundaries decreases with decreasing foil thickness. This effect can be qualitatively accounted for if the surface of the foil resists the motion of the boundary. It is clear that the thicker the foil, the smaller will be the effect of this resistance on the migration of a grain boundary, since on the whole there will be less of its boundary in contact with the surface of the foil.

Observations were made on the foils during the heating in an attempt to gain information about the mechanism of sub-grain formation and growth. It was observed that the process occurred very rapidly and jerkily and in this respect was difficult to observe since there was no indication that a particular region was about to polygonize. Attempts to record this process with a ciné camera were unsuccessful. The rapidity and jerky manner with which the process occurred, suggested that the mechanism had some of the features of a slip process.

§ 5. Discussion

According to the conventional nucleation theory (Burke and Turnbull 1952), the nucleation of new grains during recrystallization occurs by a sequence of thermal fluctuations from atomic dimensions. Now for a nucleus to grow the increase in surface free energy must be more than compensated for by the loss in the volume free energy†. Consider a spherical nucleus of radius R; if the nucleus is to grow then:

$$\{4\pi(R+\delta R)^2 - 4\pi R^2\}\sigma < 4\pi R^2 \delta R E$$

where E is the stored energy per unit volume and σ the surface energy; this reduces to

$$R > 2\sigma/E.$$

For silver deformed 25% in tension $E \sim 4$ cals/g atm and $\sigma \sim 500$ ergs/cm^2 and hence $R > \frac{1}{2}\mu$. To produce a nucleus of $\sim \frac{1}{2}\mu$ radius with the aid of thermal fluctuation seems a rather unlikely process. It is sometimes suggested that in local regions of the metal, the value of the stored energy is several orders of magnitude greater than the average value and hence that nuclei of atomic dimensions can grow since $2\sigma/E$ is then very much less than $\frac{1}{2}\mu$. The difficulty with this model is that the stored energy must drop rapidly in the surrounding regions in order to give the low average stored energy value observed, whereas if such a nucleus is to grow the stored energy density must fall off in such a manner that the radius of the growing nucleus is always greater than $2\sigma/E$. In a previous paper (Bailey and Hirsch 1960) it has been shown that the total stored energy can be accounted for in terms of the observed dislocation arrangement in the metal, i.e. dense dislocation arrangements in cell walls. In this model the local stored energy density is a maximum at the core of a dislocation. It is expected therefore, to be easiest to form a nucleus of atomic dimensions at the core; however, it can be easily shown that growth can occur only to atomic dimensions because the surrounding elastic strain energy density from a dislocation falls off too rapidly for the nucleus to grow. It may be thought that a nucleus of ~ 100 Å could grow in the cell walls. For polycrystalline silver deformed in tension the dislocation density N_f in the cell walls is about five times the average dislocation density N (Bailey and Hirsch 1960) and hence in the cell walls the stored energy E_f is $\sim 5E$; therefore $2\sigma/E_f$ is $\sim 1/10\,\mu$. To form a nucleus of this size by thermal fluctuations is quite unreasonable, but even worse, it could not grow out of the cell walls unless its radius $R \sim 1/2\,\mu$, i.e. the possibility of growth is still governed by the average value of the stored energy.

---

† The assumption is made throughout this discussion that the free energy is equal to the difference between the stored energy involved and surface energy absorbed.

It can be concluded therefore that for the distribution and density of dislocations observed in the cold-worked metal, recrystallization by a process of random nucleation is ruled out. For the nucleation process, R must be ~ 10 Å and hence this process would be possible only if $E \sim 10^3$ cals/g atm corresponding to a dislocation density of $\sim 10^{14}$ cm/cm^3; this value is very unlikely and so far there is no evidence for such high dislocation densities in local regions of a deformed metal. Furthermore, recrystallization occurs in materials with lower dislocation densities than those considered here. For this reason the theory due to Cahn (1950), which suggests that recrystallization nuclei are produced by the polygonization of dislocations to form sub-grains which then grow preferentially, seems particularly plausible.

In actual fact the observation is that in silver foils deformed in tension recrystallization occurs by the migration of the grain boundaries. Beck and Sperry (1950) observed this mechanism, which they called strain induced boundary migration, when annealing aluminium cold-rolled to moderate deformations. Their observations were on a much larger scale than those presented here. The grain size of the aluminium was $\sim 10^4\,\mu$ as compared with $\sim 10\,\mu$ for the silver used in this investigation and they observed regions of the grain boundaries of $\sim 10^3\,\mu$ in length to bulge out and grow into the neighbouring grains, as compared with regions $\sim 1\,\mu$ in length in the present case. These combined observations strongly suggest that for moderate deformation most polycrystalline metals recrystallize by this grain boundary migration mechanism. The problem now is to decide on the criterion for migration of the boundary. A simplified model is envisaged here (fig. 12) in which a circular area of grain boundary of diameter $2L$ bulges out into the shape of a spherical cap and migrates; such a model is in accordance with the observations. The boundary will migrate provided that there is a difference in free energy ΔF across the boundary; that is, provided that the energy released by the migration more than compensates for the increase in surface energy. Now the change in free energy will be given by:

$$\Delta F \,.\, \delta V = E\,\delta V - \sigma\delta A \qquad (1)$$

where δA is the increase in boundary area when the volume δV is swept through by the grain boundary and E is the stored energy difference across the boundary and σ the grain boundary energy. For migration ΔF must be positive, that is:

$$E > \sigma\,\delta A/\delta V. \quad . \quad . \quad . \quad . \quad . \quad . \quad . \quad . \quad . \qquad (2)$$

Fig. 12

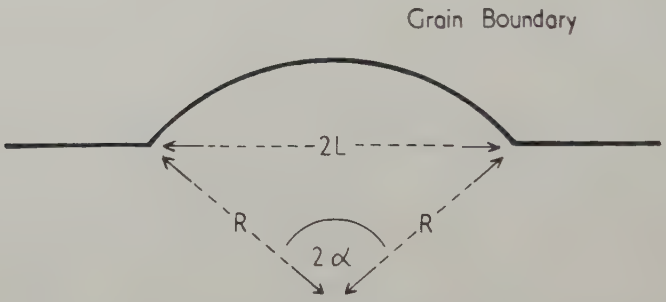

Model for the grain boundary migration process.

For the above model (fig. 12)

$$\delta A/\delta V = 2\sin\alpha/L \quad . \quad . \quad . \quad . \quad . \quad . \quad . \quad . \quad . \quad . \qquad (3)$$

which has a maximum of $2/L$ when $R=L$ and hence:

$$E \geqslant 2\sigma/L.$$

Thus provided an area of radius $>L$ moves forward there is a positive driving force. But the rate of advance or of formation of the bulge depends on the nature of the migration process on an atomic scale. For silver deformed $\sim 25\%$ in tension $E \sim 4$ cals/g atm and thus $L > \frac{1}{2}\,\mu$, which agrees favourably with the observations.

The treatments of grain boundary migration occurring in the literature (Burke and Turnbull 1952, Cole *et al.* 1954) are based on models in which an atom is transferred across the boundary and the linear rate of growth G is given by:

$$G = C\,.\,\Delta F\,.\exp(-U)/KT \quad . \quad . \quad . \quad . \quad . \quad . \quad . \qquad (4)$$

where U is the activation energy for the transfer of atoms from the cold-worked side of the boundary to the other side, T is the temperature,

K Boltzmann's constant and C a constant, at a given temperature. From eqn. (4) it is seen that G is proportional to ΔF and substituting for ΔF from eqn. (1):

$$G=B\,.\,\Delta F=B(E-\sigma\delta A/\delta V), \qquad (5)$$

B being a constant at a given temperature. It is clear from eqns. (5) and (3) that the migrating boundary region will initially decelerate until $R=L$ (i.e. when $\delta A/\delta V$ reaches a maximum) and will then accelerate again; further, unless $L>2\sigma/E$ the regions of boundary decelerate and come to a halt, otherwise ΔF would become negative. The time taken by the migrating boundary to reach the position where $R=L$ may be looked upon as a nucleation period.

The process of grain boundary migration can then be considered to proceed as follows: migration may start at an area of boundary across which there is a fairly large difference in dislocation density. As soon as the boundary has moved a dislocation free region is generated on one side so that the driving force is then governed by the average value of the stored energy. Although the stored energy associated with the dislocations is responsible for the driving force for the migration process and produces a positive value of ΔF in eqn. (4), the main rate determining factor is the activation energy U which is only affected to a very small degree by the dislocations. The above model does not enquire into the mechanism by which the boundary migrates on an atomic scale. It does not imply a particular value for the activation energy or whether the activation process is affected by dislocations ending in the boundary. Although the process may be expected to be influenced where dislocations end in the boundary, most of the boundary must migrate by the normal process and therefore, the average activation energy U is not expected to be greatly affected by dislocations. The value of U might be expected to be about that for grain boundary self diffusion. The observations discussed here do not provide information on the nature of the migration process since boundary migration was not observable in the electron microscope. It is proposed to discuss this process in more detail in a later paper.

The observations on the recrystallization of heavily rolled foils (95% reduction) are less conclusive. Although recrystallization is seen to occur by the migration of high angle boundaries, it is possible that the sub-grains which are observed to form by polygonization are also able to migrate. Due to the high misorientations observed in these foils a sub-grain boundary need only migrate a small distance before becoming essentially a high-angle boundary. For this reason and the fact that the original grain boundaries were indistinguishable, it was not possible to determine whether recrystallization occurred by the migration of the old grain boundaries or by sub-grain boundaries or by both. In a sense the distinction between these two mechanisms is trivial since the straight forward interpretation of the observations presented here is that in all cases recrystallization occurs by the migration of the high angle boundaries present in the material regardless of their origin. For this reason it would seem of great interest to investigate the conditions under which deformed single crystals recrystallize.

ACKNOWLEDGMENTS

The author is indebted to Professor N. F. Mott, F.R.S., and to Dr. W. H. Taylor for their interest and encouragement. He particularly wishes to thank Dr. P. B. Hirsch for his useful criticism and for a very full discussion of the content of this paper. Thanks are also due to Messrs. C. K. Jackson and G. Rickards for assistance in electron microscopy. The author wishes to acknowledge the receipt of a maintenance grant from the Admiralty.

REFERENCES

BAILEY, J. E., 1959, Ph.D. Dissertation, University of Cambridge.
BAILEY, J. E., and HIRSCH, P. B., 1960, *Phil. Mag.*, **5,** 485.
BECK, P. A., and SPERRY, P. R., 1950, *J. appl. Phys.*, **21,** 150.
BURKE, J. E., and TURNBULL, D., 1952, *Prog. met. Phys.*, **3,** 220 (London: Pergamon Press).
CAHN, R. W., 1950, *Proc. phys. Soc. Lond.*, A, **63,** 323.
COLE, D. G., FELTHAM, P., and GILLIAM, E., 1954, *Proc. phys. Soc. Lond.*, B, **67,** 131.
GAY, P., and KELLY, A., 1953, *Acta Cryst.*, **6,** 165.
WHELAN, M. J., 1957, Ph.D. Dissertation, University of Cambridge.

Strain-broadening of Nuclear Magnetic Resonance Lines in Copper†

By E. A. Faulkner
Division of Tribophysics, Commonwealth Scientific and Industrial Research Organization, University of Melbourne, Australia

[Received January 25, 1960]

Abstract

The mean-square width of the nuclear magnetic resonance absorption line in copper sheet has been measured with an accuracy of ± 4%, using specimens from a sample of copper (99·98% Cu) on which stored energy measurements had already been made (Clarebrough *et al.* 1957). Plastic deformation has been found to increase the mean-square line width by up to 40% and there is evidence that the broadening is proportional to the stored energy. There is also a small reduction in the integrated intensity of the line in deformed specimens, possibly caused by the high strains in regions near the cores of dislocations.

The results can be interpreted satisfactorily on a model where both the line width and the stored energy are calculated from the state of strain of the material.

§ 1. Introduction

Some preliminary measurements of the nuclear magnetic resonance in rolled copper sheet have already been reported (Faulkner 1959 a). The accuracy of these experiments was severely limited by the effects of eddy-currents and preferred orientation, but they were sufficient to show that the sensitivity of the resonance line to deformation had previously been overestimated by a factor of 10 or more (Bloembergen 1955); this was confirmed by measurements on copper sheet subjected to elastic strain (Faulkner 1959 b).

The experimental technique has now been improved so that measurements of the mean-square line width in copper sheet are possible with a standard deviation of ± 4%. Plastic deformation has been found to cause a definite broadening of the line, and this paper describes measurements of the line width and intensity as a function of the degree of plastic deformation by rolling. The material used was O.F.H.C. copper (99·98% Cu) on which stored energy measurements had already been made (Clarebrough *et al.* 1957) for similar amounts of deformation by compression.

All measurements were made at room temperature, on the ^{63}Cu resonance.

---

† Communicated by W. Boas.

§ 2. Apparatus

The spectrometer is of the marginal-oscillator type, operating at 5·5 Mc/s. It is based on a Colpitts oscillator coupled to a crystal detector which is connected through a high resistance to the grid of the oscillator valve, so that this valve also acts as the first audio-frequency amplifier. This arrangement has been found more sensitive than a simple regenerative detector (Gutowsky *et al.* 1953), and gives much better control of oscillation amplitude with change of frequency. The frequency is swept at a rate of 26 kc/s per hour by a synchronous motor which drives the tuning capacitor through a reduction gear. The detector is relatively insensitive to direct pick-up from the modulation coils, so no compensating coil is necessary.

A permanent magnet is used, with a gap of 11·4 cm diameter and 3·8 cm length, in which the field is 4·9 kilogauss. The field is sinusoidally modulated at a frequency of 350 c/s with peak-to-peak amplitude of 5·0 gauss, which is nearly equal to the line width.

The audio-frequency signal is fed to a pentode preamplifier mounted in the oscillator housing, and then to a transistor amplifier with a gain of 50 dB; this is run from a transistor-stabilized direct current supply which also provides the current for the heaters of the oscillator and preamplifier valves. The output of the amplifier, which is about 1 volt peak-to-peak, is fed to a transistor phase-sensitive detector (Faulkner 1959 c) with a time-constant of 5 sec, connected to a 0–10 millivolt Varian recorder.

§ 3. Evaluation

Three parameters are extracted from the recorded curves: these are the mean-square line width $\overline{\Delta f^2}$, the integrated intensity I, and the 'derivative maximum' $G_{\max}$. In the recorded curve the abscissa is proportional to the oscillator frequency f and the ordinate to the output voltage $G'(f)$ of the phase-sensitive detector. The curve has the same general appearance as the usual 'derivative' curve but is not quite antisymmetric, the maximum value on the high-frequency side being about 15% greater than the corresponding value on the low-frequency side. This distortion is due to eddy currents in the specimen (Chapman *et al.* 1957). A function $G(f)$ can be defined by

$$G(f)=G(f_0'+\Delta f)=\tfrac{1}{2}[G'(f_0'+\Delta f)-G'(f_0'-\Delta f)] \quad . \quad . \quad . \quad (1)$$

where f_0' is the frequency for which $G'=0$. This process is equivalent to taking a mean of the magnitudes of G' at equal intervals from f_0', and, because the distortion is small, G should be a good measure of the output voltage in the absence of distortion.

Using the analysis of Andrew (1953), one can now calculate the mean-square line width $\overline{\Delta f^2}$ from the formula

$$\overline{\Delta f^2}=\frac{\int_0^\infty (f-f_0')^3G(f)df}{3\int_0^\infty (f-f_0')G(f)df}-\frac{\gamma^2 h_m{}^2}{4} \quad . \quad . \quad . \quad . \quad . \quad (2)$$

where γ is the gyromagnetic ratio and h_{m} is the modulation amplitude; also the integrated intensity I from the formula

$$I=\int_0^\infty (f-f_0')G(f)\,df \quad . \quad . \quad . \quad . \quad . \quad . \quad . \quad . \quad (3)$$

which gives I in units which depend on the experimental parameters.

In order to carry out the integrations, the experimental curve was traced from the recorder chart on to graph paper and values of G' were read at intervals of 0·25 cm, corresponding to frequency intervals of 0·44 kc/s. This gave about 55 non-zero numerical values for each line.

The parameter which is referred to as $G_{\max}$ was obtained for each line by averaging the two highest numerical values of G. The ratio $I/G_{\max}$ for a line has the same units as the mean-square width, and has been found to be a very useful empirical measure of line width, although its value cannot be simply corrected for modulation broadening.

§ 4. SPECIMENS

A strip of copper of size 5·1 × 2·3 × 0·18 cm was machined from the bar which provided the specimens for the stored energy experiments referred to previously (Clarebrough *et al.* 1957). This was annealed for one hour at 600°C, after which strips were rolled from it of thickness 0·010, 0·005, 0·0033 and 0·0025 cm, the rolling being done in alternate directions with about 10% reduction at each pass. The thinnest of these strips had been reduced by 98·6% in thickness. The three thicker strips were recrystallized by being annealed for 10 min at 300°C and were then rolled down to a thickness of 0·0025 cm, corresponding to reductions in thickness of 75, 50 and 25%.

Each specimen consists of two pieces cut from the rolled strips, each piece measuring 6·0 × 0·6 × 0·0025 cm. These are wrapped in rice paper and wound into a tight spiral of outer radius 0·25 cm which is fitted into a glass tube; this tube can be slid into the specimen coil of the spectrometer.

In this spiral type of specimen, the effects of preferred orientation are minimized and thinner sheet can be used than in the parallel-sheet type of specimen used previously without any sacrifice of rigidity, so that eddy-current distortion of the line is greatly reduced. The specimen has good thermal contact with the wall of the glass tube, and can be heat-treated without being removed from the tube. The extra deformation involved in winding the strip has been found to be negligible compared with the deformation by rolling.

§ 5. EXPERIMENTAL PROCEDURE

Specimens were prepared from each of the rolled strips and the following experiments were done:

(1) The nuclear magnetic resonance absorption line was observed over a frequency range of 50 kc/s, which is about eight times the line width. This wide range was necessary in order to obtain an accurate zero level, because the tails of the line extended over a range of up to 25 kc/s. Lines were

recorded from two specimens of each deformation, and then a second set of strips was rolled and lines were recorded from one more specimen of each deformation. The mean-square width and integrated intensity of each line were obtained by the methods already described.

(2) Deformed specimens were heated at a rate of 6°c per minute in an oil bath, from which they were removed at suitable intervals to allow the absorption line to be recorded, and then returned to the bath for the heating to be continued. So that the experiment could be done in a reasonably short time, the frequency range was limited in these experiments to about 10 kc/s, which was sufficient to enable $G_{\max}$ to be measured but not the other line parameters. The value of $G_{\max}$ for a line can be measured with an estimated accuracy of about ± 1·5% in 25 min, so it will be seen that this is a convenient quantity to follow through the process of recrystallization.

§ 6. Results

The observed mean-square line widths and values of $I/G_{\max}$ for the various deformations are listed in the table, with the standard deviations of eight observations on three separate specimens; the results listed under zero deformation refer to nine observations on four specimens which had been recrystallized (see below) after deformations ranging from 25 to 99%. The table also shows values of stored energy obtained by interpolation from the results given by Clarebrough *et al.* (1957) for deformation by compression, which may be assumed to be approximately equal to the stored energy in specimens which have been subjected to the same amount of deformation by rolling. In fig. 1 the observed mean-square line widths are plotted against these values of stored energy.

Deformation (%)	0	25	50	75	99
Mean-square width (kc/s)^2	7·4 ±0·2	8·9 ±0·3	9·3 ±0·4	10·0 ±0·4	10·2 ±0·3
$I/G_{\max}$ (kc/s)^2	1·06±0·02	1·17±0·03	1·22±0·02	1·28±0·04	1·30±0·03
Relative value of $I/G_{\max}$	1·00	1·10	1·15	1·20	1·22
Stored energy (cal/g)	0·000	0·088	0·121	0·154	—
Relative value of $G_{\max}$ after recrystallization	1·00	1·12	1·21	1·27	1·33

The results of the annealing experiments are shown in fig. 2. It can be seen that a sudden increase in $G_{\max}$ occurs for each specimen in a range of temperature which is lower the higher the degree of deformation. It is found that this range of temperature corresponds to that in which the evolution of stored energy and changes in properties accompanying recrystallization have been observed (Clarebrough, Hargreaves and West, private communication). The increase in $G_{\max}$ on annealing is therefore attributed to recrystallization.

Relative values of $G_{\max}$ before and after recrystallization are obtained from the initial and final levels in these curves and are listed in the table.

Fig. 1

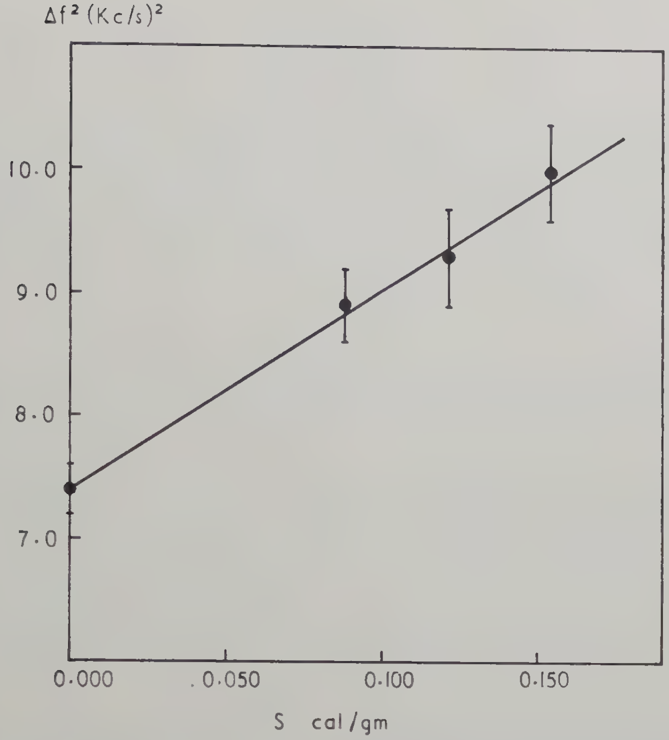

Mean-square line width in deformed and annealed copper sheet, plotted against stored energy figures. The equation of the drawn line is $\overline{\Delta f^2} = 17S + 7{\cdot}4$.

Fig. 2

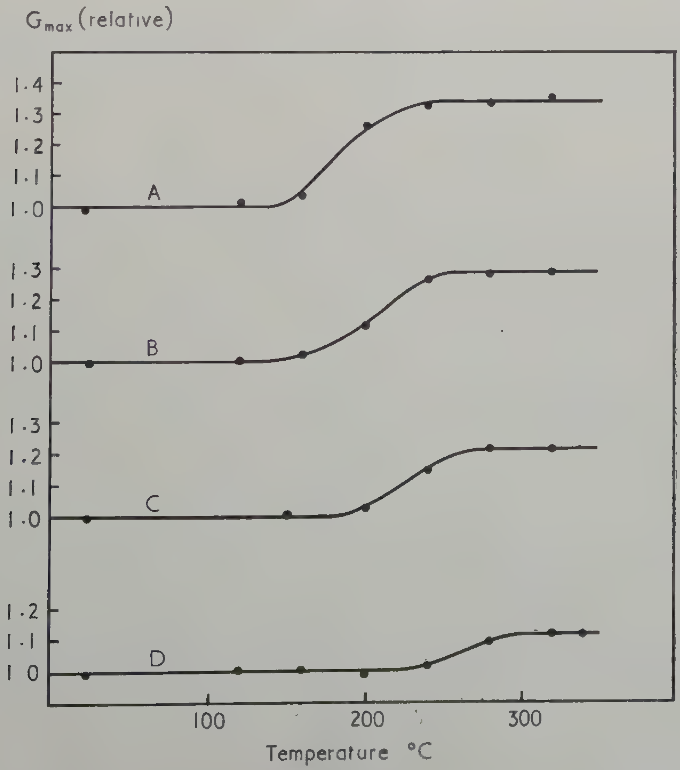

Nuclear magnetic resonance in rolled copper sheet heated at 6°c per minute. Deformation: A, 99%, B, 75%, C, 50%, D, 25%.

§ 7. Discussion

Strain-broadening of nuclear magnetic resonance lines is due to electric quadrupolar interactions, as distinct from the magnetic dipolar interactions which are the cause of the line width in a strain-free cubic crystal. Since there is no correlation between these two mechanisms, the resultant mean-square line width is simply the sum of the dipolar and quadrupolar contributions:

$$\overline{\Delta f^2} = \overline{\Delta f_{\mathrm{D}}{}^2} + \overline{\Delta f_{\mathrm{Q}}{}^2}. \qquad (4)$$

The quadrupolar perturbation of the nuclear magnetic energy levels at a given site depends on the electric field gradient grad grad ϕ, which is zero in the case of perfect cubic symmetry and which is linearly related, in the case of small strain, to the value of the strain tensor at the site (Cohen and Reif 1957). In first-order perturbation the frequency shift Δf of the nuclear magnetic resonance is proportional to $\phi_{z'z'}$ where z' is the direction of the applied magnetic field, the other components of grad grad ϕ being inoperative. Since the stored energy of a randomly strained isotropic material is proportional to the mean-square value of the strain, and since the strain distribution in polycrystalline rolled sheet approximates to a random one, it may reasonably be assumed that the mean-square value of $\phi_{z'z'}$ is proportional to the stored energy. These considerations lead to the following theoretical relation between the stored energy S and the quadrupolar contribution $\overline{\Delta f_{\mathrm{Q}}{}^2}$ to the mean-square line width:

$$\overline{\Delta f_{\mathrm{Q}}{}^2} = kS. \qquad (5)$$

It will be seen from fig. 1 that a straight line can easily be drawn through a plot of the observed values of $\overline{\Delta f^2}$ against S. Comparison of the equation of this line with eqns. (4) and (5) leads to the result

$$k = 17\ (\mathrm{kc/s})^2 \text{ per (calorie per gram)}. \qquad (6)$$

The other information that can be derived from these results concerns the integrated intensity of the lines. Experiments on alloys (Bloembergen and Rowland 1953) indicate that the quadrupolar interactions rise very sharply in the neighbourhood of a solute atom so that quadrupolar interactions at the adjacent sites are sufficient to eliminate their contribution to the observed nuclear magnetic resonance line, while the resonance at other sites is only slightly affected. A similar effect may be expected near the core of a dislocation, so that the presence of dislocations will result in a reduction in the integrated intensity I of the line (which is proportional to the number of nuclei taking part in the resonance) compared with the corresponding value for a perfect crystal. Small changes in the absolute value of I are not easy to measure experimentally because of slight variations in the overall sensitivity of the apparatus from day to day but measurements of the value of $I/G_{\max}$ are not affected by such variations. A useful indication of any change in I can therefore be obtained by comparing the ratio $G_{\max}$ (recrystallized)/$G_{\max}$ (deformed) from the annealing experiments with the relative values of $I/G_{\max}$ in the deformed and annealed states.

If I remained constant during annealing, these two ratios would be equal, but it can be seen from the table that the relative change in $G_{\max}$ is always slightly more than the corresponding ratio of $I/G_{\max}$ values so it seems that I does increase by a few per cent during recrystallization.

It will be seen from the table that the line width for the 99% deformed specimen is very little more than that for the 75% deformed specimen, although the increase in $G_{\max}$ on annealing is significantly greater. In the absence of stored energy data for this degree of deformation, no attempt will be made to interpret this fact; however, it is consistent with the fact that in copper filings, which may show a much larger increase in $G_{\max}$ on annealing, there is no very marked broadening of the line at any stage in the annealing process.

The results of the earlier annealing experiments on parallel-sheet specimens (Faulkner 1959 a) agree within experimental limits with the more accurate results quoted here except for the case of 25% deformation. [In the report of these experiments the quantity $G_{\max}$ was referred to as the *intensity* of the line, following previous practice (Bloembergen and Rowland 1953).] Because of eddy-current effects, the strain-broadening of the line was not observed in these experiments and it was assumed that changes in $G_{\max}$ on annealing were largely due to variations in the integrated intensity; however, it now appears that the main cause of such changes is variation in the line width and shape.

§ 8. CALCULATION OF STRAIN-GRADIENT TENSOR

The quadrupolar perturbation of the nuclear magnetic energy levels at a given site depends on the electric field gradient grad grad ϕ, which is connected with the strain at the site by a fourth-order tensor which may be written, by the use of the Voigt notation, in terms of components F_{ij}; in the case of cubic symmetry there are only two independent components, $F_{11}=-2F_{12}$ and F_{44}. The values of these components may be calculated from the observed constant of proportionality between stored energy and line broadening in polycrystalline material if assumptions are made about (*a*) the relation between F_{11} and F_{44} and (*b*) the strain distribution in the specimen.

(*a*) It is reasonable to suppose that the field gradient is due to the displacement of charges in a uniformly deformed lattice, and this assumption leads to the relation (Cohen and Reif 1957) $F_{44}=F_{12}$ which has been confirmed experimentally for single crystals of InSb (Shulman *et al.* 1957) and which has been used in all the calculations in this work.

(*b*) There are various possible assumptions that can be made about the strain distribution in the deformed material. The simplest one is that there is only elastic shear strain, randomly distributed in direction and magnitude, and that all the stored energy resides in the regions of the crystal which contribute to the nuclear magnetic resonance, the effect of dislocation cores being ignored. This assumption will be used in the calculation which follows.

Let the strain at any lattice site in a cubic crystal have the single component $E=E_{x''y''}$, the direction cosines of the x'' and y'' axes referred to the crystal axes being $(l_1,\ l_2,\ l_3)$ and $(m_1,\ m_2,\ m_3)$ respectively. The strain components in the crystal axes are then

$$\left.\begin{array}{lll} E_{xx}=l_1m_1E, & E_{yy}=l_2m_2E, & E_{zz}=l_3m_3E, \\ E_{yz}=(l_2m_3+l_3m_2)E, & E_{zx}=(l_3m_1+l_1m_3)E, & E_{xy}=(l_1m_2+l_2m_1)E, \end{array}\right\} \quad (7)$$

and the components of grad grad ϕ are obtained by multiplying by the tensor F, in which $F_{11}=-2F_{12}=-2F_{44}$. This gives

$$\left.\begin{array}{l} \phi_{xx}=F_{11}(E_{xx}-\tfrac{1}{2}(E_{yy}+E_{zz}))=\tfrac{3}{2}F_{11}l_1m_1E, \\ \phi_{yz}=-\tfrac{1}{2}F_{11}E_{yz}=-\tfrac{1}{2}F_{11}(l_2m_3+l_3m_2)E, \end{array}\right\} \quad . \quad . \quad . \quad . \quad (8)$$

with corresponding expressions for the other components of grad grad ϕ.

In first-order quadrupolar perturbation of nuclear magnetic energy levels the only operative component of grad grad ϕ is $\phi_{z'z'}$ where the z' axis is the direction of the applied magnetic field, with direction cosines $(\lambda_1.\ \lambda_2,\ \lambda_3)$ referred to the crystal axes. This component is given by

$$\phi_{z'z'}=\lambda_1{}^2\phi_{xx}+\lambda_2{}^2\phi_{yy}+\lambda_3{}^2\phi_{zz}+2(\lambda_2\lambda_3\phi_{yz}+\lambda_3\lambda_1\phi_{zx}+\lambda_1\lambda_2\phi_{xy}) \quad . \quad . \quad (9)$$

and its mean-square value may be obtained by averaging this expression over all the sites in a randomly oriented array of crystals

$$\overline{\phi_{z'z'}{}^2}=\tfrac{1}{5}(3\overline{\phi_{xx}{}^2}+4\overline{\phi_{yz}{}^2}+2\overline{\phi_{xx}\phi_{yy}}). \quad . \quad . \quad . \quad . \quad (10)$$

The averages in this equation are obtained from eqns. (8) by assuming a random distribution of the l's and m's, the result being

$$\overline{\phi_{z'z'}{}^2}=\tfrac{1}{10}F_{11}{}^2\overline{E^2}. \quad . \quad . \quad . \quad . \quad . \quad . \quad . \quad . \quad (11)$$

The corresponding broadening of the nuclear magnetic resonance line can be calculated from the well-known formulae for first-order quadrupole interaction (Pound 1950): the result for copper, in c.g.s. electrostatic units, is

$$\overline{\Delta f_Q{}^2}=1\cdot8\times10^{-17}\overline{\phi_{z'z'}{}^2}=1\cdot8\times10^{-18}\,F_{11}{}^2\,\overline{E^2}, \quad . \quad . \quad (12)$$

allowance having been made for the fact that the central component of the line, comprising 40% of its intensity, is not broadened in first-order approximation.

The strain energy density is simply $\frac{1}{2}\mu E^2$ where μ is the shear modulus so the stored energy per unit mass is given by

$$S=\mu\overline{E^2}/2\rho \quad . \quad . \quad . \quad . \quad . \quad . \quad . \quad . \quad . \quad (13)$$

where ρ is the density. The value of F_{11} can now be found by combining eqns. (12) and (13) and putting in the observed value of $\overline{\Delta f_Q{}^2}/S$ from eqn. (6) which is equal to 0·41 (c/s)^2 per (erg/g), and the known values of μ and ρ for copper. The final result is

$$F_{11}=7\times10^{13}\ \text{c.g.s. electrostatic units.} \quad . \quad . \quad . \quad (14)$$

This result is probably somewhat lower than the true value, because no account is taken of any reduction in integrated intensity which may be caused by the deformation; this is equivalent to ignoring the strain energy of the regions in the crystal where the strain is very high.

It is interesting to compare the result (14) with estimates of the components of F made on the assumption that the field gradient is due to the displacement of unit electronic charges e located at the lattice points of a uniformly deformed lattice. A sum over the twelve nearest neighbours in a face-centred cubic lattice gives $F_{11} = 6ea^{-3}$, where a is the nearest neighbour distance, and this is equal to $1{\cdot}75 \times 10^{14}$ c.g.s. electrostatic units for copper. The ratio of the actual value of F_{11} to this estimate has been referred to as the anti-shielding factor because its value was thought to be greater than unity; however, this calculation suggests that it is about 0·4. This is much lower than corresponding values for ionic compounds (Watkins 1952) and semi-conductors (Shulman *et al.* 1957), presumably because of the effect of conduction electrons.

ACKNOWLEDGMENT

The author wishes to acknowledge the contribution made to this work by Dr. M. E. Hargreaves, whose advice and cooperation have been invaluable. Thanks are also due to Dr. A. K. Head, Dr. J. K. Mackenzie, and Mr. G. W. West for many valuable discussions.

REFERENCES

ANDREW, E. R., 1953, *Phys. Rev.*, **91,** 425.

BLOEMBERGEN, N., 1955, *Report on the Bristol Conference*, **1** (London: The Physical Society).

BLOEMBERGEN, N., and ROWLAND, T. J., 1953, *Acta Met.*, **1,** 731.

CHAPMAN, A. C., RHODES, P., and SEYMOUR, E. F. W., 1957, *Proc. phys. Soc. Lond.*, B, **70,** 345.

CLAREBROUGH, L. M., HARGREAVES, M. E., and WEST, G. W., 1957, *Acta Met.*, **5,** 738.

COHEN, M. H., and REIF, F., 1957, *Solid State Physics*, **5,** 321 (New York: Academic Press).

FAULKNER, E. A., 1959 a, *Nature, Lond.*, **183,** 1043; 1959 b, *Ibid.*, **184,** 442; 1959 c, *J. sci. Instrum.*, **36,** 321.

GUTOWSKY, H. S., MEYER, L. H., and MCCLURE, R. E., 1953, *Rev. sci. Instrum.*, **24,** 644.

POUND, R. V., 1950, *Phys. Rev.*, **79,** 685.

SHULMAN, R. G., WYLUDA, B. J., and ANDERSON, P. W., 1957, *Phys. Rev.*, **107,** 953.

WATKINS, G. D., 1952, *Ph.D. Thesis*, Harvard University.

Observation of Interstitial Atoms in F.C.C. Metals†

By A. Seeger, P. Schiller, and H. Kronmüller
Max-Planck-Institut für Metallforschung, Stuttgart, and Institut für theoretische und angewandte Physik der Technischen Hochschule Stuttgart, Germany

[Received May 8, 1960]

For a number of years, among the outstanding problems in the study of lattice defects in f.c.c. metals there have been the properties of atoms on interstitial lattice sites as produced by cold-work or radiation damage. Considering copper as an example, the key problem was whether the energy of migration of interstitial atoms was about 0·1 ev or about 0·6 ev. In the first case, the interstitial atoms would anneal out below 60°K, whereas in the second case the so-called annealing stage III (at about 250°K) would have to be ascribed to the annealing out of the interstitial atoms. So far no specific experiment has been published that would demonstrate directly the presence or the behaviour of isolated interstitial atoms in f.c.c. metals. The two views mentioned above are based on the analysis of a large body of experimental material, the interpretation of which includes the assignment of migration and formation energies to lattice defects other than interstitials. Recent reviews emphasizing the one or the other of the two principal viewpoints are those by Seitz (1959; small migration energy of interstitials) and by Seeger (1958, 1960; large migration energy of interstitials).

A recent theoretical study of interstitials in copper (Seeger *et al.* 1960) using the model of Seeger and Mann (1960) has given the following results:

(i) The interstitialcy configuration (fig. 1 *b*; Huntington and Seitz (1942)) has a lower energy than the position in the cube centre (fig. 1 *a*), in agreement with the results of Gibson *et al.* (1960).

(ii) The energy difference between the interstitialcy configuration (fig. 1 *b*) and the configuration with cubic symmetry (fig. 1 *a*) is of the order 0·6 ev–0·7 ev. This suggests that the energy of migration of an interstitial atom is of about the same magnitude.

An experimental check of these theoretical results appears possible as follows: According to the calculations, the stable configuration of an interstitial has a tetragonal symmetry with a preferred ⟨100⟩ axis. In an unstressed cubic crystal an equal number of interstitials will have their preferred directions parallel to each of the three cube axes, whereas under the action of an applied stress or (in a ferromagnetic crystal) in the

---

† Communicated by the Authors.

presence of a magnetic field an asymmetric distribution will have a lower free energy. The transition of a random distribution to such a partially ordered one should give rise to a relaxation phenomenon similar to the so-called Snoek–effect of carbon atoms in α-iron. Estimates show the mechanical 'relaxation strength' per atom should be about the same in both cases.

There are, however, two important differences between the interstitial atoms in f.c.c. metals and the carbon (or other) impurities in b.c.c. metals:

(i) The f.c.c. interstitials cannot be present in thermal equilibrium. They anneal out at temperatures at which they are sufficiently mobile. This means that there are practical upper limits to the measuring frequencies and measuring times that can be used.

Fig. 1

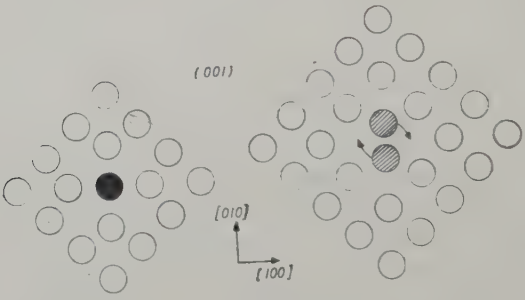

(*a*) (*b*)

Section through a (001)-plane in a f.c.c. crystal containing an interstitial atom. (*a*) Interstitial (full circle) in cube centre, cubic symmetry of the environment. (*b*) Interstitial in intersticialcy (dumb-bell) configuration (hatched circles). Tetragonal symmetry with tetragonal axis along [010].

(ii) The activation energy of the relaxation process will in general be different from (lower than) the energy of migration of the interstitials as determined from diffusion experiments. The larger this difference the less stringent are the conditions mentioned under (i). Consider fig. 1: For interstitial migration by the interstitialcy mechanism the configuration of fig. 1 *b* must change (approximately) into that of fig. 1 *a* and may then relax into the interstitialcy configuration again, possibly with a different preferred ⟨100⟩–axis than before. However, the dumb-bell configuration of the two hatched 'half-interstitials' may 'rotate' into another ⟨100⟩–axis. The projection of such a movement on the (001)–plane is indicated by arrows in fig. 1 *b*. This movement leads over a saddle-point configuration lower in energy than that of fig. 1 *a*. Since this 'rotation' does not shift the 'centre of gravity' of the interstitialcy, it cannot contribute to the interstitial diffusion.

Keeping in mind the above mentioned complications over and above the Snoek–effect as caused by impurities, we have searched for the relaxation process due to the dumb-bell rotation. The noble metals were inconvenient for this, since the interstitial atoms anneal out in a very short time at ambient temperature. According to Sosin and Brinkman (1959), interstitials in nickel have an energy of migration of 1·03 ev. They should therefore be quite persistent at room temperature. Allowing for the different scales of temperatures or activation energies, the spectra of migration energies of point defects appear to be very similar for copper and nickel. We have therefore chosen nickel for an experimental investigation. This has the additional advantage that we are able to demonstrate the ferromagnetic analogue to the Snoek–effect (in the case of C in α–Fe called Richter–after-effect).

We have employed two different experimental techniques: (1) Internal friction as measured in the torsion pendulum (apparatus described by Bangert 1952); (2) The disaccommodation of the initial ferromagnetic susceptibility as measured in a mutual inductance bridge (Wilde 1952, Gerstner 1960).

All our measurements were performed on polycrystalline nickel wires drawn at room temperature and stored at liquid oxygen temperature. As a function of temperature the logarithmic decrement showed peaks of the order of magnitude 10^{-3} superimposed on a rather large background increasing uniformly with temperatures. The shift in the peak temperature was observed for a frequency variation by a factor of 5. The corresponding relaxation times τ are plotted as a function of the reciprocal absolute temperature in fig. 2 (full circles). The half-width of the peaks corresponds to an activation energy of 0·8 ev.

The disaccommodation of the initial susceptibility μ was measured between 0°c and 21·4°c. To a good approximation the time variation of μ was exponential. The corresponding relaxation times τ are shown as open circles in fig. 2.

The magnetic and mechanical measurements can be described by the equation

$$\tau=\tau_0 \exp\left(\frac{Q}{kT}\right) \quad . \; . \; . \; . \; . \; . \; . \; . \; . \quad (1)$$

with $Q=(0{\cdot}79\pm0{\cdot}03)$ ev. For $Q=0{\cdot}79$ ev we find $\tau_0=4\times10^{-12}$ sec. The relaxation times that can be deduced from the disaccommodation measurements of Morkowski (1959) between 10·3°c and 59·6°c agree with the relation shown in fig. 2.

We have also performed annealing experiments. The relaxation effect annealed out with an activation energy of migration of about 1 ev. Allowing for differences in the amount of cold-work, the annealing characteristics were the same as those observed in resistivity annealing studies of stage III and attributed to interstitial migration (Sosin and Brinkman 1959). We consider this as strong evidence for the assignment of both the annealing stage III and the relaxation effect reported in this note to the movement of individual interstitial atoms. Any other explanation (for instance one involving diinterstitials) appears to be far less satisfactory.

The present results are in complete agreement with the view that the migration energies of interstitials are rather high, and with the results of the calculations mentioned above. For copper, where according to Meechan and Brinkman (1956) the activation energy of interstitial migration is 0·6 ev, we expect an activation energy Q for the relaxation mechanism of about 0·45 ev. A relaxation peak in cold-worked copper with such an activation energy was observed by Hasiguti and Okuda (1959). We are not sure, however, whether this peak has the same origin as that studied in the present paper, since the annealing behaviour of the two peaks seems to be different. We are planning to undertake experiments on the noble metals in order to investigate these questions further.

Fig. 2

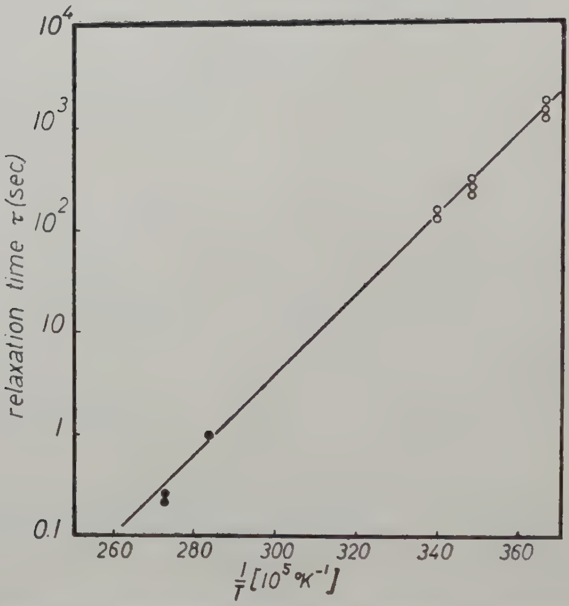

Relaxation time τ (in logarithmic scale) as a function of the reciprocal of the absolute temperature T.

The relaxation effect reported in the present paper appears not only to decide the question of the migration energy of interstitials in f.c.c. metals discussed above, but promises to provide a quantitative tool for the study of atoms on interstitial sites. Experiments on radiation damaged metals would be particularly interesting in this respect.

Note added in proof.—Experiments on pile-irradiated nickel have now been performed, and the results agree in all respects with those reported here (Kronmüller *et al.* 1960).

REFERENCES

BANGERT, L., 1952, Thesis T. H., Stuttgart.

GERSTNER, D., 1960, (to be published).

GIBSON, J. B., GOLAND, A. N., MILGRAM, M., and VINEYARD, G. H., 1960, *Bull. Amer. phys. Soc.*, **5,** 26.

HASIGUTI, R. R., and OKUDA, S., 1959, *Proc. imp. Acad. Japan.*, **35,** 284.

HUNTINGTON, H. B., and SEITZ, F., 1942, *Phys. Rev.*, **61,** 315.

KRONMÜLLER, H., SEEGER. A., and SCHILLER, P., 1960, *Z. Naturforschg.* (in the press).

MEECHAN, J. C., and BRINKMAN, J. A., 1956, *Phys. Rev.*, **103,** 1193.

MORKOWSKI, J., 1959, *Acta phys. polon.*, **18,** 75.

SEEGER, A., 1958, *Proceedings of the Second United Nations International Conference on the Peaceful Uses of Atomic Energy*, Vol. 6, 250 (Geneva); 1960, *Prog. nucl. Energ.*, Vol. 3 (in the press).

SEEGER, A., and MANN, E., 1960, *J. Phys. Chem. Solids*, **12,** 326.

SEEGER, A., MANN, E., and v. JAN, R., 1960, (to be published).

SEITZ, F., 1959, *Trans. met. Soc., A.I.M.E.*, **215,** 354.

SOSIN, A., and BRINKMAN, J. A., 1959, *Acta Met.*, **7,** 478.

WILDE, H., 1952, *Arch. elektr. Übertr.*, **6,** 354.

Lattice Vibrations of Sodium Chloride: Experimental and Theoretical Heat Capacity Data†

By J. R. Hardy
Department of Physics, University of Reading, Berkshire

and A. M. Karo
Lawrence Radiation Laboratory, University of California, Livermore, California

[Received May 3, 1960]

Abstract

Vibrational frequency spectra of sodium chloride derived from two theoretical models which allow for ionic deformability, instead of treating the ions as rigid point charges, have been used to calculate ' effective ' Debye temperatures and distribution function moments.

The results are compared with those deduced from specific heat measurements. For the second, more refined, model the agreement with experiment is considerably better than that achieved when the ions are treated as rigid point charges as in the simple Born theory.

§ 1. Introduction

There has recently been a revival of interest in the theory of the lattice dynamics of the alkali halide crystals. This has been stimulated by high-precision, specific heat measurements on these materials by Morrison *et al.* (1955), Morrison and Patterson (1956), Berg and Morrison (1957), Briscoe and Squire (1957), Briscoe and Norwood (1958). At the same time preliminary results on inelastic neutron scattering in sodium iodide (Woods *et al.* 1959) have shown that the simple Born–Mayer model does not adequately describe the dynamical behaviour of this crystal. This model assumes that the crystal is composed of point charges held apart by nearest-neighbour repulsion, and it has long been known that it does not adequately describe the dielectric properties of these crystals even when the ions themselves are regarded as polarizable. Cochran (1959 a) has interpreted the frequency *versus* wave number dispersion curves for lattice vibrations obtained from neutron scattering data in terms of a model advanced by Hanlon and Lawson (1959) to explain the dielectric properties and claims good agreement with experiment for sodium iodide. A similar model for germanium reproduces the experimental dispersion curves very closely (Cochran 1959 b).

Recently one of us (Karo 1959, denoted by A hereafter, 1960) has carried out a systematic investigation of the frequency spectra of most of the alkali halides on the basis of the simple Born–Mayer model. This represents an extension of Kellermann's (1940, 1941) classic work on sodium chloride and uses improved compressibility data (Born and Huang 1954). The

---

† Communicated by the Authors.

results of this investigation are directly comparable with those of Barron *et al.* (1957) deduced from the experimental data of the last two authors. The agreement between theory and experiment is, in many respects, very good. However, in view of the large difference between the frequency spectrum of lattice normal modes calculated in this way and that calculated by one of us (Hardy 1959, denoted by B hereafter, fig. (2)†) using a more refined model of the crystal, it is obviously necessary to show that these new results can also be reconciled with the thermal data. This is the object of the present paper.

§ 2. Outline of the Theory

A typical normal mode of a perfect crystal lattice is a plane wave of frequency ω_i, and one mole of sodium chloride has a total of six L distinct modes, where L is Avogadro's number. The standard technique, originated

Fig. 1 (*a*)

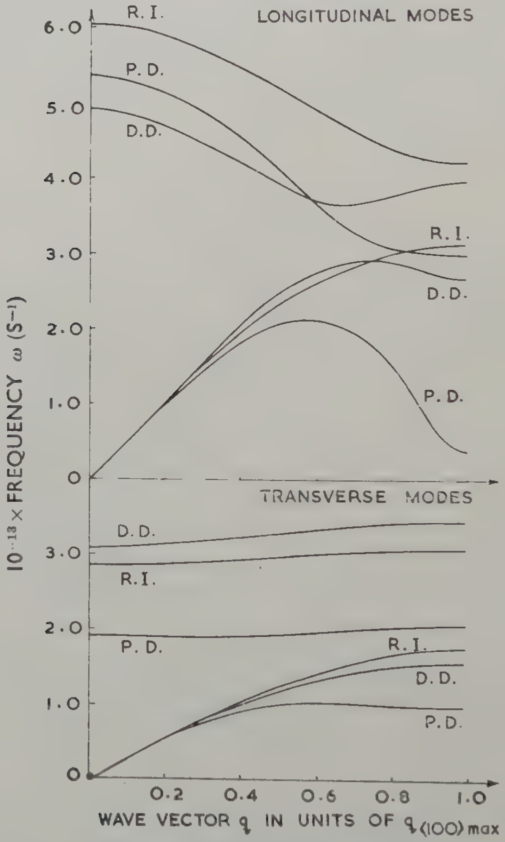

Phonon dispersion curves.
ω versus q along a $\langle 100 \rangle$ direction.

---

† The peaks A and D of the frequency spectrum in fig. 2 of reference B are wrongly assigned in the text. The former is due to transverse *acoustic* modes and the latter to longitudinal *optical* modes.

by Blackmann (1935, 1937) for determining the frequency distribution function $N(\omega)$ (number of normal modes/unit frequency at ω) is to take a sample of wave vectors chosen to satisfy the Born–von Kármán periodic boundary conditions. One then determines the corresponding ω_i's by solving the equation of motion for the model lattice in question. This was the method used in both references A and B, resulting in the determination of about 6000 frequencies in each case.

Fig. 1 (*b*)

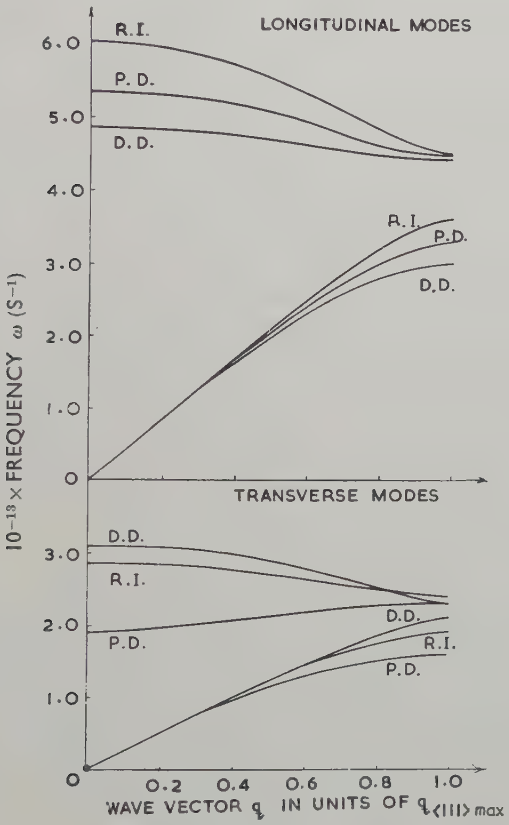

Phonon dispersion curves.
ω versus q along a $\langle 111 \rangle$ direction.

The work in B represents an attempt to construct a theoretical model which allows for the fact that the ions certainly do not behave as point charges when displaced from their equilibrium positions. There are two stages to this work. First, one assumes that each ion acquires a dipole moment proportional to the electrostatic field acting on it, and the resulting $N(\omega)$ versus ω curve is shown as fig. 1 in B. The resulting thermal data have now been calculated and will be discussed in detail in the next section, but the agreement between theory and experiment is completely destroyed.

The good agreement between Born–Mayer theory and experiment now appears rather puzzling, and the second stage of the work is to introduce a further modification of the model, which one hopes will remove this anomaly. This modification is, however, introduced quite independently, and is necessary in order to fit the observed macroscopic dielectric constants (static and optical frequencies) and the reststrahlen frequency. The new concept is that of a 'deformation' dipole (D.D.) associated with each chlorine–sodium bond. This idea was originally due to Szigeti (1950) who pointed out that overlap causes a distortion of the ionic charge distributions which can be described, to the lowest approximation, by these dipoles. Their exact location is not important when conditions are homogeneous, but, for the purpose of the calculations in B, they were assumed to lie at the centre of the chlorine ion, and to vary in magnitude with interionic separation in the same way as the overlap repulsive potential.

The advantage of this mechanism, as far as sodium chloride is concerned, is that it is possible to fit the observed reststrahlen frequency and compressibility simultaneously. This is not possible if one uses Hanlon and Lawson's (1959) model as Cochran (1959 a) does.

In fig. 1 (*a*) and (*b*) the dispersion curves for the $\langle 100\rangle$ and $\langle 111\rangle$ directions are shown. Those marked R.I. (rigid ions) are derived from Kellermann's (1940) data, those marked P.D. (polarization dipoles) result when ionic polarization alone is included, and those marked D.D. (deformation dipoles) follow when both polarization and deformation are taken into account. The D.D. curves for the $\langle 100\rangle$ direction are very similar to those published by Cochran (1959 a) and, in view of the differences between the two approaches, this agreement is very encouraging.

§ 3. COMPARISON BETWEEN THE RESULTS OF THEORY AND EXPERIMENT

Barron *et al.* (1957) have analysed the sodium chloride experimental data in such a way as to extract effective Debye temperatures and certain positive and negative moments of the frequency distribution. The former quantity $\Theta_{\mathrm{D}}(T)$ is defined as $\hbar\omega_m(T)/k$ where $\omega_m(T)$ is the cut-off frequency imposed on the Debye spectrum in order to fit the observed specific heat at a temperature T. The nth moment is defined as

$$\mu_n = \int_0^\infty \omega^n N(\omega)\, d\omega \Big/ \int_0^\infty N(\omega)\, d\omega$$

(this is in fact $(2\pi)^n$ times the values given by Barron *et al.*).

In fig. 2 the values of Θ_{D} derived from the two models (P.D. and D.D.) are compared with values of Θ_{D} from A. On the same figure are plotted the experimental results of Morrison and his co-workers (1955, 1956).

In the table the calculated moments of both distributions are compared with the experimental results. Also shown are the results given in (A) derived for rigid ions using both room temperature and absolute zero compressibilities. Finally in fig. 3 a plot of the function

$$\omega_{\mathrm{D}}(n) = [\tfrac{1}{3}(n+3)\,\mu_n]^{1/n},$$

Fig. 2

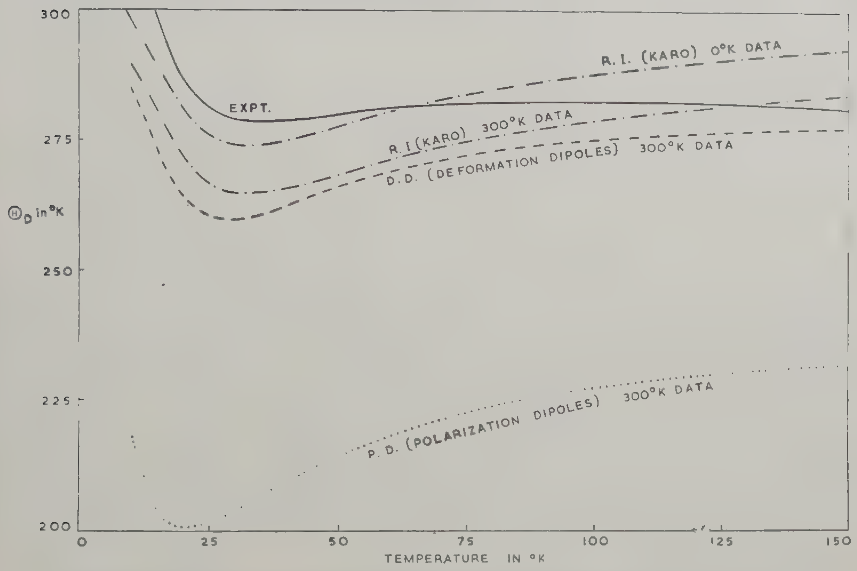

Effective Debye temperatures Θ_D versus absolute temperature.

Fig. 3

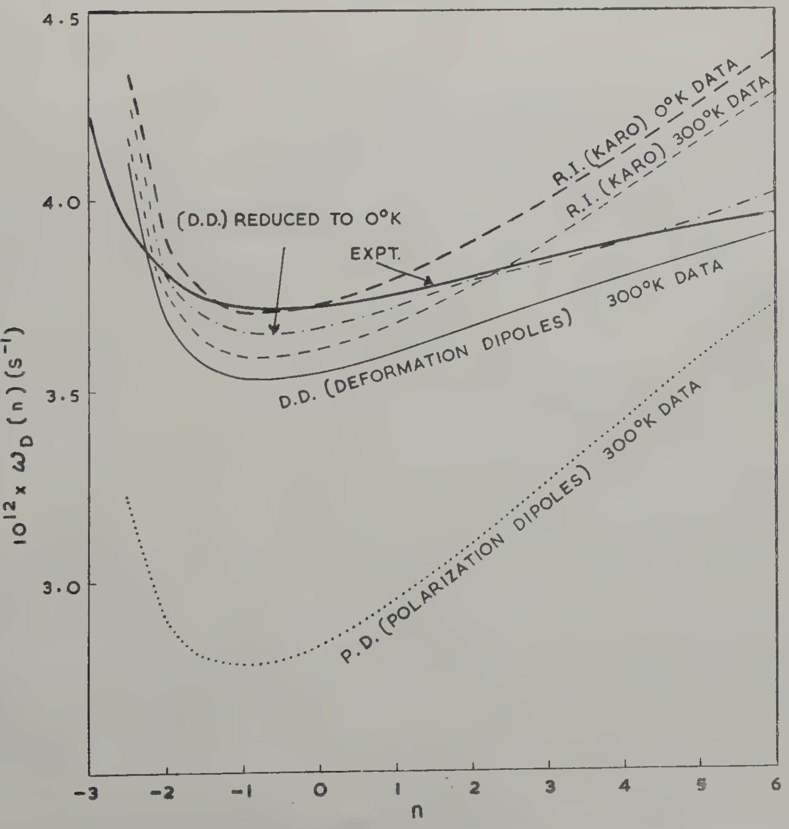

Moment function $\omega_D(n) = [\frac{1}{3}(n+3)\mu_n]^{1/n}$ as a function of n for the various data.

defined by Barron *et al.* (1957) as a means of correlating the various moments, is given for the various sets of results ($\omega_D(n)$ is in fact 2π times the function $\nu_D(n)$ used by these authors).

Moments of the Various Distribution Functions

Moment μ_n	Experimental	P.D.	D.D.	Karo 0°K data	1959 R.T. data
$10\mu_1{}^{-13}$ (s^{-1})	2·81	2·21	2·70	2·85	2·76
$10\mu_2{}^{-26}$ (s^{-2})	8·65	5·75	8·07	9·09	8·56
$10\mu_4{}^{-52}$ (s^{-4})	98·2	58·6	89·3	125	113
$10\mu_6{}^{-78}$ (s^{-6})	1,290	885	1,200	2,360	2,060
$10\mu_{-1}{}^{13}$ (s)	0·403	0·539	0·425	0·404	0·418
$10\mu_{-1\cdot5}{}^{19\cdot5}$ ($\mathrm{s}^{3/2}$)	0·276	0·427	0·297	0·276	0·289
$10\mu_{-2}{}^{26}$ (s^{2})	0·208	0·358	0·221	0·199	0·213
$10\mu_{-2\cdot5}{}^{32\cdot5}$ ($\mathrm{s}^{5/2}$)	0·197	0·320	0·176	0·155	0·168

§ 4. DISCUSSION

When one examines the curves shown in figs. 2 and 3, one must remember that the results from B (P.D. and D.D.) are derived from spectra calculated from room temperature data. For the moments, no direct comparison can be made with experimental values, since they have been derived from an ‘ effective ’ harmonic spectrum of the crystal at absolute zero. However, it is possible to correct for this, to a first approximation, by assuming that room temperature and absolute zero results differ by the same amounts as those deduced in (A). This has been done for the moment function $\omega_D(n)$ shown in fig. 3 and the resulting curve (D.D. reduced to 0°K) is remarkably close to that determined experimentally. This is particularly striking in view of the large discrepancy between the curve P.D. and the experimental results. Furthermore the overall agreement between theory and experiment is noticeably better, particularly for large n, than that of the simple Born–Mayer theory.

The Θ_D versus T curves have not been corrected in any way ; the theoretical curves are compared with the experimental curve taken directly from the results of Morrison and his co-workers (1955, 1956). However, comparison with the results of A shows that the values of Θ_D from B would be about 10°K higher if absolute zero data had been used. The use of such data is advisable below 100–150°K and for the D.D. case, much of the discrepancy between theory and experiment is removed between the minimum and 150°K. (The empirical Θ_D is too low, above about 30°K, and must be corrected to remove anharmonic effects.)

There are, however, still certain discrepancies in the D.D. curve:

(1) In the region of the minimum and below, the calculated Θ_D versus T curve is about 5–10°K too low even when corrected.

(2) The theoretical moment curve is a little too low in the intermediate range.

(3) The calculated moments increase too rapidly as $n \to -3$.

It would be unwise to draw any conclusions from (1) and (3) alone, as both effects depend critically on the low frequency end of the distribution and are strongly influenced by the coarseness of our 'net' of chosen wave vectors. Thus (2) is the only definite anomaly. This discrepancy might be removed if the first two peaks in the D.D. $N(\omega)$ versus ω curve were more distinct since this would probably raise the lower-order moments ($|n| \leqslant 1{\cdot}5$) without much affecting the others. This might happen if the calculations were carried out exactly using absolute zero data. Unfortunately the relevant information, in particular the reststrahlen frequency, does not seem to be available.

It is worth noting that these first two peaks coincide with the two proposed by Barron and Morrison (1960), and that the high central peak, found by Kellermann (1940) and in (A) is in fact split by the present theory, as they suggest might be the case, into the second and third peaks of the D.D. spectrum.

§ 5. Conclusion

In view of the good agreement between theory and experiment, in particular with respect to the moment curves, the results in this paper tend to confirm that the model of sodium chloride, used during calculations on the frequency spectrum of this crystal in reference B, provides a better description of its dynamical properties than any used previously in such calculations. There remains some discrepancy in the specific heat, but improvement could result when accurate low-temperature dielectric constants and reststrahlen frequency are available to use as input data, and when the calculation is carried out for more points in the reciprocal lattice.

Acknowledgments

We should like to thank Dr. T. H. K. Barron and Dr. J. A. Morrison, for communicating their results to us prior to publication and for access to unpublished data.

One of us (A.M.K.) would like to acknowledge the support of the U.S. Atomic Energy Commission and the other author (J.R.H.) would like to thank A.E.I. for a Research Fellowship during the tenure of which this work was carried out.

REFERENCES

BARRON, T. H. K., BERG, W. T., and MORRISON, J. A., 1957, *Proc. roy. Soc.* A, **242,** 478.

BARRON, T. H. K., and MORRISON, J. A., 1960, *Proc. roy. Soc.* (in the press).

BERG, W. T., and MORRISON, J. A., 1957, *Proc. roy. Soc.* A, **242,** 476.

BLACKMANN, M., 1935, *Proc. roy. Soc.* A, **148,** 384; 1937, *Ibid.* A, **159,** 416.

BORN, M., and HUANG, K., 1954, *Dynamical Theory of Crystal Lattices* (Oxford: Clarendon Press).

BRISCOE, C. V., and NORWOOD, M. H., 1958, *Phys. Rev.*, **112,** 45.

BRISCOE, C. V., and SQUIRE, C. F., 1957, *Phys. Rev.*, **106,** 1175.

COCHRAN, W., 1959 a, *Phil. Mag.*, **4,** 1082; 1959 b, *Proc. roy. Soc.* A, **253,** 260.

HANLON, J. E., and LAWSON, A. W., 1959, *Phys. Rev.*, **113,** 472.

HARDY, J. R., 1959, *Phil. Mag.*, **4,** 1278.

KARO, A. M., 1959, *J. chem. Phys.*, **31,** 1489 ; 1960, *Ibid.* (in the press).

KELLERMANN, E. W., 1940, *Phil. Trans. roy. Soc.*, **238,** 513 ; 1941, *Proc. roy. Soc.* A, **178,** 17.

MORRISON, J. A., PATTERSON, D., and DUGDALE, J. S., 1955, *Canad. J. Chem.*, **33,** 375.

MORRISON, J. A., and PATTERSON, D., 1956, *Trans. Faraday Soc.*, **52,** 764.

SZIGETI, B., 1950, *Proc. roy. Soc.* A, **204,** 51.

WOODS, A. D. B., COCHRAN, W., and BROCKHOUSE, B. N., 1959, *Bull. Amer. phys. Soc.*, **4,** 246.

CORRESPONDENCE

Measurements of Thermoelectricity below 1°K—IV

By D. K. C. MacDonald, W. B. Pearson and I. M. Templeton
Division of Pure Physics, National Research Council, Ottawa, Canada

[Received July 18, 1960]

It is well known that metals such as copper may show anomalous resistive and thermoelectric behaviour at low temperatures. It now seems clear (cf. Gold *et al.* 1960) that the large negative thermoelectric power which develops at temperatures of the order of 10°K to 20°K in certain specimens of the 'pure' metal or specially prepared dilute alloys must be attributed primarily to the presence of very small quantities of iron in solid solution. It also appears that other magnetic ions in solid solution will give rise to similar behaviour (cf. e.g. Jacobs and Schmitt 1959). It has been suggested (Schmitt 1956, cf. also Brailsford and Overhauser 1959) that, for example, the appearance of a maximum (and consequently also a minimum) in the electrical resistance at low temperatures can be explained in terms of scattering by magnetic impurity ions, if the spin degeneracy of the ground state is split and the electron scattering cross sections of the lower levels are higher than those of the upper levels. No detailed analysis appears to have been made of the thermoelectric behaviour to be expected on such a model, but it is suggested (cf. Schmitt loc. cit.) that this might be predicted if due account is taken of the inelastic electron scattering involved. One might remark that the experimental situation is to some extent complicated by the fact that electron scattering by excited lattice vibrations (phonons) becomes important above, say, 15°K in Cu in comparison with electron scattering by impurity sites.

In a previous letter to this Journal (MacDonald *et al.* 1959) we presented some data on the thermoelectric power of a number of metals at very low temperatures, and remarked in particular on the puzzling change of sign which we observed (in Ni, Pd and Fe) when the residual resistivity was altered by a relatively modest amount. Following that work we decided to have a number of alloys of the transition metals, Pd and Pt, specifically prepared with Cu, Sn and Fe as solutes in relatively small concentrations. We are grateful to Dr. J. C. Chaston of Messrs. Johnson, Matthey and Co., Wembley, for his interest in preparing a series of eighteen such alloys for us. We have now surveyed the thermoelectric power of a number of these alloys. Some of the results are shown in figs. 1 and 2 where for the present we have restricted ourselves to the most concentrated alloys (nominal 0·5 at. % solute in each case) for comparison of behaviour.

The following points seem to us noteworthy :

(i) The behaviour of the thermoelectric power is monotonic from the absolute zero (up to at least 3°K) when copper and tin are present as the dominant impurity in Pd or Pt. We note however that, when dissolved in Pd, Cu gives rise to a negative, and Sn to a positive absolute thermoelectric power.

(ii) The presence of Fe as a solute in Pd or Pt gives rise to a thermoelectric power which goes through a positive maximum (which in Pt as parent occurs at a temperature as low as about 0·5°K) and then changes sign, becoming negative (and in the case of Pt almost linear in temperature dependence above about 1°K).

Fig. 1

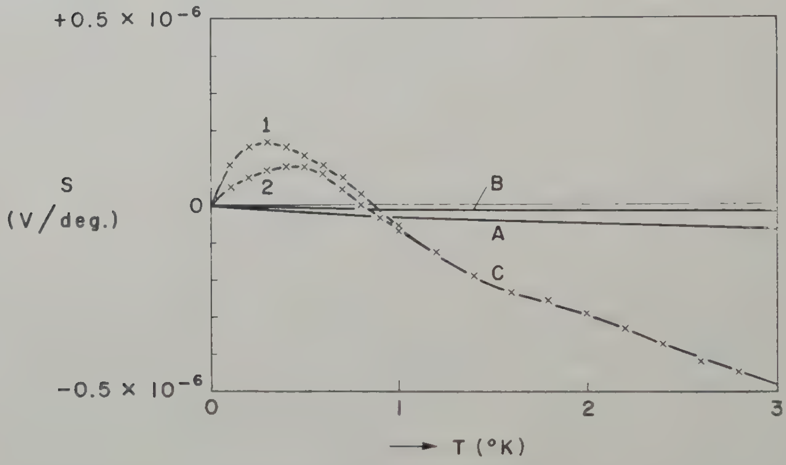

Measurements of absolute thermoelectric power of alloys of Cu, Sn and Fe in Pt. Solute concentration: 0·5 nominal at. % in each case.

A: Cu in Pt. B: Sn in Pt. C: Fe in Pt; 1: points derived from measurements of thermo-e.m.f. to ~2°K; 2: points derived from measurements of thermo-e.m.f. to ~3°K.

(iii) Comparing the monotonic temperature dependences (and in the case of the Pt alloys the relative magnitude) of the alloys containing Cu and Sn with that of the alloys containing Fe, it seems most improbable that ‘ phonon-drag ’ effects could be responsible for the anomalous behaviour of the alloys containing Fe. Apart from this direct comparison, one might expect that the amount of impurity present (0·5 nominal at. % in each case) would play some role in scattering the phonons, and we recall moreover that the characteristic temperatures (θ) of Pt and Pd are about 230°K and 270°K respectively.

(iv) We are thus led to believe that the anomalous behaviour we have observed at these very low temperatures in the alloys containing Fe cannot be attributed to 'phonon-drag', nor more generally to electron-scattering by thermal vibrations of the lattice but rather that we must seek an explanation in terms specifically of electron-scattering by Fe ions. It is thus of considerable interest to find that scattering by Fe ions can give rise to a maximum in S and also a change of *sign* at these very low temperatures, particularly as the conventional theory of 'diffusion' thermoelectricity predicts uncompromisingly that $S \propto T$ (e.g. Wilson 1953, Mott and Jones 1936).

Fig. 2

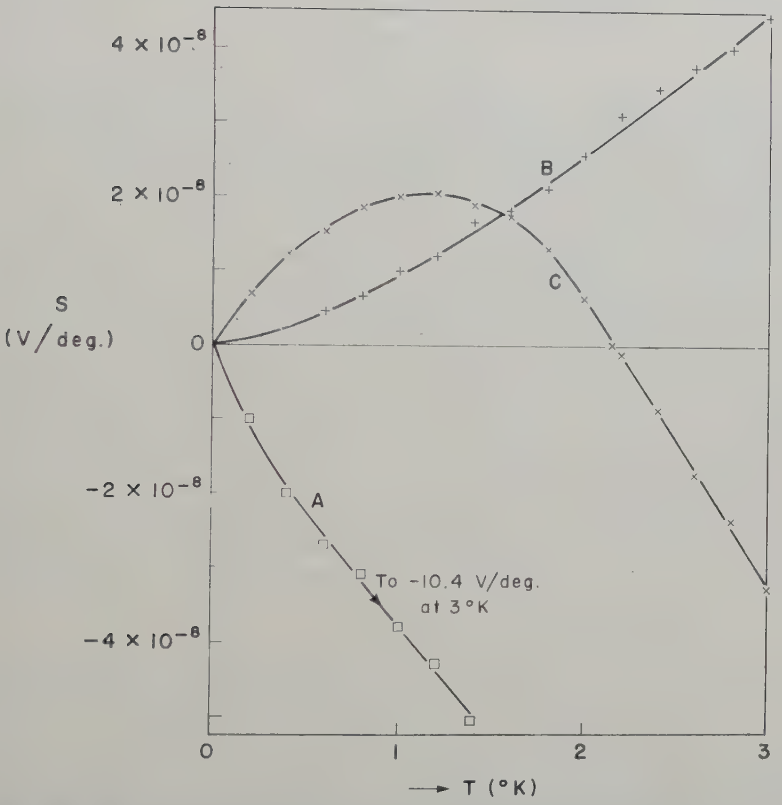

Measurements of absolute thermoelectric power of alloys of Cu, Sn and Fe in Pd. Solute concentration: 0·5 nominal at. % in each case.

A: Cu in Pd. B: Sn in Pd. C: Fe in Pd.

Since similar concentrations of Fe behave differently in different parent metals, experiments of this kind should be fruitful in studying the influence of the matrix on the interaction involved (presumably magnetic) between the scattering ions, if the general type of mechanism suggested by Schmitt and others (foregoing references) is accepted as responsible.

We are studying a number of other metals at these very low temperatures, with magnetic ions as solutes, and we hope to publish a fuller account of this work later.

ACKNOWLEDGMENT

We should like to thank Mr. J. E. Dunick for technical assistance in some of these experiments.

REFERENCES

BRAILSFORD, A. D., and OVERHAUSER, A. W., 1959, *Phys. Rev. Letters*, **3**, 331.

GOLD, A. V., MACDONALD, D. K. C., PEARSON, W. B., and TEMPLETON, I. M., 1960, *Phil. Mag.*, **5**, 765.

JACOBS, I. S., and SCHMITT, R. W., 1959, *Phys. Rev.*, **113**, 459.

MACDONALD, D. K. C., PEARSON, W. B., and TEMPLETON, I. M., 1959, *Phil. Mag.*, **4**, 380.

MOTT, N. F., and JONES, H., 1936, *Theory of Properties of Metals and Alloys* (Oxford : Clarendon Press).

SCHMITT, R. W., 1956, *Phys. Rev.*, **103**, 83.

WILSON, A. H., 1953, *Theory of Metals*, 2nd edition (Cambridge : University Press).

REVIEWS OF BOOKS

Similarity and Dimensional Methods in Mechanics. By L. I. SEDOV. Translated by M. HOLT and M. FRIEDMAN. (London : Cleaver Hume for Infosearch.) [Pp. 363.] No price given by publishers.

THIS is a translation of the 4th Russian edition (1956) of this well-known work. The chapter headings are : (1) General dimensional theory ; (2) Similarity, modelling and examples of the application of dimensional analysis ; (3) Application to the theory of motion of a viscous fluid and to the theory of turbulence ; (4) One-dimensional unsteady motion of a gas ; (5) Application to astrophysical results.

With a few exceptions the problems treated in this book are taken from fluid mechanics and illustrate the various roles played by dimensional analysis in modern applications. In its simplest form the dimensional argument follows from the known equations of motion and shows, e.g. that the drag coefficient of a sphere in steady motion (which cannot easily be calculated) is a function only of Reynolds' number ; this has been verified by measurements. When several dimensionless variables enter, simplification may sometimes be achieved in limiting cases by use of intuitive physical arguments. Numerous diagrams show how far these are supported by experiments. In Chapter 3 some of the arguments are less obvious, and less use is made of the equations of motion. Boundary layers, isotropic turbulence and pipe-flow turbulence are discussed, with a short excursion into mixing-length theory. Chapter 4 is the longest in the book (150 pages). Dimensional analysis is applied to those special solutions of the equations of motion in which the scale but not the form of the solution changes with time, the *self-similar* solutions. The equations of motion then reduce to a system of ordinary differential equations. This part is mainly theoretical and few comparisons with experiment are given.

This book can be warmly recommended both as a study of dimensional analysis and as a study of certain parts of fluid mechanics. F. U.

Mathematics in Physics and Engineering. By J. IRVING and N. MULLINEUX. (New York : Academic Press Inc., 1960.) [Pp. 883.] $11.50.

THE subject-matter of this book has formed the basis of lecture courses at British universities to undergraduate and postgraduate students of mathematics, physics and engineering. Chapter headings are : 1. Introduction to Partial Differential Equations ; 2. Ordinary Differential Equations : Frobenius' and Other Methods of Solution ; 3. Bessel and Legendre Functions ; 4. The Laplace and Other Transforms ; 5. Matrices ; 6. Analytical Methods in Classical and Wave Mechanics ; 7. Calculus of Variations ; 8. Complex Variable Theory and Conformal Transformations ; 9. The Calculus of Residues ; 10. Transform Theory ; 11. Numerical Methods ; 12. Integral Equations.

There is an appendix on certain mathematical topics which could not find a place in the text. Many examples are worked in the text, and at the end of each chapter there are problems the solutions of which are given at the end of the book. The authors intend that a good knowledge of elementary differential and integral calculus should be sufficient for an understanding of this work.

The reviewer believes that this book will appeal most to those who, trained as applied physicists or engineers, wish to take a serious interest in the mathematical side of their subject. It is clear that the authors are not only competent mathematicians but also convinced of the importance and utility of mathematics in applied science and it is to be wished that they may open the eyes of some of those engineering students who were obliged by degree requirements to learn mathematical methods without their applications, and who have naturally acquired a harmful distaste for all theory. The book appears well suited for this purpose. Technologists will probably like the authors' style. A different selection of topics might have been made by different authors. The reviewer has only one serious criticism. It seems to him that more references should have been given, to papers as well as to books.

F. U.

[*The Editors do not hold themselves responsible for the views expressed by their correspondents.*]

Fig. 2

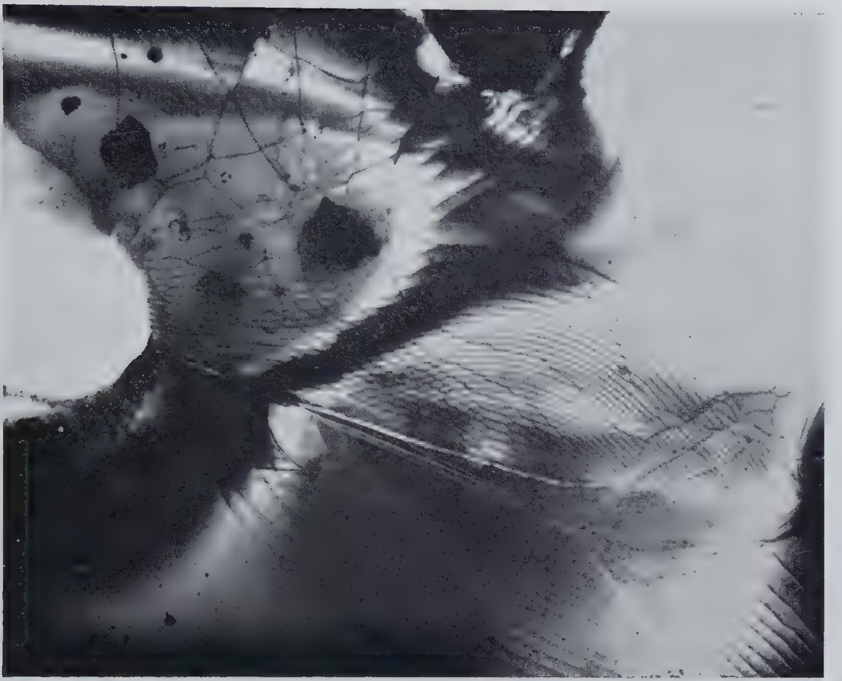

An array of dislocations associated with deformation of the crystal during mounting on specimen grid. ×10 000.

Fig. 3

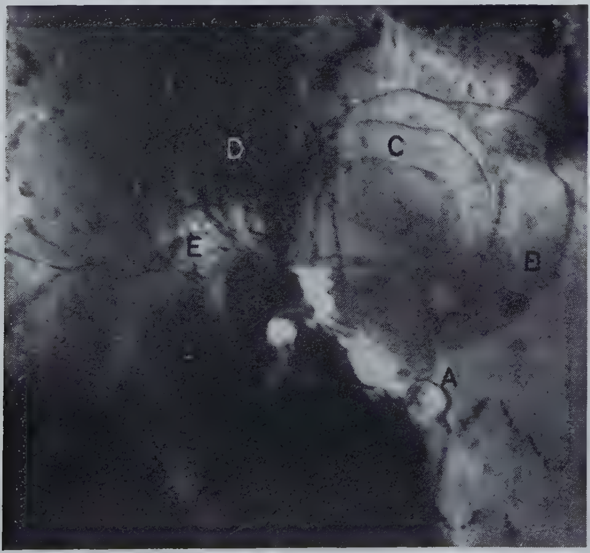

An array of pre-existing dislocations which is clearly composed of a number of families of loops A, B, C, D, E. ×18 000.

Fig. 4

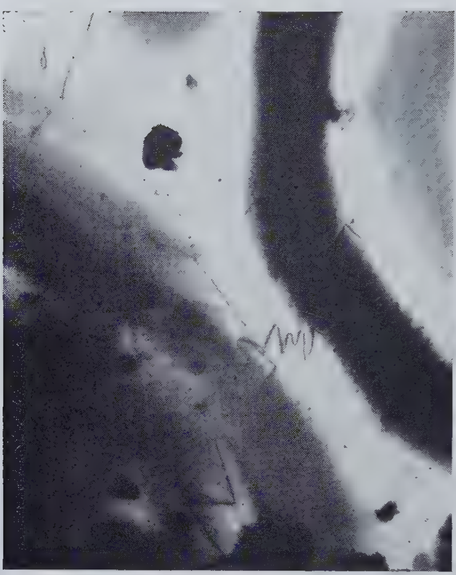

Helices produced by the climb of pre-existing dislocations. ×18 000.

Fig. 5

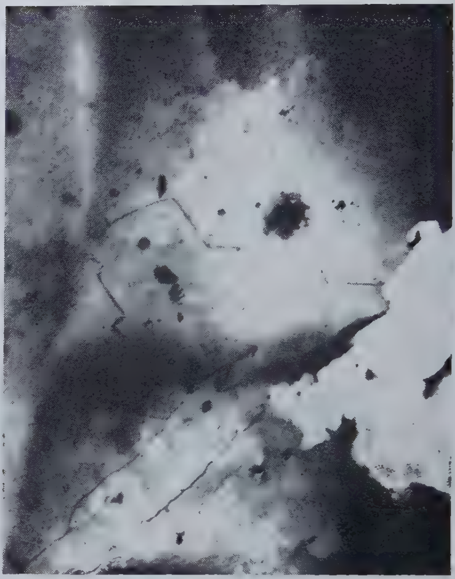

The climb of a loop of dislocation. ×18 000.

Fig. 6

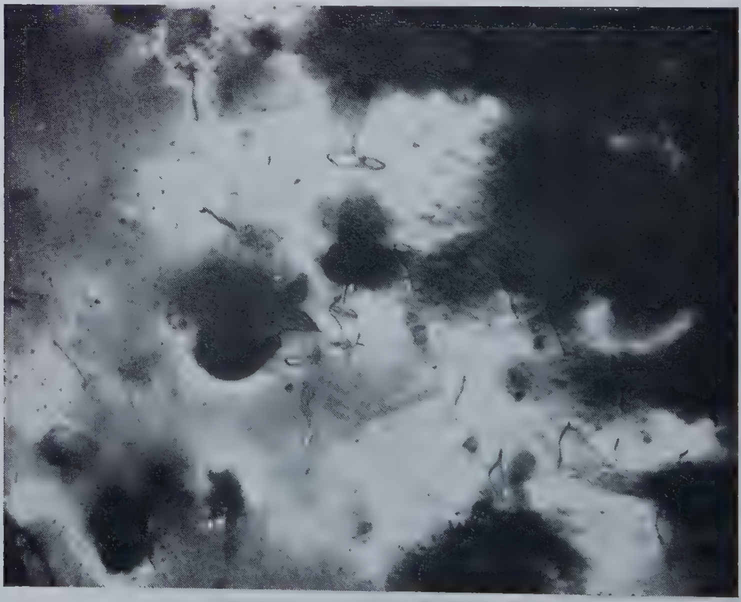

Illustrating the formation of a loop in a dislocation line by localized condensation of vacancies. Note also the large numbers of small isolated loops and the several zig-zag dislocations. ×24 000.

Fig. 7

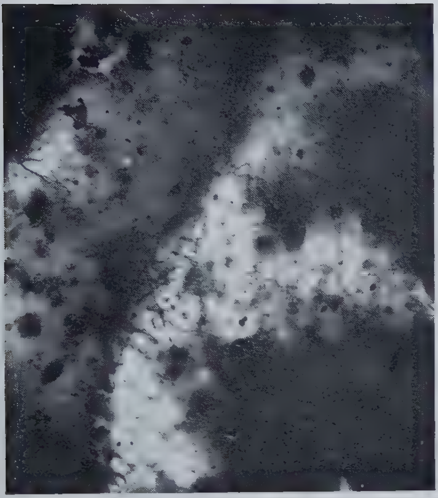

Illustrating chains of loops formed during climb from an array of pre-existing dislocations. ×15 000.

Fig. 8

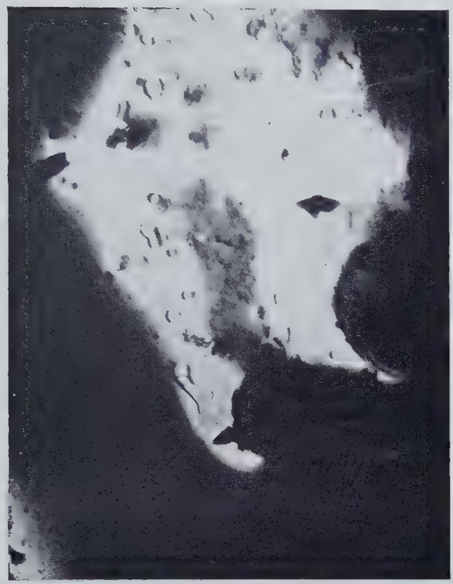

Isolated loops of dislocation, apparently lying in an inclined plane. ×24 000.

Fig. 9

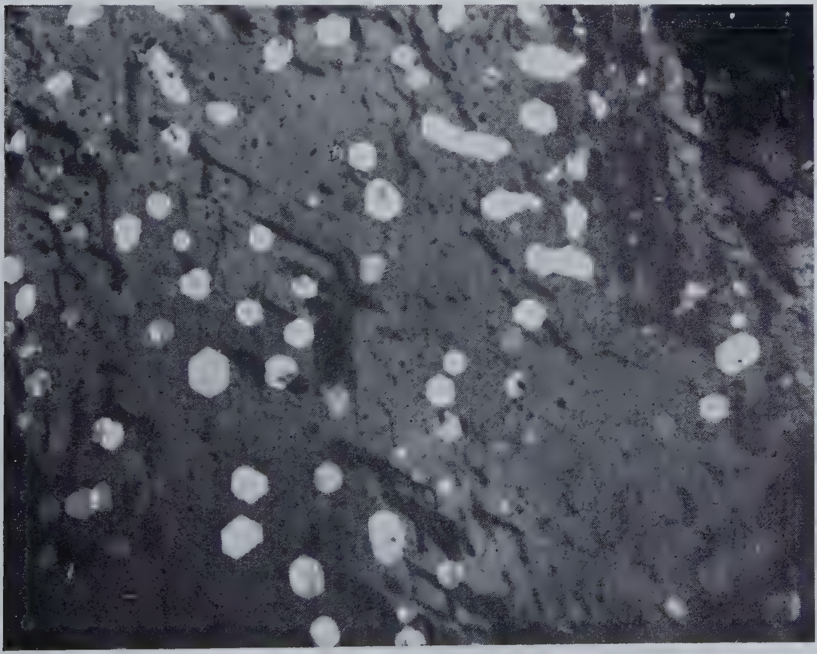

Bright patches formed during the intermediate stage of decomposition. The outlines follow ⟨10$\bar{1}$0⟩ directions. ×20 000.

Fig. 10

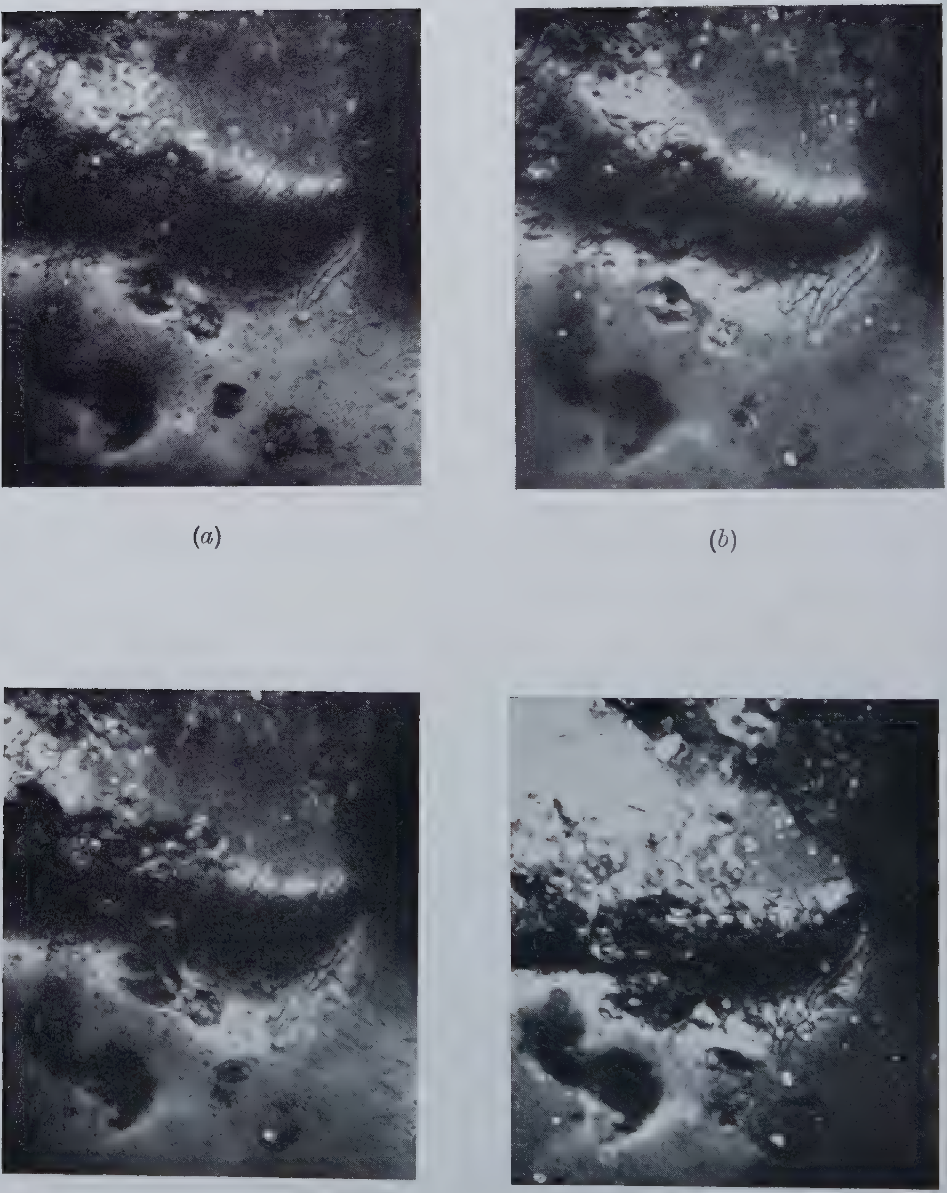

(a) (b)

(c) (d)

Sequence illustrating the movement of a number of bright patches and the extension of dislocations associated with them. ×15 000.

Fig. 11

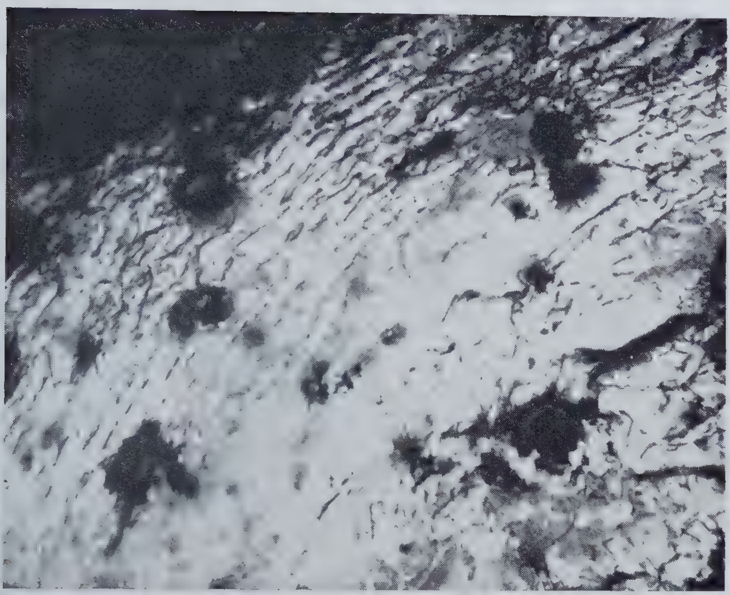

A highly dislocated region produced by the passage of a wave of bright patches. ×15 000.

Fig. 12

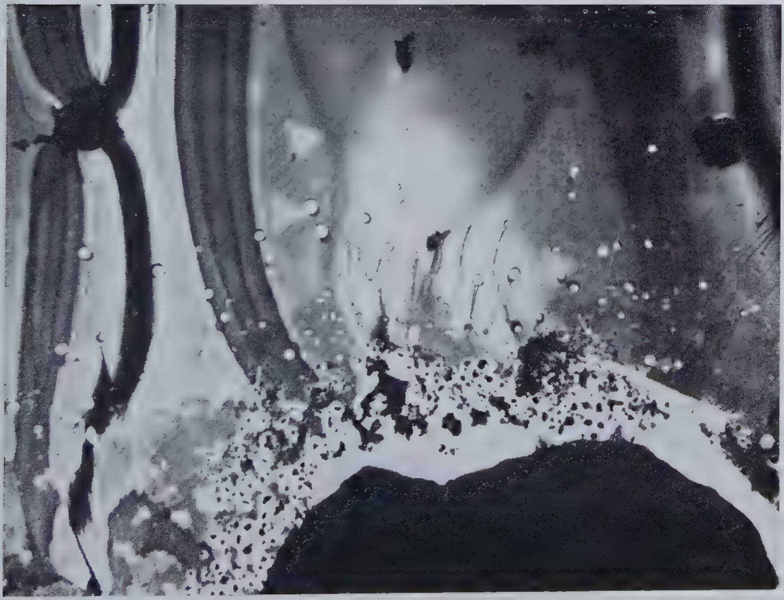

The commencement of the final stage of decomposition. A wave of bright patches is leaving a completely decomposed zone. ×15 000.

Fig. 13

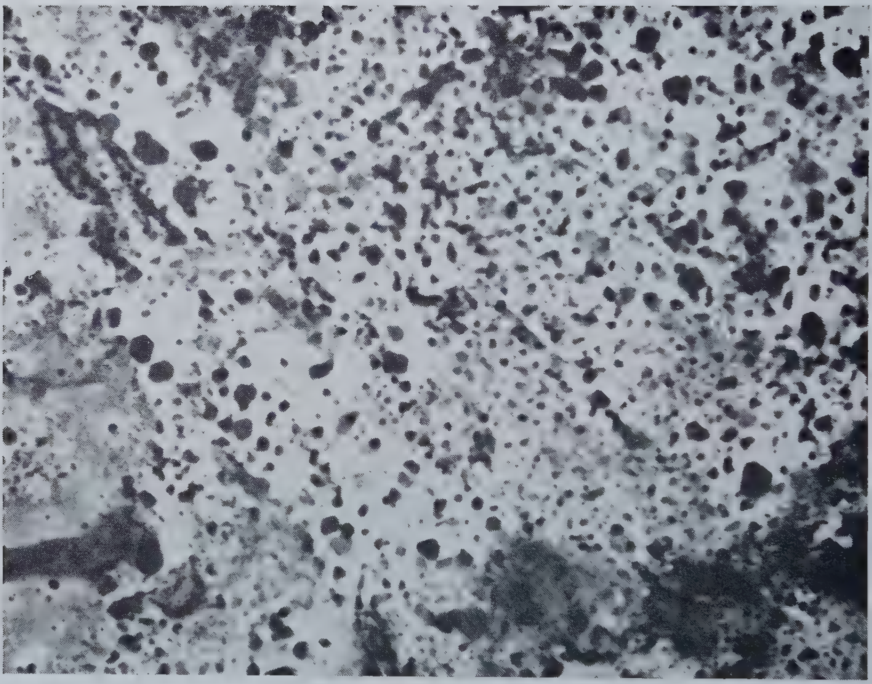

An aggregate of dense crystallites remaining after complete decomposition. ×24 000.

Fig. 14

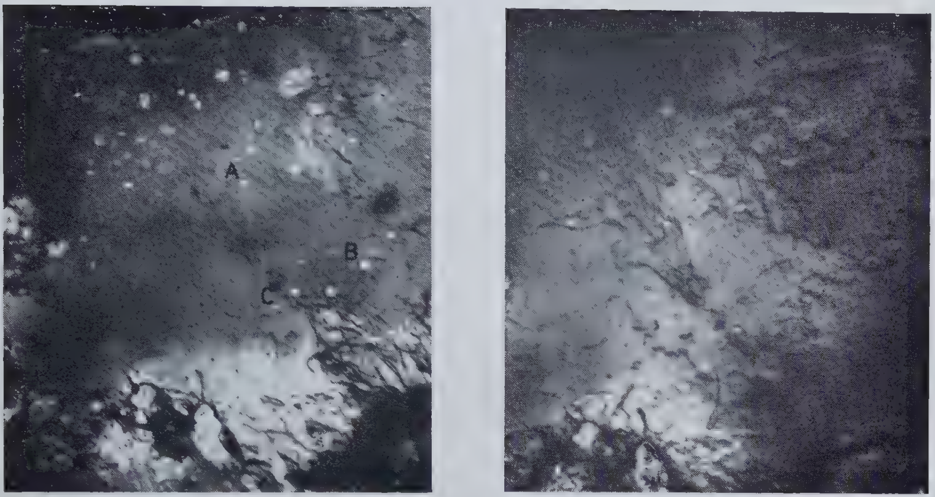

(*a*) (*b*)

Illustrating the change in appearance of bright patches after a slight deflection of the electron beam. ×15 000.

Fig. 15

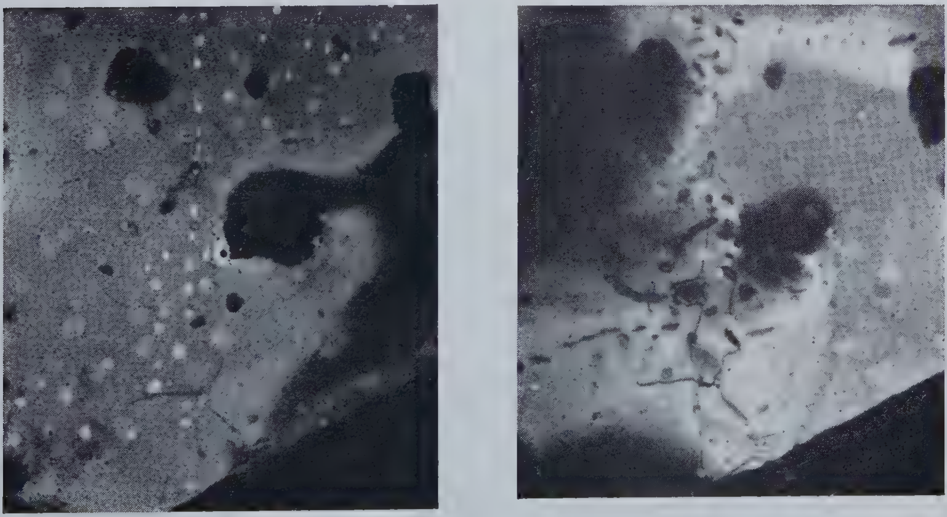

(*a*) (*b*)

Illustrating the reversal of contrast of patches after deflection of the electron beam. ×20 000.

Fig. 3

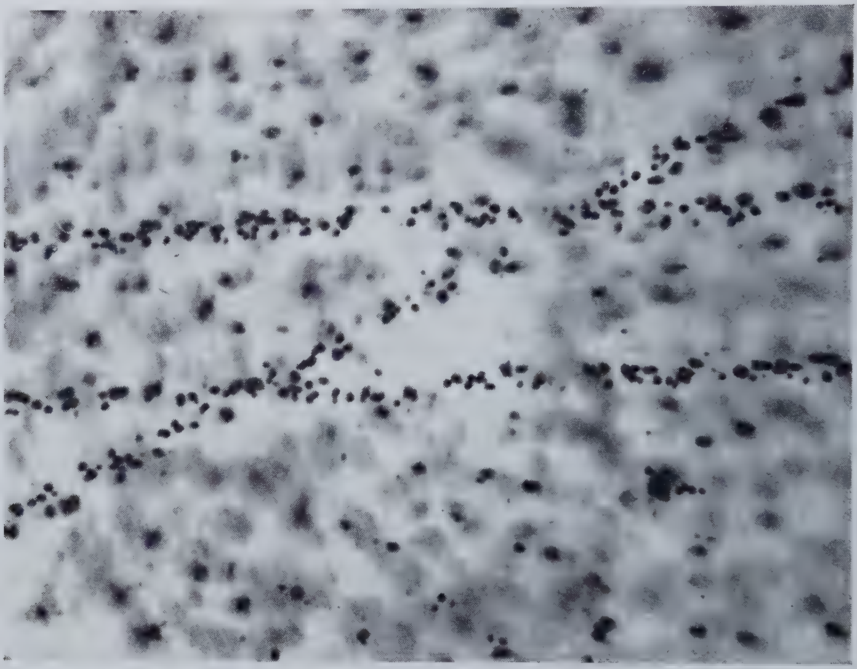

Surface terraces associated with dislocation loops made visible by the separation of particles of silver. ×1600.

Fig. 4

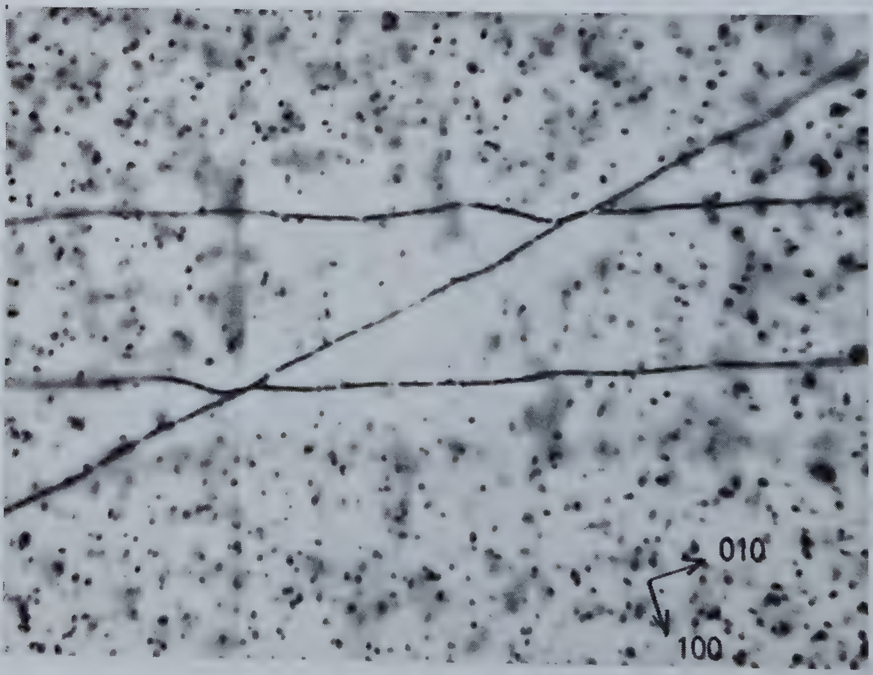

Dislocations approximately in the edge orientation corresponding with the surface terraces of fig. 3 and made visible by the separation of silver. ×1600.

Fig. 1

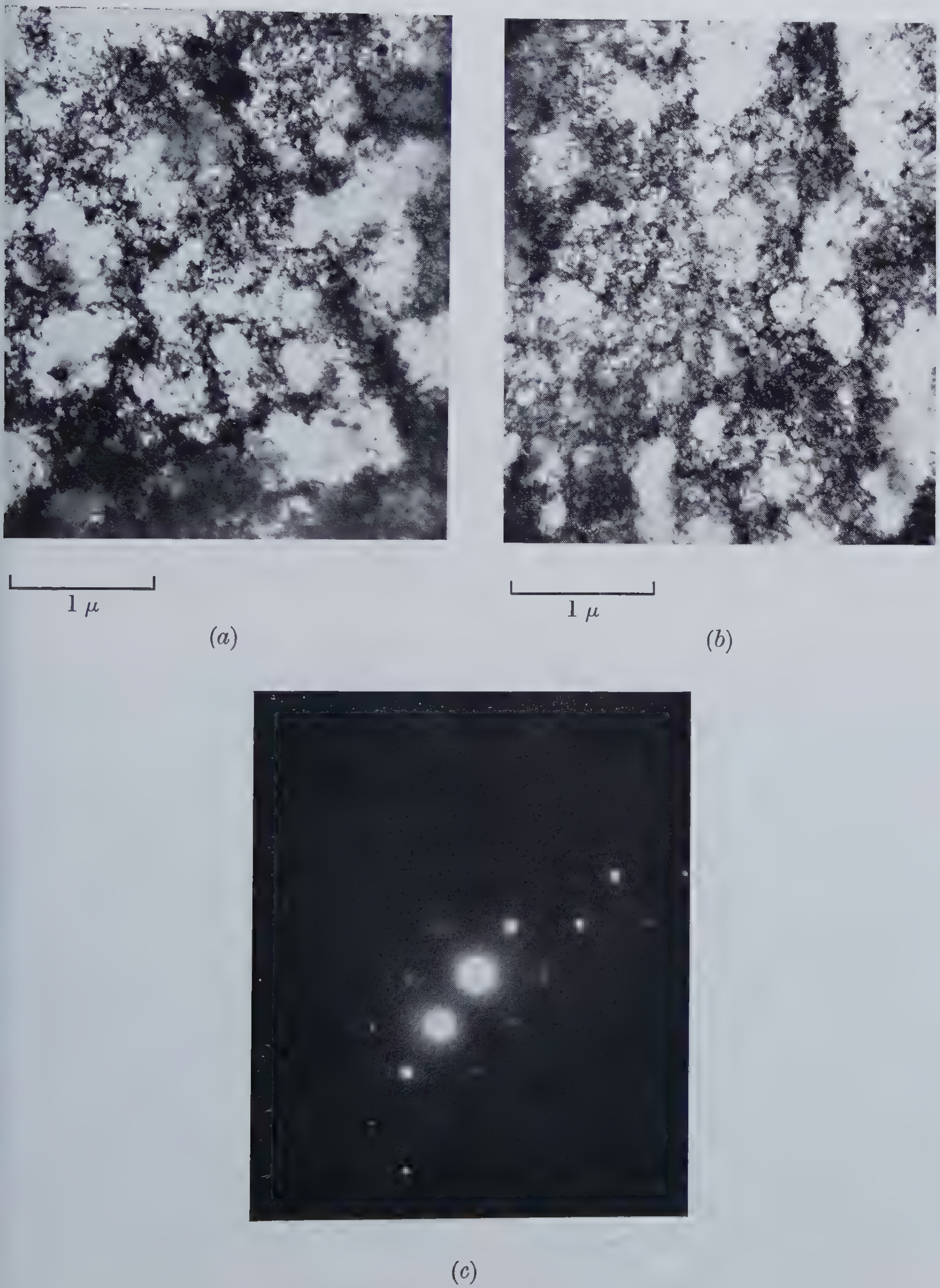

(a)

(b)

(c)

(a) Electron micrograph of a typical area within one grain of polycrystalline silver deformed 25% in tension. (b) Unrecrystallized area within one grain of polycrystalline silver deformed 25% in tension and annealed for 1 hour at 200°C. (c) Electron diffraction pattern from an area $\frac{4}{3}$ μ in diameter within one grain of polycrystalline silver deformed 25% in tension. Mag. ×20 000.

Fig. 2

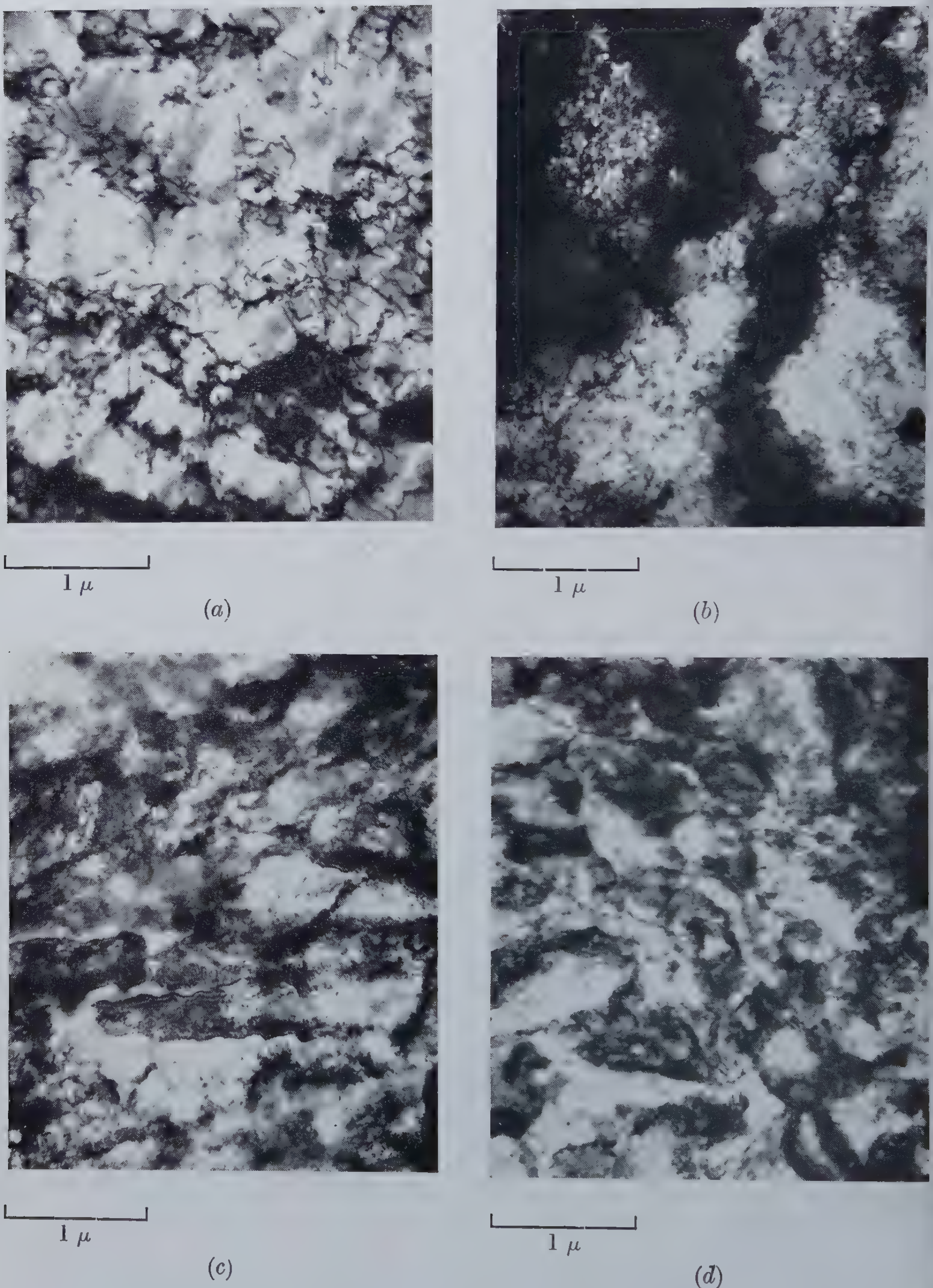

(*a*) Typical area of polycrystalline silver reduced 20% by cold rolling. (*b*) Typical area of polycrystalline silver reduced 40% by cold rolling. (*c*) Typical area of polycrystalline silver reduced 60% by cold rolling. (*d*) Typical area of polycrystalline silver reduced 95% by cold rolling. Mag. × 20 000.

Fig. 3

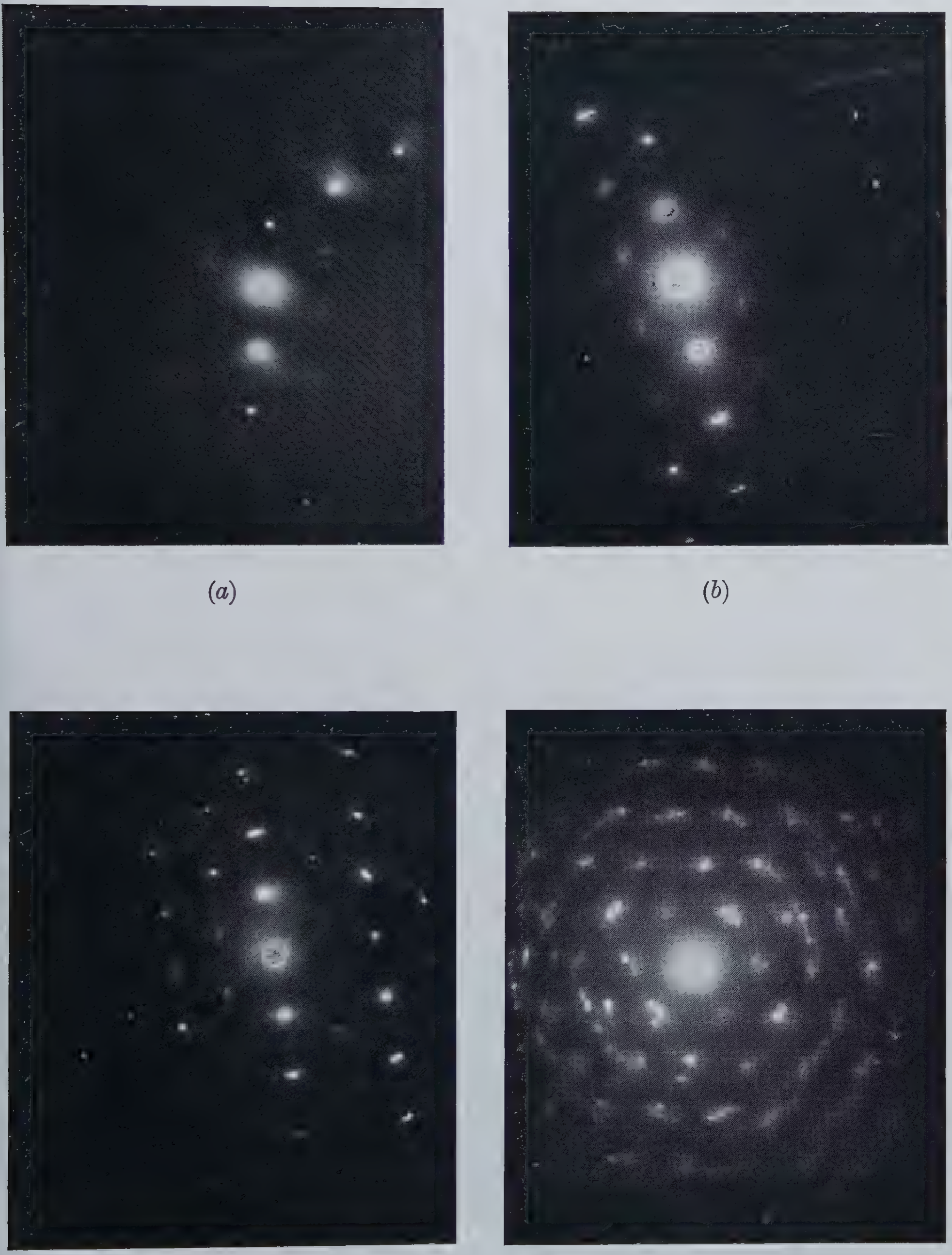

(*a*) (*b*)

(*c*) (*d*)

Set of electron diffraction patterns of the central region ($\frac{4}{3}\,\mu$ diameter) of the areas shown in fig. 2 (*a*), (*b*), (*c*) and (*d*) respectively.

Fig. 4

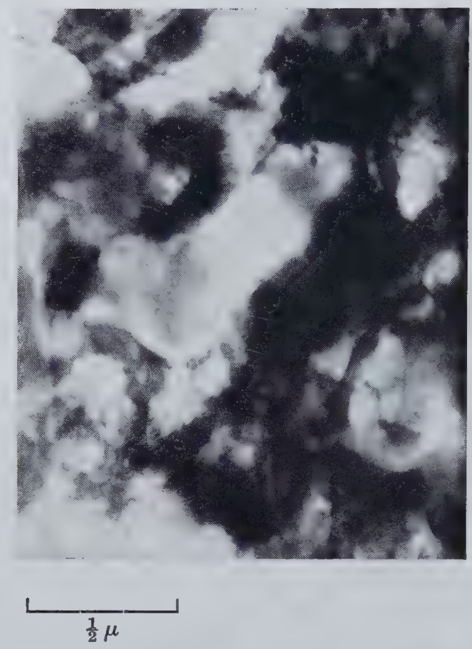

Sub-boundaries in heavily rolled (95% reduction) polycrystalline silver. Mag. × 40 000.

Fig. 5

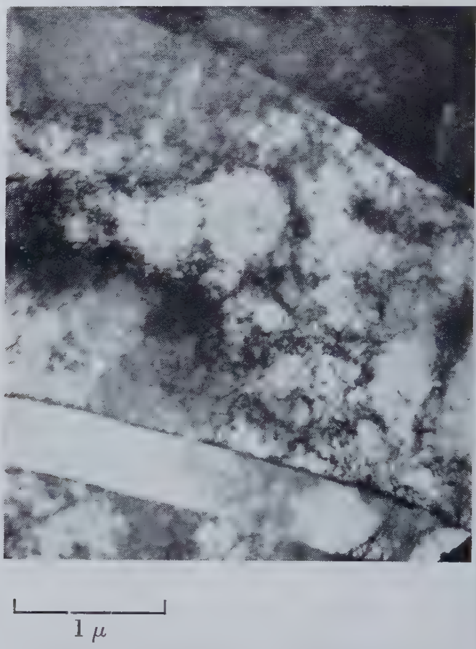

Grain boundaries in polycrystalline silver deformed 25% in tension. Mag. × 20 000.

Fig. 6

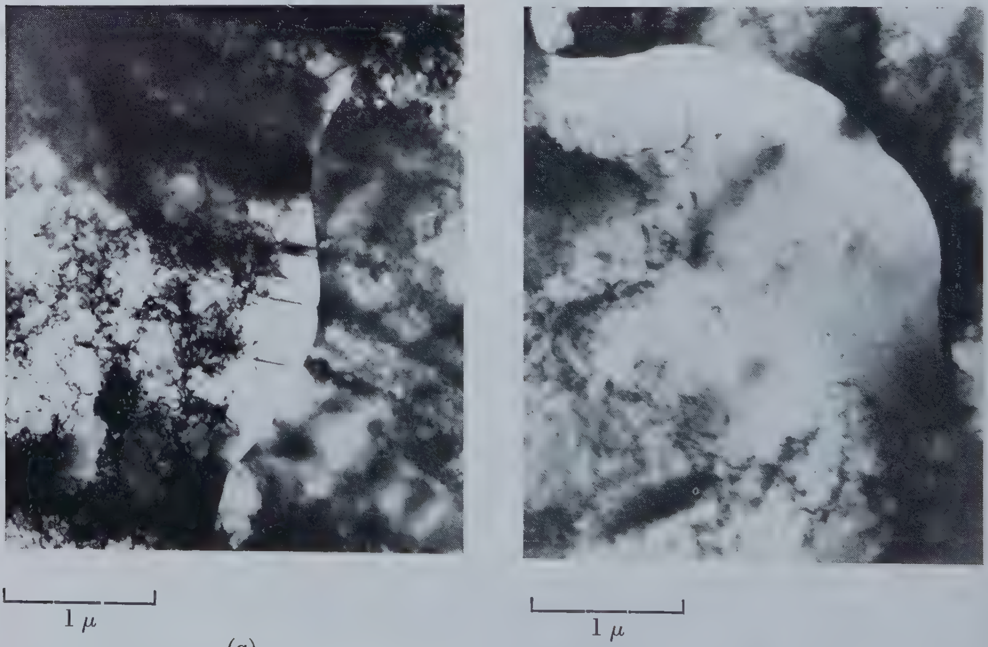

(a) (b)

Examples of the early stage of grain boundary migration in polycrystalline silver deformed 25% in tension and annealed 1 hour at 210°c. Mag. × 20 000.

Fig. 6 (*continued*)

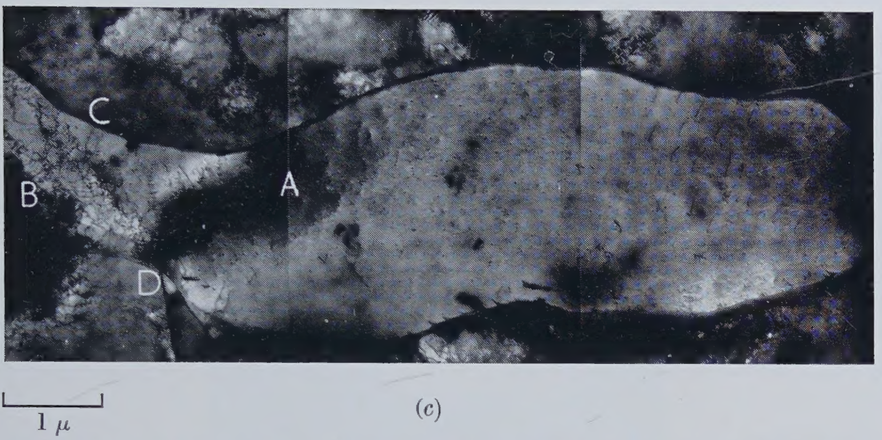

(*c*)

Advanced stage of grain boundary migration in polycrystalline silver deformed 25% in tension and annealed 1 hour at 200°c. Mag. ×13 000.

Fig. 7

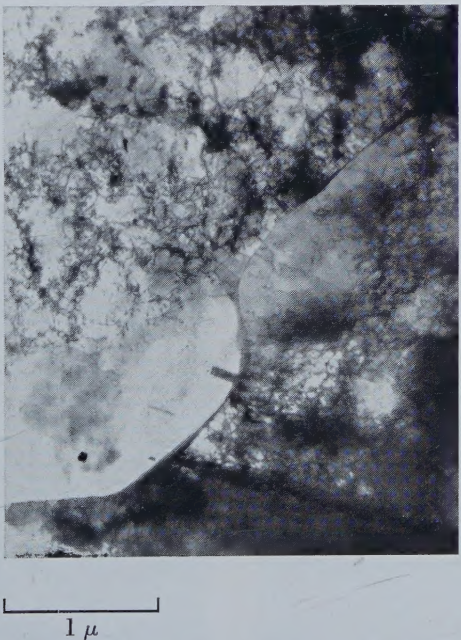

Neighbouring regions of a grain boundary attempting to migrate in opposite directions. Mag. ×20 000.

Fig. 8

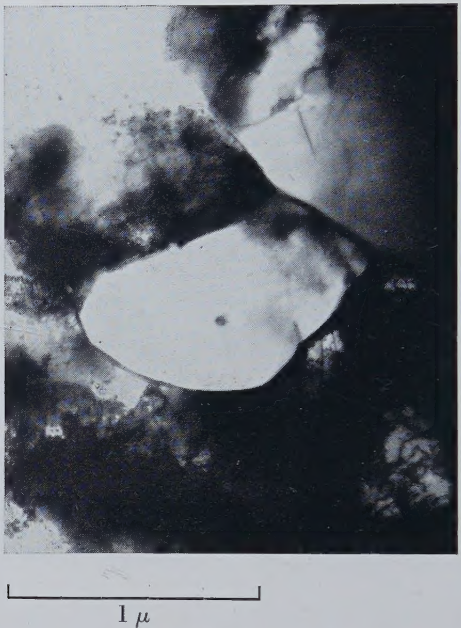

Micrograph showing completely enclosed recrystallizing grain. Mag. ×33 000.

Fig. 9

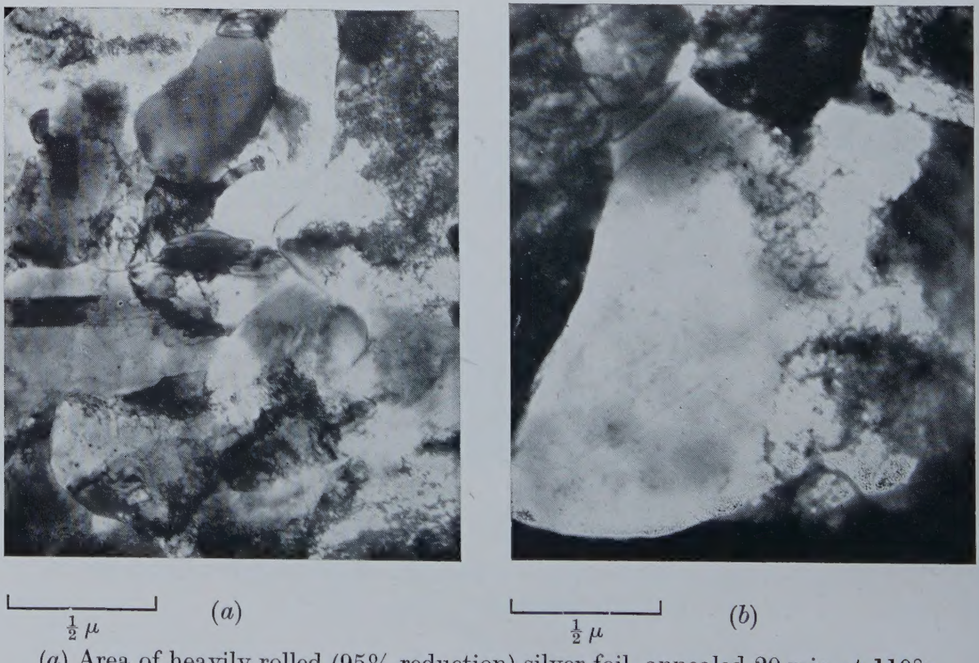

(*a*) (*b*)

(*a*) Area of heavily rolled (95% reduction) silver foil, annealed 20 min at 110°C showing sub-grain formation. (*b*) Early stage in the growth of a recrystallizing grain in heavily rolled silver (95% reduction) after annealing for 20 min at 110°C. Mag. ×40 000.

Fig. 10

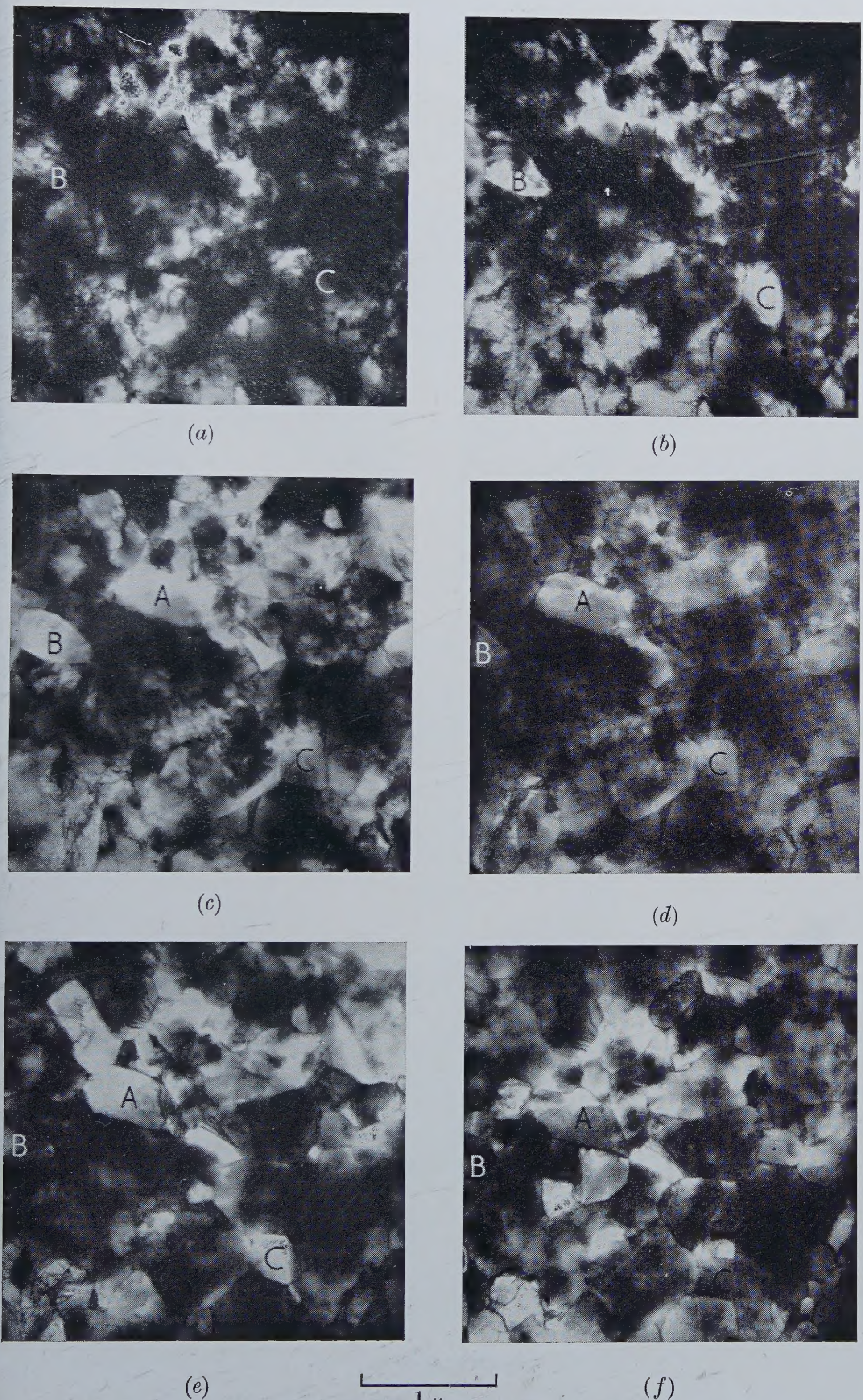

(a) (b) (c) (d) (e) (f)

Sequence of heating stage observations on heavily rolled (95% reduction) polycrystalline silver foil, showing: (*a*) Area at room temperature. (*b*) Same area after heating for 4 min at 200°c. (*c*) Same area after heating for $1\frac{1}{2}$ min at 400°c. (*d*) Same area after heating for $\frac{3}{4}$ min at 500°c. (*e*) Same area after heating for $\frac{1}{4}$ min at 600°c. (*f*) Same area after heating for $\frac{1}{4}$ min at 700°c. Mag. ×20 000.

Fig. 11

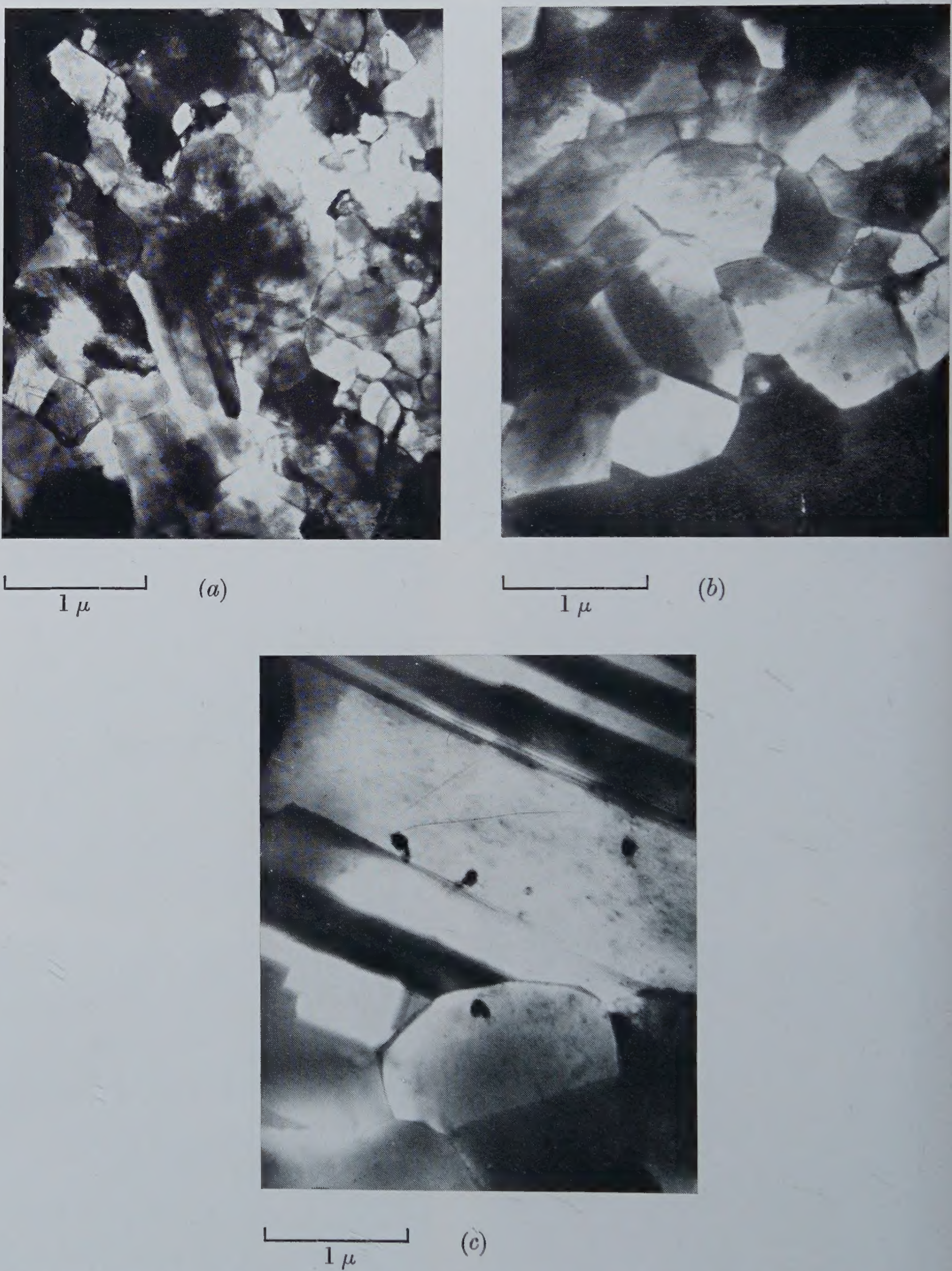

Micrographs of heavily rolled (95% reduction) polycrystalline silver foil after heating to a high temperature in the electron microscope, showing the increase of the grain size with increasing thickness of the foil. Mag. × 20 000.